REPORT DOCUMENTATION PAGE

Form Approved OMB NO. 0704-0188

1. REPORT DATE (DD-MM-YYYY)	2. REPORT TYPE	3. DATES COVERED (From - To)
19-01-2015	Ph.D. Dissertation	-

4. TITLE AND SUBTITLE	5a. CONTRACT NUMBER
Effect of Hydration on the Mechanical Properties of Anion Exchange Memebranes	W911NF-10-1-0520
	5b. GRANT NUMBER
	5c. PROGRAM ELEMENT NUMBER
	611103

6. AUTHORS	5d. PROJECT NUMBER
Melissa A. Vandiver	
	5e. TASK NUMBER
	5f. WORK UNIT NUMBER

7. PERFORMING ORGANIZATION NAMES AND ADDRESSES	8. PERFORMING ORGANIZATION REPORT NUMBER
Colorado School of Mines 1500 Illinois Street, Guggenheim Hall, Room 130 Golden, CO 80401 -1887	

9. SPONSORING/MONITORING AGENCY NAME(S) AND ADDRESS (ES)	10. SPONSOR/MONITOR'S ACRONYM(S) ARO
U.S. Army Research Office P.O. Box 12211 Research Triangle Park, NC 27709-2211	11. SPONSOR/MONITOR'S REPORT NUMBER(S) 58161-CH-MUR.63

12. DISTRIBUTION AVAILIBILITY STATEMENT

Approved for public release; distribution is unlimited.

13. SUPPLEMENTARY NOTES

The views, opinions and/or findings contained in this report are those of the author(s) and should not contrued as an official Department of the Army position, policy or decision, unless so designated by other documentation.

14. ABSTRACT

Anion exchange membranes (AEM) are promising solid polymer electrolytes for use in alkali fuel cells and electrochemical conversion devices. The dynamic nature of the fuel cell environment requires that AEMs operate at a range of hydration levels. Water sorption is critical for ion conduction, but excess water uptake causes dimensional swelling and mechanical instability. Ion conduction is slower in AEMs, compared to proton exchange membranes (PEM), making it important to minimize overall transport resistance by reducing membrane thickness; however, maintaining mechanical durability is difficult as thickness is reduced. Achieving an AEM with high

15. SUBJECT TERMS

Anion Exchange Membrane, Polymer Rheology, Mechanical Properties

16. SECURITY CLASSIFICATION OF:			17. LIMITATION OF ABSTRACT	15. NUMBER OF PAGES	19a. NAME OF RESPONSIBLE PERSON
a. REPORT	b. ABSTRACT	c. THIS PAGE			Andrew Herring
UU	UU	UU	UU		19b. TELEPHONE NUMBER 303-384-2082

Report Title

Effect of Hydration on the Mechanical Properties of Anion Exchange Memebranes

ABSTRACT

Anion exchange membranes (AEM) are promising solid polymer electrolytes for use in alkali fuel cells and electrochemical conversion devices. The dynamic nature of the fuel cell environment requires that AEMs operate at a range of hydration levels. Water sorption is critical for ion conduction, but excess water uptake causes dimensional swelling and mechanical instability. Ion conduction is slower in AEMs, compared to proton exchange membranes (PEM), making it important to minimize overall transport resistance by reducing membrane thickness; however, maintaining mechanical durability is difficult as thickness is reduced. Achieving an AEM with high conductivity and good mechanical durability is a difficult balance, which was the focus of this thesis.

Various polymer chemistries were investigated with respect to ion conduction, morphology, swelling, and mechanical properties as potential AEMs. The success of perfluorosulfonic acid PEMs inspired synthesis of perfluorinated AEMs, but cation functionalization was low, and proved chemically unstable, resulting in poor performance. Random polyiosoprene copolymers with high ion concentration were solution processed into films and subsequently crosslinked to generate solid AEMs. Diblock copolymers were studied due to their ability to phase separate into organized morphologies for efficient ion transport, but polymer chemistry greatly influenced mechanical performance. A polystyrene based diblock resulted in stiff, brittle AEMs with insufficient strength, but a polyethylene based diblock AEM produced large, flexible films.

Mechanical performance was investigated by extensional and dynamic mechanical testing. The addition of cation functionalities increased membrane stiffness, leading to brittle films. Water in the membrane acts as a plasticizer increasing elasticity and elongation, but also

iii

weakening membranes. Changing polymer chemistry to a polyethylene based diblock and optimizing casting conditions produced large (~300 cm2) area membranes of consistent (10 ?m) thickness. These membranes were flexible and showed good mechanical performance. Mechanical softening, due to hydration level, was identified by dynamic mechanical analysis. Conductivity measured as a function of humidity suggested increased ion conduction correlated with the hygromechanical softening point. Understanding the relationship between ion conduction and mechanical properties is critical to the development of robust, well-performing AEMs for use in fuel cells and electrochemical devices.

EFFECT OF HYDRATION ON THE MECHANICAL PROPERTIES

OF ANION EXCHANGE MEMBRANES

by

Melissa A. Vandiver

A thesis submitted to the Faculty and Board of Trustees of the Colorado School of Mines in partial fulfillment of the requirements for the degree of Doctor of Philosophy (Chemical Engineering).

Golden, Colorado

Date _____

<div style="text-align: right;">

Signed: _____
Melissa A. Vandiver

Signed: _____
Dr. Matthew W. Liberatore
Thesis Advisor

Signed: _____
Dr. Andrew M. Herring
Thesis Advisor

</div>

Golden, Colorado

Date _____

<div style="text-align: right;">

Signed: _____
Dr. David W.M. Marr
Professor and Head
Department of Chemical and Biological Engineering

</div>

ii

ABSTRACT

Anion exchange membranes (AEM) are promising solid polymer electrolytes for use in alkali fuel cells and electrochemical conversion devices. The dynamic nature of the fuel cell environment requires that AEMs operate at a range of hydration levels. Water sorption is critical for ion conduction, but excess water uptake causes dimensional swelling and mechanical instability. Ion conduction is slower in AEMs, compared to proton exchange membranes (PEM), making it important to minimize overall transport resistance by reducing membrane thickness; however, maintaining mechanical durability is difficult as thickness is reduced. Achieving an AEM with high conductivity and good mechanical durability is a difficult balance, which was the focus of this thesis.

Various polymer chemistries were investigated with respect to ion conduction, morphology, swelling, and mechanical properties as potential AEMs. The success of perfluorosulfonic acid PEMs inspired synthesis of perfluorinated AEMs, but cation functionalization was low, and proved chemically unstable, resulting in poor performance. Random polyiosoprene copolymers with high ion concentration were solution processed into films and subsequently crosslinked to generate solid AEMs. Diblock copolymers were studied due to their ability to phase separate into organized morphologies for efficient ion transport, but polymer chemistry greatly influenced mechanical performance. A polystyrene based diblock resulted in stiff, brittle AEMs with insufficient strength, but a polyethylene based diblock AEM produced large, flexible films.

Mechanical performance was investigated by extensional and dynamic mechanical testing. The addition of cation functionalities increased membrane stiffness, leading to brittle films. Water in the membrane acts as a plasticizer increasing elasticity and elongation, but also

iii

weakening membranes. Changing polymer chemistry to a polyethylene based diblock and optimizing casting conditions produced large (~300 cm^2) area membranes of consistent (10 μm) thickness. These membranes were flexible and showed good mechanical performance. Mechanical softening, due to hydration level, was identified by dynamic mechanical analysis. Conductivity measured as a function of humidity suggested increased ion conduction correlated with the hygromechanical softening point. Understanding the relationship between ion conduction and mechanical properties is critical to the development of robust, well-performing AEMs for use in fuel cells and electrochemical devices.

TABLE OF CONTENTS

LIST OF FIGURES

xiv

LIST OF TABLES

ACKNOWLEDGEMENTS

CHAPTER 1 : INTRODUCTION

Fuel cell devices directly convert the chemical energy in fuel to electrical energy for powering electronic or electrical devices [1]. Polymer electrolyte membrane fuel cells are one of the most promising low temperature fuel cell technologies, owing to their high power density and quick start-up, and have been highly developed in the last several decades [2, 3]. Proton exchange membranes (PEM), specifically perfluorinated sulfonic acid (PFSA) membranes have dominated the industry due to their high proton conductivity and good chemical and mechanical stability [4, 5]. Current PEM fuel cells remain cost prohibitive due to the high catalyst costs and limited fuel options due to the acid based catalyst systems that need Pt based materials, as well as long-term durability issues [2, 6, 7]. These issues make implementation of PEM fuel cells difficult without significant research into next generation membranes and improved catalysts.

Alkali fuel cells (AFC) offer an alternative to PEM fuel cells in that non-precious metals can be used that reduce catalyst costs and increase fuel options. The concept of the alkali fuel cell with a liquid potassium hydroxide electrolyte was developed by Francis Bacon in the late 1930s [8]. In the 1960s AFCs were implemented on the NASA Apollo space craft, replacing the unstable PEMFCs based on sulfonated polystyrene used in earlier Gemini space craft [8-12]. Alkali fuel cells utilize a liquid potassium hydroxide electrolyte to transport hydroxide ions from the anode to the cathode (Figure 1.1). The ion transport in an AFC is opposite to PEMFCs reducing the chance of fuel crossover due to electro-osmotic drag [4, 9, 13]. The kinetics of fuel oxidation are more favorable in an alkali environment giving AFCs a potential benefit over PEMFCs [9, 10, 12, 13]. The increase oxidation in alkali media encourages use of non-precious metal catalysts, decreasing the cost of the fuel cell [4, 8-10, 12]. While liquid electrolyte AFCs found some use in early niche applications, fundamental hurdles prevented wide-scale

commercial application. Exposure to carbon dioxide causes the hydroxide ions in the liquid electrolyte to form insoluble potassium carbonate/bicarbonate precipitates that can block active sites of the electrodes reducing performance [9-12, 14]. To prevent electrolyte degradation very pure oxygen streams or frequent regeneration of the electrolyte solution is necessary, neither of which are reasonable for long-term or terrestrial application. To overcome these shortfalls, while maintaining the kinetic and cost benefits of AFCs, current research is focused on the development of an alkali fuel cell containing a solid anion exchange membrane as the electrolyte. Anion exchange membranes have cations covalently bonded to the polymer so carbonation can change the counter ion association in the polymer, but will not result in solid precipitates [9, 10]. Alkali anion exchange membrane fuel cells will benefit from the increased kinetics of the methanol oxidation and allow for use of cheaper non-precious metal catalyst.
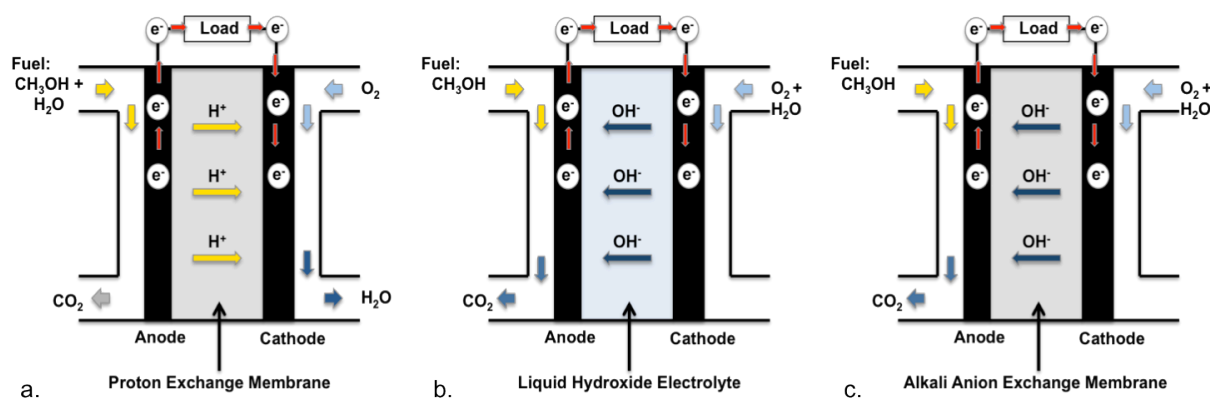
Figure 1.1: Schemtatics of a.) a proton exchange membrane fuel cell, b.) a liquid electrolyte alkali fuel cell, and c.) a solid alkali anion exchange membrane fuel cell.

An anion exchange membrane has several basic requirements for use in an alkali fuel cell. The membrane requirements include 1) a high ionic conductivity, 2) a selective permeability to transport ions while preventing crossover of fuel/oxygen, 3) an adequate hydration level to facilitate conductivity/transport while limiting geometric swelling, 4) chemical stability of the polymer backbone and cationic group, 5) mechanical stability over the lifetime of the device [8-

10]. All of these requirements must be considered when developing anion exchange materials. Careful characterization of these properties is critical during development of an optimized film for practical use. While anion exchange membrane fuel cells have the potential to produce an efficient low cost direct methanol fuel cell, there are fundamental challenges to be addressed before application can be fully realized. The main issues facing anion exchange membrane are the inherently lower conductivity of hydroxide compared to protons and the chemical and mechanical stability of the membrane over its lifetime.

Conductivity and transport of hydroxide ions is inherently slower than protons; the diffusivity of hydroxide is approximately half that of the proton [15], making it challenging to develop an AEM with performance of a PEM. Anion exchange membrane fuel cell often rely on increased ion exchange capacity (IEC), the number of charge groups per unit polymer mass, to overcome the inherently lower transport of hydroxide systems. Higher IECs increase conductivity, but can negatively affect mechanical stability due to increased swelling of the membrane at high hydrations that can weaken the membrane and be detrimental to the membrane electrode assembly (MEA). Both hydronium (proton) and hydroxide ions have significantly higher diffusivities than other ions of similar size due to their ability to participate in charge shuttling with water molecules [16]. This phenomenon is called the Grotthuss diffusion mechanism and accounts for the increased diffusivity of hydronium/hydroxide ions over other ions that rely solely on a translational diffusion [10, 16]. Adequate hydration provides the water molecules that facilitate Grotthuss diffusion, critical to maintain high conductivity.

Chemical stability is a fundamental requirement for an anion exchange membrane, however it is also one of the biggest challenges. AEMs must withstand the basic environment created by hydroxide transport through the membrane. Common cation groups used in AEMs

include quaternary ammonium, quaternary phosphonium, tertiary sulfonium, and guanidinium based compounds [8]. Unfortunately, degradation is a concern for all of these cations, making implementation of a stable AEM difficult. The most widely used cations for AEMs are quaternary ammonium compounds, which suffer a number hydroxide degradation routes, including Hoffman elimination, nucleophilic substitution, or subtraction of hydrogen to form water and an ylide [8, 9, 17]. In addition to cation stability the backbone of the polymer must be chemically stable and produce a durable membrane.

The lower transport efficiency of AEMs makes thin membranes critical to minimize area specific resistance, however, maintaining mechanical integrity of thin membranes is difficult [18]. Considering mechanical properties of new AEMs and tailoring membrane design towards robust, thin films are critical for the realization of AEM energy conversion devices in the future. A number of design factors can influence membrane strength and durability. Polymer chemistry is responsible for the basic mechanical properties of the membrane [8]. Block copolymer AEMs offer the opportunity to tailor mechanical properties by selecting the polymer chemistry of the hydrophobic block to tune desired properties. PEM research has shown that a higher degree of crystallinity can improve mechanical properties [19]. Increasing polymer crystallinity can be achieved by altering polymer chemistry, such as reducing the side chain length in PFSA PEMs [20, 21], or through various annealing techniques. Crosslinking is another common technique to improve membrane strength [19, 22]. Chemically crosslinking polymer chains increases the modulus and strength, however the method of crosslinking may reduce the ionic concentration and a high degree of crosslinking may cause membrane embrittlement. Physical reinforcement of membranes with a nonconductive, porous polymer film can also significantly improve durability, as long as it is also chemically stable to hydroxide [23]. Porous polytetrafluoroethylene (PTFE)

membranes and fibers have been incorporated into PFSAs to improve mechanical durability [6, 19, 24]. Reinforcing an ion exchange membrane also helps resist dimensional swelling, retaining membrane properties between dry and hydrated states. While physical reinforcement can strengthen the membrane and resist changes with hydration, the addition of a nonconductive material lowers the ion exchange capacity of the membrane. While a number of design factors can impact the mechanical durability of an AEM, consideration of these factors early in AEM research is important to develop satisfactory fuel cell membranes.

Thorough studies have been performed on the mechanical strength, durability, and failure mechanisms of PEMs [6, 7, 25] and this information can be used to guide AEM development and testing. A working fuel cell has a dynamic temperature and humidity environment resulting in changes in membrane hydration. Sorption and desorption of water can produce significant swelling and hygrothermal stresses in the membrane [6, 7, 26]. As the membrane is constrained in the membrane electrode assembly (MEA), dimensional swelling of the membrane results in stresses on the assembly and membrane. The hygrothermal stresses experienced by the membrane due to swelling and contraction can lead to pinhole and crack formation [27]. These defects weaken the membrane, leading to mechanical failure, and allowing crossover in electrochemical energy conversion devices. Durability tests to gauge membrane lifetime of PEMs include rapid humidity cycling while monitoring gas crossover [28] and pressurized blister tests [29]. These tests have been shown to accurately predict relative membrane lifetimes. Traditional tensile tests are a less accurate predictor of membrane lifetime in a fuel cell, but remain the standard characterization for comparing mechanical properties of polymer films [6]. Dynamic mechanical analysis can measure the dynamic membrane response to changing temperature and humidity.

Fabrication of defect free membranes, mechanical durability, and relating mechanical properties to ion conduction is critical for successful AEM applications. For this reason, a various AEM polymer systems were investigated to test the hypothesis that ion conduction is dependent hydration and chain flexibility and can be correlated to a membrane's mechanical properties. The objectives identified to test the hypothesis that hydration and mechanical properties can be correlated to ion conduction are as follows:

1. Identify quantifiable metrics for tensile properties of AEMs at a range of hydration levels.

2. Study the effects cationic functionalization, film formation technique, hydration level on the mechanical properties and ion conduction in AEMs.

3. Relate ion conduction to mechanical properties by identifying hygrothermal mechanical transitions and measuring ionic conductivity around these transition points.

This document focuses on the development of mechanically robust anion exchange membranes and the interplay of conductivity and mechanical durability at a range of hydration levels. Chapter 2 explains experimental methods to characterize membrane properties including ionic conductivity, water sorption, morphology, and mechanical durability. Chapter 3 describes the functionalization and characterization of the 3M ionomer with various cationic species to make perfluorinated AEMs. Chapter 4 describes the benchmark mechanical characterization of three common anion exchange membranes by extensional rheology at different hydration levels. Chapter 5 compares the properties of a polystyrene-b-poly(vinylbenzyl trimethylammonium) membrane with the equivalent homopolymer blend, focusing on the effect of film casting method on mechanical performance of the membrane. Chapter 6 explores the effect of crosslinking

technique and duration on mechanical properties of random polyiosoprene based AEM copolymers. Chapter 7 describes the effect of hydration on the mechanical performance and ion conduction in a polyethylene-b-poly(vinylbenzyl trimethylammonium) AEM. Finally, Chapter 8 provides general conclusions and makes recommendations for future work.

CHAPTER 2 : EXPERIMENTAL DESIGN

This chapter describes the experimental methods and techniques utilized throughout the remainder of this document.

2.1 Ion Exchange Capacity

Ion exchange capacity (IEC) is defined as the number of cationic functional groups per mass of polymer and can be determined by titration methods. For polymer materials that are stable in base, an acid-base titration can be performed [30, 31]. The polymer, in the hydroxide form, is placed in a know volume of sodium chloride solution for at least 24 hours. The solution is then titrated with a standardized weak acid to determine the hydroxide content in the solution. Based on the volume of titrant used the ion exchange capacity of the material is calculated. For materials that are not stable in base, an alternative Mohr titration can be performed on the polymer material in the chloride form [32]. The polymer, in the chloride form, is placed in a known volume of bicarbonate solution for at least 24 hours. This solution is then titrated using standardized silver nitrate solution and a potassium chromate indicator. The silver nitrate produces white-silver precipitates of silver chloride. The formation of rust colored silver chromate precipitate indicates the titration equivalence point. The amount of chloride ions is back calculated based on the titrant volume and the ion exchange capacity is calculated by Equation (2.1).

$$\text{IEC}\left(\frac{\text{mmol}}{\text{g}}\right) = \frac{\text{mmol}}{\text{mL}}(\text{AgNO}_3) \cdot \text{mL}(\text{AgNO}_3) \cdot \frac{1\,\text{mmolCl}^-}{1\,\text{mmol Ag}^+} \cdot \frac{1}{\text{m}_{\text{membrane}}(\text{g})} \qquad (\,2.1\,)$$

The titration solution is typically divided into several aliquots and multiple titrations performed so a standard error can be calculated.

2.2 Conductivity by Impedance Spectroscopy

The ability of a membrane to conduct ions is one of the most important parameters for successful application in a fuel cell. Accurate characterization of membrane conductivity at a range of operating conditions is necessary to gauge potential anion exchange membranes. The in-plane conductivity was calculated using electrochemical impedance spectroscopy to measure membrane resistance as given by Equation (2.2) below.

$$\sigma = \frac{l}{R \cdot w \cdot t} \tag{2.2}$$

where R is the membrane resistance, l is the distance between the electrodes, w is the width of the membrane samples, and t is the thickness of the sample. The cell consists of two Teflon blocks that sandwich the membrane to contact platinum wire electrodes connected to a potentiostat (Figure 2.1).
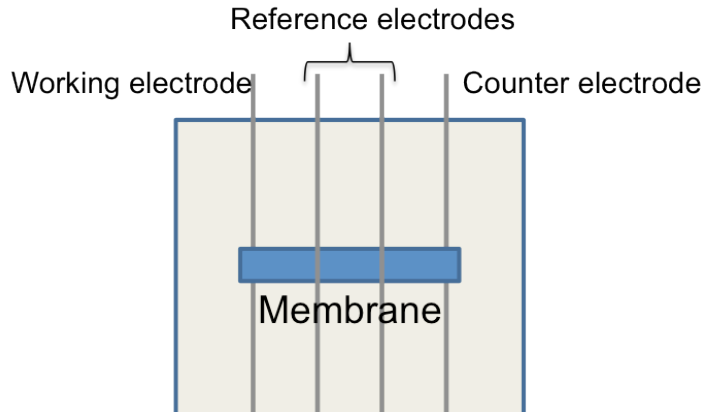
Figure 2.1: Schematic of the in-plane conductivity cell.

Impedance spectra were obtained over a frequency range of 1 to 10^5 Hz using a four-electrode test cell connected to a multi-channel potentiostat (BioLogic VMP3, Knoxville, TN). The test cell outer electrodes are the working and counter electrodes while the inner electrodes represent the reference and sense electrodes. The measurements were made in an environmental chamber (TestEquity Model 1007H, Moorpark, CA) to control sample temperature and humidity.

The TestEquity oven is a well-insulated system and at steady state the temperature varies by less than 0.5°C and the humidity varies by less than 1%RH. Impedance measurements were represented in a Nyquist impedance plot of the real impedance vs. the imaginary impedance. Typical impedance spectra are given as a semi-circle starting at the origin for high frequency and approaching the x-axis at lower frequencies (Figure 2.2). The resistance of the membrane is determined from the low frequency intercept.
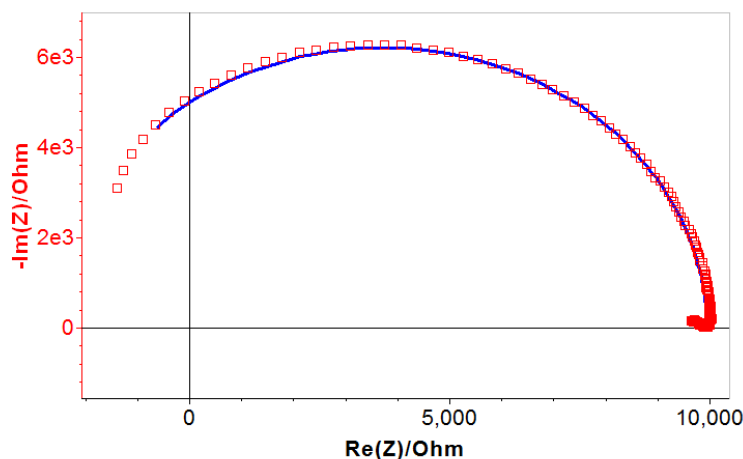
Figure 2.2: Typcial Nyquist plot of an impedance loop, the red squares are the expeirmental data and the blue line is the fit to a theoretical circuit.

The environmental chamber allows independent control of temperature and humidity. A typical experiment will maintain a constant relative humidity and ramp the temperature from 50 to 90°C in 10°C increments. The TestEquity oven maintains each temperature set point for 64 minutes, during this interval the potentiostat takes impedance measurements continuously in 4-minute cycles. The membrane resistance and conductivity is calculated for each impedance loop, the measurements that reduce to a consistent resistance and conductivity are taken as the steady-state data while earlier measurements are disregarded in calculations.

2.3 Water Sorption

Water uptake by the membrane was characterized using a dynamic vapor sorption apparatus (SMS DVS Advantage 1, Allentown, PA). A small membrane sample was placed on a glass weigh plate and the gravimetric change in mass was measured under different humidity conditions. Humidity was ramped from a dry set point of 0% RH to a maximum set point of 95% RH stepping up by 20% RH in two-hour interval steps. An additional two-hour drying step at the start of the experiment allowed the membrane to come to an "equilibrium" dry state before taking measurements. Each sample was cycled at least twice to determine possible hysteresis of the membrane.

The water uptake, WU, of the membrane was calculated using Equation (2.3)

$$WU = \frac{m_{\%RH} - m_{dry}}{m_{dry}} \times 100 \qquad (\,2.3\,)$$

where $m_{\%RH}$ is the mass of the sample at the given relative humidity and m_{dry} is the mass of the dry sample. The water uptake represents the mass change in the sample due to water sorption into the membrane. Given the water uptake at saturated conditions and the known ion exchange capacity, the hydration level (λ), or number of waters per cation functional group, can be calculated using Equation (2.4)

$$\lambda = \frac{n(H_2O)}{n(NR_4^+)} = \frac{WU}{m(H_2O) \cdot IEC} \qquad (\,2.4\,)$$

where $n(H_2O)$ is the number of waters, $n(NR_4^+)$ is the number of cation groups, $m(H_2O)$ is the molar mass of water, and IEC is the ion exchange capacity in mol/g. The water uptake is a key parameter used to correlate membrane performance properties. Membrane conductivity, transport, and morphology can all be correlated to the water content in the membrane.

2.4 Small Angle X-ray Scattering

Small angle x-ray scattering (SAXS) is an experimental technique used to determine morphological characteristics of materials on size scale of 1.5 to 150 Å. SAXS is complimentary to wide angle x-ray scattering (WAXS) which probes the crystal structure of materials on the scale of 0.45 to 1.15 Å. Combined SAXS and WAXS have the potential to reveal a large amount of information about polymer structure and morphology. X-ray scattering detects structural features based on the scattering of x-rays by electrons in the material [33]. Contrast in SAXS is based on the differences of the average electron density of the materials, which results in changes in the scattering intensity. Electrons in the material resonate at the frequency of the x-rays generating secondary waves, scattering, that can be detected. This change, or scattering, of the x-rays corresponds to material domain size and spacing. The length scale probed is related by the scattering vector, q, as given in Equation (2.5)

$$q = \frac{4\pi \sin(\theta/2)}{\lambda}$$ (2.5)

where θ is the scattering angle and λ is the x-ray wavelength. Bragg's law relates the scattering vector, q, to the size of a domain (d-spacing) of the material as shown in Equation (2.6).

$$d = \frac{2\pi}{q}$$ (2.6)

X-rays generated by synchrotron sources are much higher flux than lab scale x-ray sources, thus allowing shorter sampling times (as low as 0.1 seconds) and ability to sample through gas/humidity environments. Therefore, synchrotron SAXS can observe the swelling behavior of polymer membranes and perform dynamic studies on these samples.

SAXS experiments were performed at The Basic Energy Sciences Synchrotron Radiation Center (BESSRC), beamline 12-ID-B, at the Advanced Photon Source at Argonne National Lab.

Measurements were taken in a transmission geometry using a Pilatus 2M SAXS detector and a Pilatus 300K WAXS detector with an acquisition time of 1 s. The 2D scattering pattern was radially integrated to obtain data of intensity versus scattering vector, q. The transmission intensity was normalized to exposure time and flux of the direct beam through the sample. However, due to of the swelling of the membranes, absolute thickness and atomic density could not be determined in-situ. Therefore, the intensity units become arbitrary. Incoming X-ray wavelength for all experiments was 1 Å.

A custom built four-sample oven was used to control the humidity and temperature of the samples during scattering experiments. The sample oven has Kapton windows on both sides of the sample area. Typical experiments contain three membrane samples and one empty window to obtain a background spectrum at each humidity throughout the scattering experiment. A Vaisala HMT337 humidity probe monitors humidity in the oven. Humidity is controlled by operator adjustment of the wet and dry gas flow using LabView software. Two mass flow controllers (MKS Mass-Flo RS-485 Controller) regulate the dry and wet gas flow. The house nitrogen feed at the APS was used directly for the dry gas line, while the humidified gas line was bubbled through a humidifying bottle (Fuel Cell Technologies, Inc.). A helical mixing tube upstream from the oven mixes the dry and humidified gas streams prior to entering the sample oven. A Watlow PID temperature controller controlled the temperature of the oven, gas lines, and humidity bottle.

2.5 Film processing

Generation of uniform films is critical to membrane integrity, and can be greatly enhanced by controlled film processing. Defect areas and non-uniform thickness in films are

more susceptible to failure as the film undergoes different stresses. Controlled film processing will increase film uniformity and overall strength.

2.5.1 Solution casting

Solution casting is one of the most utilized film formation techniques [34]. The polymer is dissolved in a suitable solvent and poured on to a flat substrate. The solution is then allowed to evaporate leaving a solid polymer film, which is subsequently removed from the substrate for application. Evaporation of the solvent can be achieved at ambient conditions, with the addition of heat, under reduced pressure to drive the drying process, or a combination of the three.

2.5.2 Film formation using flow

Shear flow can orient polymer chains and provide structured morphology in a film [35, 36]. Commercial films are often produced by extrusion methods where a polymer is brought above its melting temperature, drawn through a die, and rapidly cooled to produce a well defined, uniform film. The extrusion process is difficult to perform on a lab scale, but the shearing effects of extrusion can be reproduced by other lab techniques including use of a doctor blade [37]. The doctor blade uses a sharp blade at a fixed gap distance above the substrate [34]. Polymer solution is placed in front of the blade, which is then moved linearly over the solution producing a thin, wet film. Along with the gap thickness, the final thickness of the film is dependent on the surface energy of the substrate, the surface tension and viscosity of the polymer solution, and the shear field produced by the blade [34]. The basic empirical relationship given in Equation (2.7) can be used to estimate the final film thickness.

$$d = \frac{1}{2}\left(g\frac{c}{\rho}\right) \qquad (2.7)$$

Where g is the gap distance, c is the concentration of solid polymer, ρ is the density of the material in the final film [34]. In addition to simulating the effects of extrusion, doctor blading

can be directly scaled to commercial processing on a roll to roll basis utilizing a knife over edge coating technique [34]. An automatic film applicator (MTI Corporation's MSK-AFA-III, Richmond, CA) with a micrometer adjustable blade was used to draw the polymer solution at a consistent speed and thickness.

2.6 Mechanical Analysis

Mechanical analysis of polymer membranes was performed on an ARES G2 rheometer (TA Instruments, New Castle, DE). While the ARES G2 is designed as a traditional rotational rheometer, additional capabilities allow small amplitude axial tests for Dynamic Mechanical Analysis (DMA). A Sentmanat Extensional Rheometer (SER) fixture (Xpansion Instruments, Tallmadge, OH) was used to perform simulated tensile tests [38]. A Film/Fiber fixture was used for tension DMA measurements. A custom-built humidity delivery system allowed control of sample temperature and humidity simultaneously.

2.6.1 Simulated Tensile Test with SER geometry

Tensile like tests were performed using a SER fixture on an ARES G2 rheometer. The SER fixture suspends the membrane across two counter rotating drums. The rheometer controls the rotation of the drums, which stretch the sample to failure. The stress on the membrane sample is measured by the rheometer during film extension. The SER fixture is generally used to measure the elongation viscosity of polymers in their melt state, but has been shown to accurately measure tensile properties in the solid state [38]. The stress vs. strain data is used to determine the elastic modulus, ultimate strength, and elongation of the film. The modulus is defined as the slope of the stress vs. strain curve in the initial liner region that corresponds to elastic deformation. The engineering stress at break is defined as the stress measured

immediately prior to break, based on the initial film dimensions. The elongation of the membrane is the percent increase in film length as determined by the strain at break.

Polymer films are cut into strips of 25 mm(L) x 3 mm(W), about 5 – 10 mg, for testing. New drums were manufactured for the SER fixture to allow for silicon coated screw-down pins to secured the film to the drum surface. The Hencky strain rate at which the films were stretched is based on the ultimate elongation: $0.0033s^{-1}$ (0.021mm/s) for elongations less than 20%, 0.0167 s^{-1} (0.106 mm/s) for elongations between 20 and 100%, and 0.33 s^{-1} (2.12 mm/s) for elongations greater than 100%. These strain rates were calculated based on ASTM D882-12 for tensile testing of thin plastic sheeting, but modified to account for the predefined sample distance between the drums.
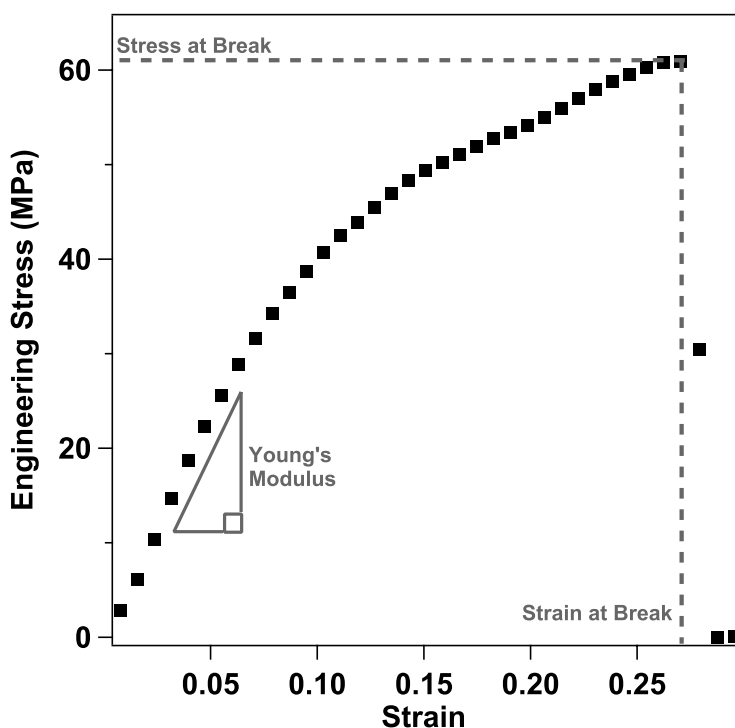
Figure 2.3: General stress *vs.* strain curve for an SER extensional test with stress at break, strain at break, and Young's modulus labeled.

2.6.2 Dynamic Mechanical Analysis

Dynamic Mechanical Analysis was performed using the rectangular film/fiber geometry on the ARES G2 rheometer. The film/fiber geometry holds a sample in linear tension. Polymers are viscoelastic materials, meaning they exhibit both solid (elastic) and fluid (viscous) like behavior. DMA probes the viscoelastic properties of a material by applying and oscillatory stress or strain and measuring the material response (Figure 2.4). The complex modulus (E*) is defined by the relationship between the sinusoidal waves of the force applied (stress or strain) and material response (strain or stress). The complex modulus can be separated into the storage modulus (E'), which is elastic component related to sample stiffness, and the loss modulus (E''), which is the viscous component related to energy loss in the material. Additionally, the ratio of E' to E'', called Tan δ is representative of damping in the material.
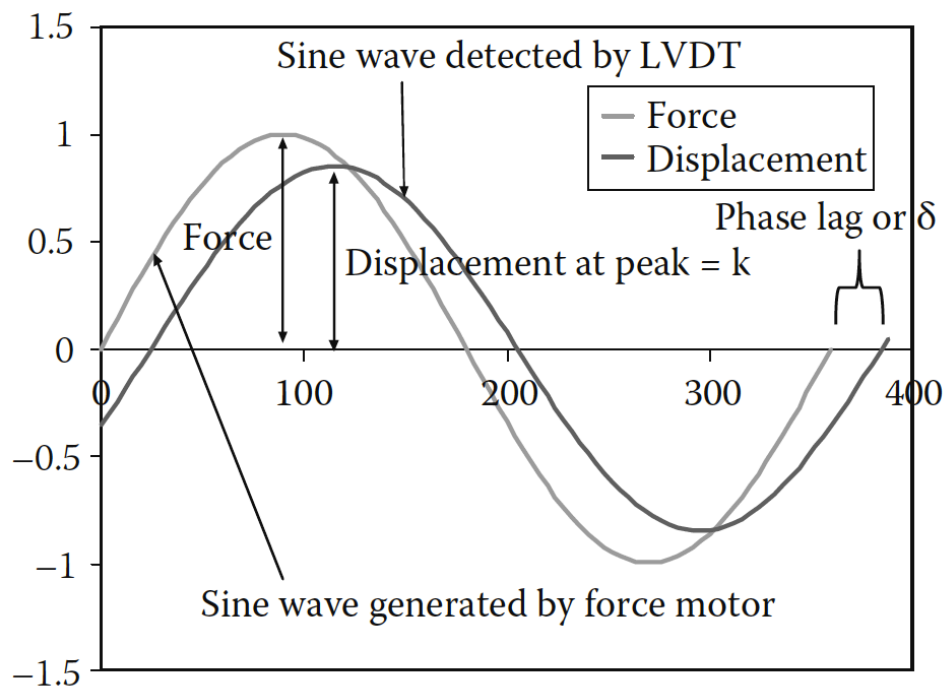
Figure 2.4: Sinusoidal waves of the applied force and resultant displacement in a standard DMA experiment used to measure the complex modulus [39].

$$E^* = E' + iE''$$
$$\text{Tan } \delta = E''/E'$$
$$\eta^* = E^*/\omega$$
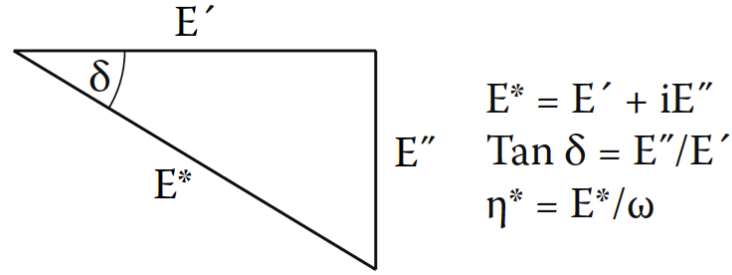
Figure 2.5: Relationships between the complex modulus (E*), storage modulus (E'), loss modulus (E''), and the phase lag (δ) [39].

Typical DMA experiments apply an oscillatory force while changing the environment such as temperature or frequency to probe transition points of the material. One of the most widely used applications of DMA is to determine the glass transition temperature (T_g) of polymers. To determine T_g, DMA is performed at a constant strain and frequency while slowly ramping temperature. The T_g of the material is identified by a sharp drop in storage modulus as a function of temperature, and a peak in Tan δ.

AEMs mechanical properties are highly dependent on hydration level, so DMA will be utilized to probe transitions and material response as a function of both temperature and humidity level using a custom-built humidity controlled sample chamber (discussed below). Thermomechanical transitions will be investigated by DMA while ramping temperature, at a constant relative humidity. Because mechanical properties are significantly different between dry and hydrated states, temperature ramps were performed at dry and saturated conditions to determine thermal changes in the membrane. Hygromechanical transitions, due to humidity/hydration, were investigated by performing DMA while ramping humidity, at a constant temperature. Performing DMA at hydrated conditions proved challenging as AEMs undergo softening at hydrated conditions, and this softening caused moduli to become immeasurable by the instrument. The instrument has a defined stiffness range, and while the

18

modulus is an intrinsic material property, stiffness is dependent on sample dimensions as described by Equation (2.8) [40]

$$K_s = E^* \cdot \left(\frac{A}{L}\right)$$ (2.8)

where K_s is the stiffness, E^* is the complex modulus, and A and L are the cross-sectional area and length of the sample respectively. Cross-sectional area is inherently low, due to the thin nature of the AEM films, and at hydrated conditions moduli are also low, causing the stiffness to be reduced below the measurable range of the instrument. In order to maintain sample stiffness within a measureable range, hydrated sample length was reduced significantly. At dry conditions samples were loaded at starting gap height of 5 mm and moduli were measurable at all temperatures; while under hydrated conditions, samples were loaded at a starting gap height of 1 mm in order to remain measurable at all conditions. The film/fiber geometry requires the sample be held in tension throughout the experiment, and this tension must be greater than the oscillation force to strain the sample. As moduli are reduced, due to increased temperature or humidity, the instrument maintains tension by increasing the gap height. Maintaining tension on soft samples can result in significant sample elongation and care must be taken that sample elongation remains in the elastic region during testing.

2.6.3 Humidity Control for Mechanical Testing

A custom-built oven with controlled humidity delivery was developed to accurately control temperature and humidity level simultaneously during mechanical testing. The aluminum oven utilizes four electric cartridge heaters wired in parallel to control the sample temperature. Humidified gas is supplied by a combination of dry and wet gas flows controlled by to two mass flow controllers (10,000 cm^3/min capacity, MKS 1179A). The wet gas passes through a humidity

bottle (FCT, Inc.) with 10 m of Nafion® tubing to saturate the air with water. The wet and dry gas flows are combined and delivered to the sample oven through heated lines, to prevent condensation in the tubing. A humidity probe (Vaisala HMT 337) measures the dew point in the sample chamber and provides real time humidity conditions. PID feedback loops control temperature through the heaters and relative humidity by wet/dry gas flow.

CHAPTER 3 : SYNTHESIS AND CHARACTERIZATION OF PERFLUORO QUATERNARY AMMONIUM ANION EXCHANGE MEMBRANES

This chapter is modified from a paper published in

Journal of Polymer Science, Part B: Polymer Physics[1]

Melissa A. Vandiver[2], James L. Horan[3], Yuan Yang[4], Emily T. Tansey[5],

Sönke Seifert[6], Matthew W. Liberatore[7], and Andrew M. Herring[8]

3.1 Abstract

In this work new alkaline exchange membranes were prepared from the perfluorinated 3M ionomer with various quaternary ammonium cations attached with sulfonamide linkage. The degree of functionalization varied depending on the cation species resulting in different ion exchange capacities (IEC), $0.33 - 0.72$ meq g^{-1}. There was evidence of polymer degradation when the films were exposed to hydroxide, so all membrane characterization was performed in the chloride form. Conductivity was dependent on cation species and IEC, $E_a = 36 - 51$ kJ mol^{-1}. Diffusion of water through the membrane was relatively high 1.6×10^{-5} cm^2/s and indicated restriction over a range of diffusion times, $6 - 700$ ms. Water uptake in the membranes was generally low and the hydration level varied based on cation species, $\lambda = 6 - 11$. Small angle scattering experiments suggested ionic aggregation, $37 - 42$ Å, independent of cation species but slight differences in long-range order with cation species.

3.2 Introduction

The proton exchange membrane (PEM) fuel cell is a very attractive energy conversion device due to its high power density; however, it suffers from a number of disadvantages including the requirement for precious metal catalysts and the challenge of oxidizing complex fuels under acidic conditions [3, 9, 41]. Recently there has been increasing interest in using alkaline fuel cells (AFCs) owing to the potential to utilize less expensive metal catalysts and the ability to oxidize more complex fuels such as ethanol [4, 8, 9, 18]. Traditional AFCs utilize a liquid electrolyte of aqueous potassium hydroxide, however, exposure to carbon dioxide generates insoluble potassium carbonate/bicarbonate precipitates that can block active sites on the electrodes reducing performance [8, 9, 11, 18]. Recent research on alkali fuel cells has focused on development of a solid anion exchange membrane (AEM) electrolyte that would combine the engineering benefit of a solid polymer electrolyte and kinetic advantages of an alkali fuel cell. The role of water in ion conduction and AEM stability needs to be understood for practical commercialization of an AEM fuel cell. Although adequate hydroxyl conductivity has been demonstrated in AEMs under very wet conditions [31, 42, 43], conductivity rapidly diminishes at lower relative humidity, and the stability of the cations in the polymers may be an issue for long-term operation [8, 9, 18]. It is, therefore, important that anion conductivity in AEMs be understood in detail with respect to polymer morphology, water content, and cation chemistry.

Perfluorosulfonic acid (PFSA) membranes have dominated the PEM fuel cell industry due to their high proton conductivity, and sufficient chemical and mechanical stability [4, 5]. Du Pont introduced their PFSA membrane, Nafion™, in the 1970s which exhibited higher conductivity and a longer lifetime compared to earlier PEMs [3]. Today Nafion and other PFSA

membranes remain the industry standard for PEMs and the benchmark to which all new PEMs and AEMs are compared [2, 3]. The performance and stability of PFSAs, along with the vast literature available for comparison [44], has generated interest in synthesis of a perfluorinated AEM based on the same polymer architecture. There have been several studies on perfluorinated AEMs synthesized by the functionalization of a PFSA precursor with a cationic species [45-48]. The reported conductivity and cation stability varied greatly for these membranes, indicating further study is necessary to evaluate the potential for perfluorinated AEMs.

Chemical stability is a fundamental requirement for an AEM, however most common cation species used in AEMs exhibit some level of degradation in hydroxide[9]. Common cation groups used in AEMs include quaternary ammonium, quaternary phosphonium, tertiary sulfonium, and guanidinium based compounds [8]. Unfortunately, degradation is a concern for all of these cations, making production of a stable AEM difficult. The most widely used cations for AEMs are quaternary ammonium compounds, which suffer a number hydroxide degradation routes. Quaternary ammonium compounds can undergo Hoffman elimination to form an amine and an olefin, nucleophilic substitution to produce an amine and an alcohol, and elimination of hydrogen to form water and an ylide, which further reacts to form an amine and an olefin [8, 9, 17]. Some of these degradation pathways can be avoided or reduced by careful selection of cation species [9]. Degradation of quaternary ammonium cations by hydroxide has been studied for cations in solution [17, 49], but the stabilities of these cations tether to a polymer have not been fully characterized. Direct comparison of cation species effects on membrane conductivity, morphology, and stability is necessary as AEM development progresses towards practical application.

In this work we have functionalized a commercially produced perfluorinated ionomer with three different quaternary ammonium cation species to produce perfluoroquaternary ammonium (PFQA) anion exchange membranes. The three cation species reacted to different degrees resulting in a range of ion exchange capacities (IECs). These polymer membranes were evaluated as potential AEMs based on conductivity, water diffusion, water uptake (WU), and polymer morphology. Membrane conductivity, WU, and morphology all varied, to some degree, based on the cation species tethered to the polymer with the smallest methyl ammonium cation having the highest conductivity and WU. Unfortunately, all of these membranes displayed significant degradation by hydroxide and further work would be needed to produce stable cation species on a perfluorinated AEM.

3.3 Experimental

3.3.1 Materials

The sulfonyl fluoride version of the perfluorinated ionomer at 800 EW was supplied in powder form by 3M Company. All other chemicals were purchased from Sigma Aldrich and were reagent grade.

3.3.2 Synthesis and Processing

The reaction scheme to synthesize the PFQA polymer was based on the patent by Matsui [50], with modifications to the solvent to increase polymer swelling, extension of reaction times to improve conversion, and an additional washing step with triethylamine to remove an acid by-product that would have hindered the alkylation step. In a typical synthesis the dried (vacuum oven, overnight, 50°C) 3M ionomer (10 g) was first swelled in anhydrous dimethylacetamide, about 25 cm^3, decanted from molecular sieves, at a temperature of 100°C. The perfluorosulfonyl material was aminated using a 10-fold molecular excess of the diamine, consisting of a 3 carbon

24

methylene chain with a primary amine on one end and a tertiary amine on the other, such as 3-(dimethylamino)-1-proypylamine. The solvent was then removed and treated with triethylamine (15 cm^3) to completely remove the HF byproduct and the product again dried by rotovap. A 10-fold excess of alkyl iodide was then introduced to the reaction vessel to quaternize the terminal amine. The material was then dried and treated with a 5-fold excess LiCl in MeOH (25 cm^3) overnight, followed by solvent removal and drying in a vacuum oven. The final product was separated from the excess LiCl by thorough washing with water, and a final drying step to give a light brown powder. After quaternization the counter-ion associated with the cation can be changed by an ion exchange reaction. The ion exchange reaction involves soaking the material in a 1 M solution of the desired ion solution for at least 24 hours. Following the ion exchange reaction the material must be washed thoroughly with water to remove excess ions from the polymer. The overall reaction scheme followed is given in Figure 3.1 and Figure 3.2 shows the functionalized cation structures of the resulting materials. The polymers were cast into membranes from dimethylacetamide on Teflon blocks and dried under reduced pressure (200 mbar) at 70°C, to give light brown brittle films, 70 -150 μm.
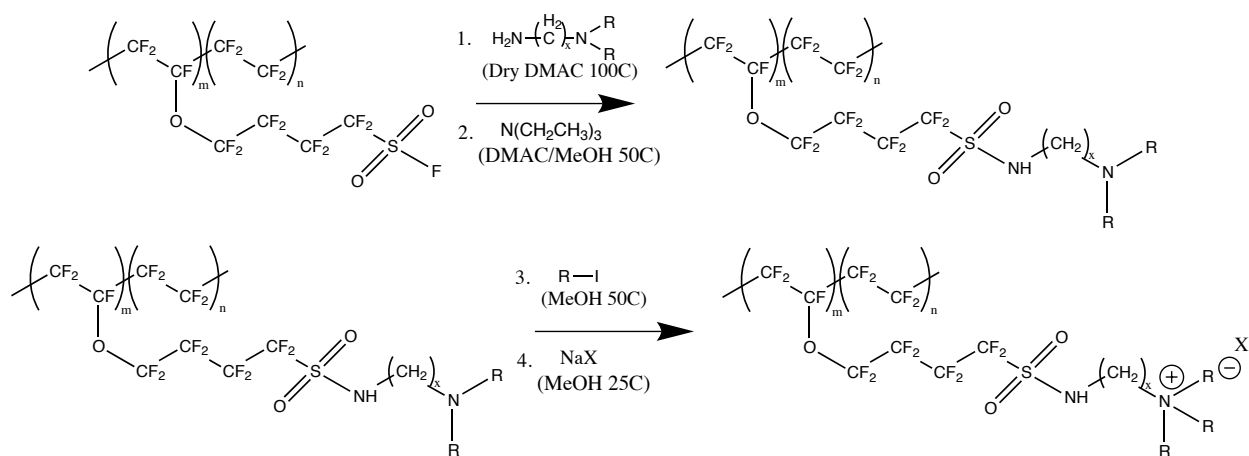
Figure 3.1: Reaction scheme for the functionalization of the 3M sulfonyl fluoride iononmer with quaternary ammonium cations.
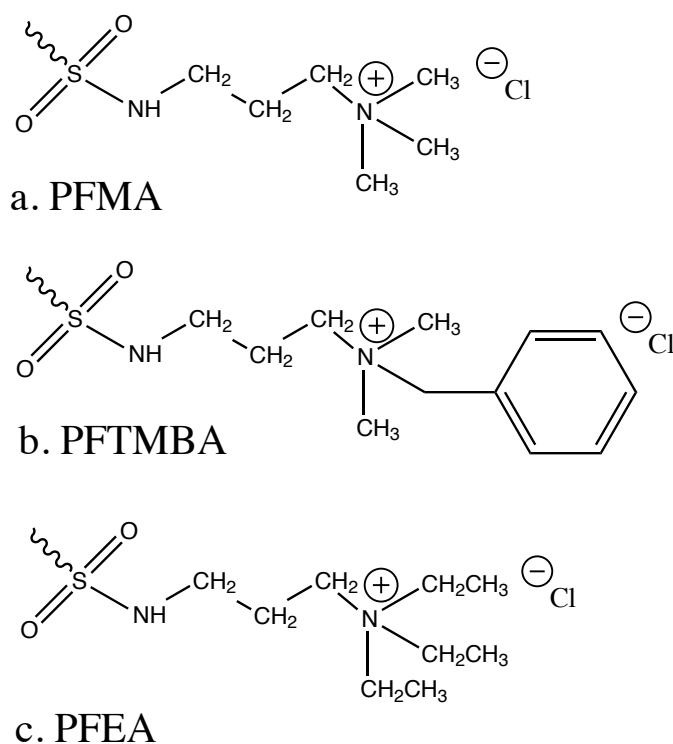
Figure 3.2: Resulting cation structures after functionalization of the sulfonyl group, the curved bond represents the sulfur attachment to the pendant chain of polymer. The resulting species are a.) methyl ammonium (PFMA), b.) trimethylbenzyl ammonium (PFTMBA), c.) ethyl ammonium (PFEA).

3.3.3 Measurements

Fourier transform infrared (FTIR) spectra were obtained on a Nicolet Nexux 470 FT-IR ESP with an attached Specac Diamond attenuated total reflectance (ATR) attachment. Typical spectrum range was 4000-500 cm^{-1} with a resolution of 4 cm^{-1} and 128 scans. The ^{1}H NMR spectrum was obtained using a Jeol ECA-500 Spectrometer at 500 MHz. Analysis of the spectra was performed using the Delta spectral software.

The ion exchange capacity (IEC) of the material was determined by titrating the chloride ions in solution after soaking chloride form membranes in 1M sodium bicarbonate solutions for 48 hours. Standardized silver nitrate solution was used to titrate the membrane solutions with a

potassium chromate indicator. The end point for the titration was defined as the point where permanent rust colored precipitates were observed in solution.

The in-plane conductivities of the membranes were calculated using electrochemical impedance spectroscopy to measure membrane resistance as given by Equation (3.1) below.

$$\sigma = \frac{l}{R \cdot w \cdot t}$$

(3.1)

Where R is the membrane resistance, l is the distance between the electrodes, w is the width of the membrane samples, and t is the thickness of the sample. Impedance spectra were obtained over a frequency range of 1 to 10^5 Hz using a four-electrode test cell connected to a BioLogic VMP3 multi-channel Potentiostat. The measurements were made in a TestEquity environmental chamber to control sample temperature and humidity. The resistance of the membrane was determined from the low frequency intercept of the Nyquist impedance plot. All samples were in the chloride form and experiments were performed at constant relative humidity of 80 or 95%RH, varying temperature from 50-90°C in 10°C steps.

Self-diffusion coefficients were measured by pulsed-field gradient nuclear magnetic resonance (PFG-NMR) spectroscopy with a stimulated echo pulse sequence. Pulse gradient NMR experimental data was analyzed using the Stejskal-Tanner-Equation[51, 52] given in Equation (3.2)

$$\frac{S}{S_0} = e^{-\gamma^2 G^2 \delta^2 \left(\Delta - \frac{\delta}{3}\right) D}$$

(3.2)

Where S and S_0 represent the signal amplitude and the signal amplitude at zero gradient, γ is the gyro magnetic ratio, G is the gradient strength, δ is the gradient pulse length, Δ is the diffusion time, and D is the apparent diffusion coefficient. Membrane samples were wound into a cylinder and suspended above saturated salt solution in a 5 mm NMR tube to generate an environment of

80% relative humidity. A pulse gradient stimulated echo sequence was performed using a Bruker AVANCEIII NMR spectrometer and 400MHz wide bore Magnex Magnet. Proton diffusion measurements were made using a 5mm Bruker single-axis DIFF60L Z-diffusion probe. The 90° pulse length was on the order of 5.0 μs. Typical parameters at 25° C were G = 0-128 G cm^{-1}, incremented in 16 steps, δ = 1 ms, Δ = 6-700 ms. The Bruker TopSpin software was used for data acquisition and analysis. Multiple diffusion experiments were performed varying the time between pulses, (Δ), between 6 and 700 ms with a constant gyromagnetic ratio (γ) of 4258 Hz G^{-1} and pulse length (δ) of 1 ms. The maximum gradient strength for each experiment was chosen to produce a full decay of the signal intensity over the length of the experiment. The decay of the signal intensity was plotted against gradient strength for each experiment and fit to Equation (3.2) to determine the diffusion coefficient.

WU was characterized using a SMS dynamic vapor sorption apparatus. A small membrane sample, about 25 mm^2, was placed on a glass weigh plate and change in mass was measured gravimetrically under different humidity conditions. Humidity was cycled between dry and saturated conditions in steps of 20%RH. The WU of the membrane was calculated based on Equation (3.3)

$$WU = \frac{m_{\%RH} - m_{dry}}{m_{dry}} \times 100$$

(3.3)

where $m_{\%RH}$ is the mass of the sample at the given relative humidity and m_{dry} is the mass of the dry sample. Given the WU at saturated conditions and the known IEC of the membrane the hydration level, λ, which is the number of waters per cation functional group can be calculated using Equation (3.4)

$$\lambda = \frac{n(H_2O)}{n(NR_4^+)} = \frac{WU}{m(H_2O) \cdot IEC}$$

(3.4)

where m(H_2O) is the molar mass of water. The mass of the membrane was monitored as a function of time while incrementally changing the relative humidity. The mass of the dry membrane was taken as the measured mass at the end of the initial 4-h drying period. The WU was calculated based on Equation (3.3) using the measured mass at the steady state of each 2-h humidity step.

Small angle X-ray scattering experiments were performed at The Basic Energy Sciences Synchrotron Radiation Center (BESSRC), beamline 12-ID-B, at the Advanced Photon Source at Argonne National Lab. Measurements were taken in a transmission geometry using a Pilatus 2M SAXS detector and a Pilatus 300K WAXS detector with an acquisition time of 1 s at a beam energy of 12 keV and incoming X-ray wavelength of 1 Å. The 2D scatter was radially integrated to obtain data of intensity versus scattering vector q. The transmission intensity was normalized to exposure time and flux of the direct beam through the sample. However, because of the swelling of the samples tested, absolute thickness and atomic density could not be determined *in-situ* and the intensity units become arbitrary. A custom built four-sample oven controlled the humidity and temperature of the samples during scattering experiments. Typical experiments contained three membrane samples and one empty window so a background spectrum could be obtained throughout the scattering experiment. The humidity of sample environment was controlled using a combination of wet and dry nitrogen. Samples were removed from water, blotted dry and mounted on the sample holders using Kapton™ tape. Samples were inserted into the oven maintained at 60°C and 95% relative humidity. The samples were allowed to take up water for 20 minutes before X-ray spectra were taken. Humidity was then stepped down to 75%, 50%, 25%, and dry gas in 15-minute steps. After the dry step was completed, the humidity was set directly to 95% relative humidity for 15 minutes to test for hysteresis of the membranes.

3.4 Results and Discussion

The synthesis of the polymer followed the reaction scheme in Figure 3.1, to produce the three polymers depicted in Figure 3.2. Characterization of the progress of the reaction and final reaction product were performed using a combination of FTIR, NMR, and chloride titration. FTIR spectra were obtained for the precursor material and following the amination and quaternization reactions, Figure 3.3. All of the aminated materials displayed new peaks
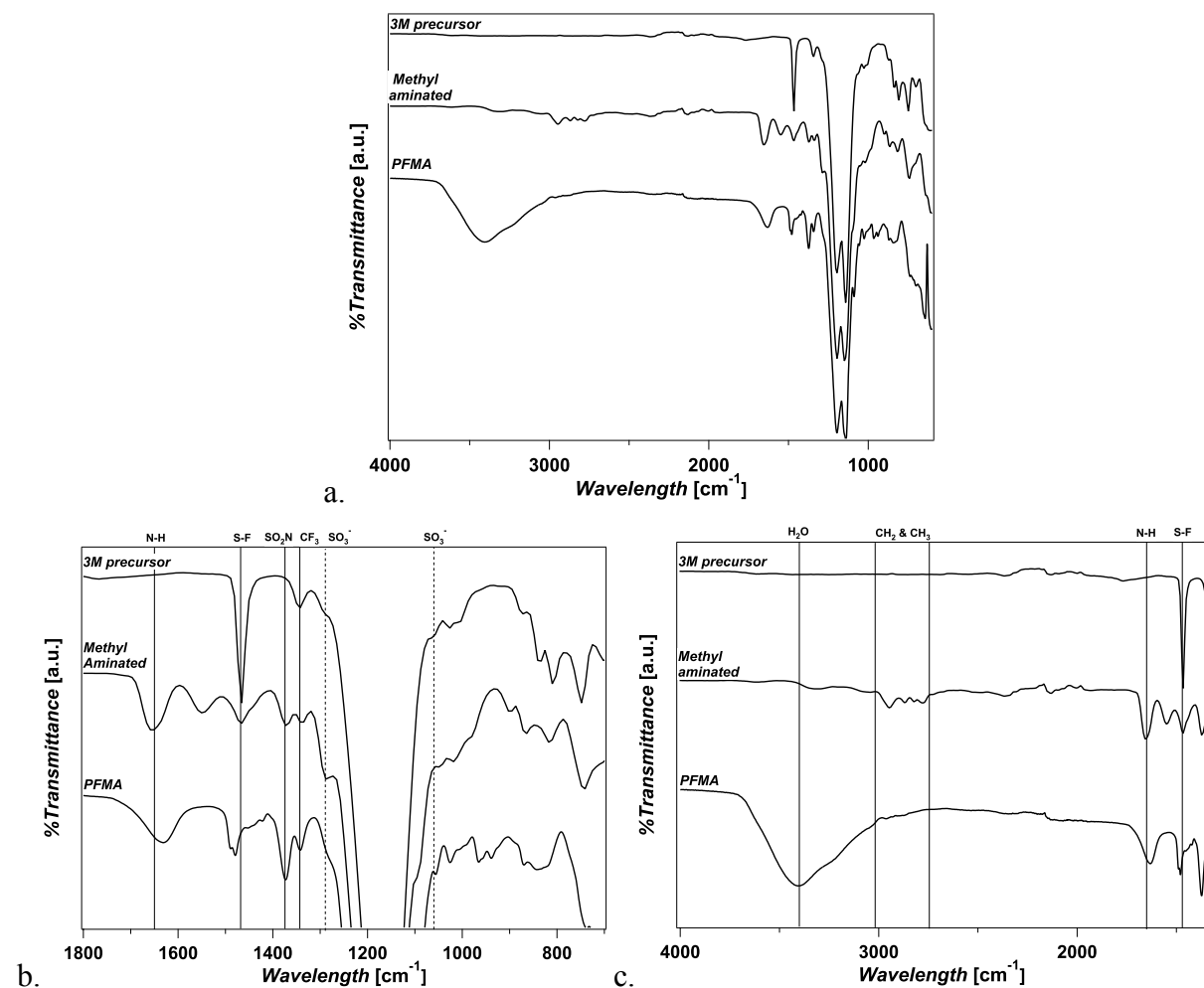
Figure 3.3: a.) Full IR spectra of the 3M sulfonyl precursor, methyl aminated polymer, and quaternized methyl ammonium polymer. b.) Magnification of the spectra to highlight the reduction of the S-F peak at 1470 cm-1, addition of the SO2N peak at 1375 cm-1 and N-H peak at 1650 cm-1, and the possible sulfonic acid peaks at 1290 and 1060 cm-1. c.) Magnification of the spectra to highlight the CH2 and CH3 peaks between 3000 and 2700 cm-1 and the broad peak between 3600 and 3000 cm-1 due to water association with the cation group.
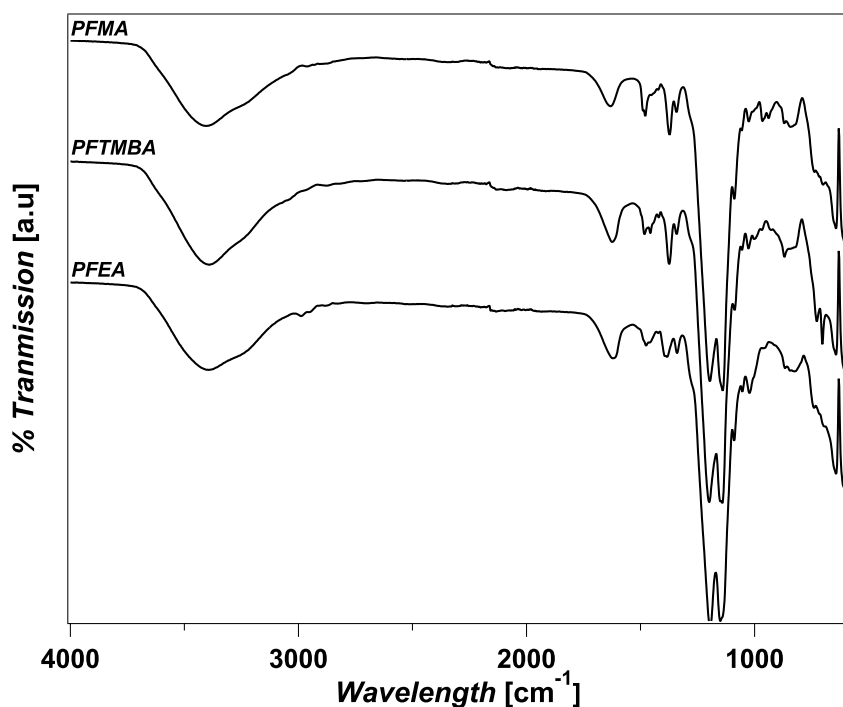
Figure 3.4: IR spectra of all PFQA polymers following the quaternization reaction step. The PFMA, PFTMBA, and PFEA all show a broad peak at 3500 cm^{-1} due to the coordination of water to the ammonium as well as the alkyl peaks from the amine.

indicating attachment of the amine to the polymer. Following the quaternization reaction all of the materials showed a broad peak at 3500 cm^{-1}. The 3M-sulfonyl precursor material showed broad absorbance peaks between 1300 and 1100 cm^{-1} corresponding to the C-F bonds along the backbone and side chain. All spectra were normalized to the high intensity peak at 1200 cm^{-1} owing to the stability of the C-F backbone throughout the reaction. The precursor material also showed a distinct peak at 1470 cm^{-1} that is associated with S-F motion [53] or the asymmetric stretch of the SO_2F group [47]. This peak is drastically reduced upon amination where the S-F bond is replaced by an S-N bond. The S-N bond produces new peak at 1375 cm^{-1} [54]. The peak at 1470 cm^{-1} was not reduced completely suggesting incomplete reaction of the sulfonyl groups. The unreacted sulfonyl groups can hydrolyze to sulfonic acid upon exposure to water, which would produce distinct new peaks at 1290 and 1060 cm^{-1} [55]. However the regions at 1290 and

31

1060 cm^{-1} display only low absorbance shoulders similar to the precursor spectra suggesting conversion to sulfonic acid was very minor. The attachment of the diamine to the sulfonyl produces new peaks at 1650 cm^{-1} corresponding the to N-H bond and 3000 and 2700 cm^{-1} corresponding to the C-H bonds of the alkyl groups of the diamine. Figure 3.4 shows the spectra of all perfluorinated polymers following the quaternization reaction step. A broad peak between 3600 and 3000 cm^{-1} is present after the alkylation reaction due to the O-H bond of water coordinating with the newly formed quaternary ammonium cation group. There is little difference between the FTIR of the quaternized polymers owing to their similar chemical compositions.

^{1}H NMR experiments were performed on the methyl and trimethylbenzyl ammonium samples to confirm the chemical attachment and structure of the quaternized polymer species. The ethyl ammonium polymer did not adequately dissolve in any common NMR solvents preventing ^{1}H NMR characterization. All materials were thoroughly washed to remove residual salts following the LiCl ion exchange treatment and dried overnight in a vacuum oven before NMR sample preparation. The ^{1}H NMR spectra for the methyl and trimethylbenzyl ammonium polymers showed peaks representing the alkyl chain of the amine and quaternary ammonium groups, however the spectra had additional peaks that were not easy identified. In the ^{1}H NMR, Figure 3.5, the methylene protons are assigned to the protons at 1.1, 2.15 and 2.4 ppm and the methyl of the quaternary ammonium at 2.6 ppm. The proton on the sulfonamide is tentatively assigned to the shoulder at 3.0 ppm. Three additional peaks marked with asterisks in the figure were observed. From separate experiments it was shown that the reaction of the diamine with alkyl iodide produced a white salt that was insoluble in water and common organic solvents. Tentatively we assign these peaks to the fully quaternized diamine, which would now be

symmetrical giving rise to methylene peaks at 0.2, and 1.0 ppm and the methyl's of the quaternary ammonium at 2.5 ppm. It is suspected that excess diamine was preserved in the polymer and quaternized during alkylation or that the diamine detached during the quaternization reaction and was further alkylated producing the insoluble salt that is responsible for the additional proton peaks in the ^{1}H NMR spectra. Further evidence for this was shown in the ^{1}H NMR of the trimethylbenzyl polymer where the dication co-product is now not symmetrical resulting in a complex ^{1}H NMR spectrum (data not shown).
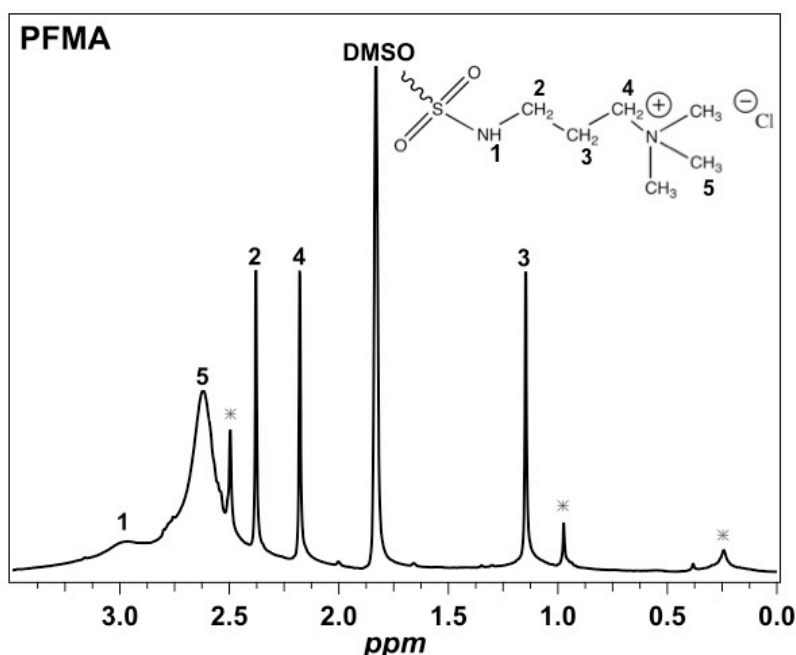
Figure 3.5: ^{1}H NMR spectra of the PFMA polymer. The peaks identified as the alkyl and ammonium hydrogen's are shown on corresponding chemical structure. Unidentified peaks, thought to be a result of insoluble diamine salts, are labeled with a star.

One objective of this study was to study the anionic transport of this material in the hydroxide form. However, several experiments clearly proved that the cationic linkage chemistry was not sufficiently stable for this characterization. In a standard acid/base titration to determine membrane IEC, in which the membranes were treated with sodium hydroxide in the first step, the calculated IECs were exceedingly low, three orders of magnitude lower than when a chloride

ion titration was performed (see below). The extremely low IEC values calculated from the acid/base titration suggested that the membranes were not stable in hydroxide solution and resulted in the loss of cation groups. An attempt was also made to measure the ionic conductivity of the PFQA membrane in the hydroxide form using a modified BekkTech cell that allowed *in-situ* hydroxide exchange, followed by thorough washing, and measurement with rigorous exclusion of carbon dioxide. During this test the membrane conductivity steadily decreased with time, again suggesting chemical degradation by hydroxide. Membranes exposed to hydroxide and later exchanged back to the chloride form produced much lower conductivities than pristine membrane samples confirming that hydroxide irreversibly altered membrane chemistry. There is evidence in literature that ammonium [48] and guanidinium [56] cations attached directly to the side chain of a perfluorinated polymer are unstable in hydroxide. In order to understand the relationship of anion conductivity to cation size and polymer morphology, all characterization and testing were performed on the polymers in the chloride form to ensure that the data was not biased by the instability of the polymer in the hydroxide form.

Table 3.1: Summary of the IEC, conductivity and corresponding activation energy, water uptake, and diffusion coefficient for PFQA polymer membranes. The conductivity and water uptake are for saturated conditions at 60°C. The diffusion coefficient was measured at 80%RH and 25°C.

Material	IEC (meq g^{-1})	σ (mS cm^{-1})	Ea (kJ mol^{-1})	WU (%)	λ	D (cm^2 s^{-1})
PFMA	0.72±0.02	4.8±0.1	36±5	8.0±0.2	6.2±0.2	1.6×10^{-5}
PFTMBA	0.52±0.02	3.3±0.2	59±5	7.1±0.1	7.6±0.3	-
PFEA	0.33±0.01	0.6±0.5	50±14	6.6±0.1	11.0±0.4	-

The extent of quaternization, reflected by the IEC (Table 3.1) had a significant effect on polymer performance as will be shown in the characterization of the materials. The methyl ammonium material quaternized to the fullest extent giving it the highest IEC, 0.72 meq g^{-1}, the maximum theoretical IEC being about 1.0 meq g^{-1}. The trimethylbenzyl ammonium and ethyl ammonium materials had IEC values of 0.52 and 0.33 meq g^{-1} respectively. The lower IECs of

the larger cations were a result of the steric hindrance of the larger alkyl groups on the amine and larger alkylating group that restricted quaternization of the amine.

Ionic conductivity of the quaternized species was performed using electrochemical impedance spectroscopy at temperatures of 50 - 90°C and constant RH. This experimental method allowed calculation of the energy of activation (E_a) for ion conduction in the material by an Arrhenius relation (Table 3.1). Figure 3.6 shows the conductivity for all polymer samples at 80% and 95% relative humidity. The conductivity increased for all polymer samples with increased temperature and humidity. The conductivity was highest for the methyl ammonium
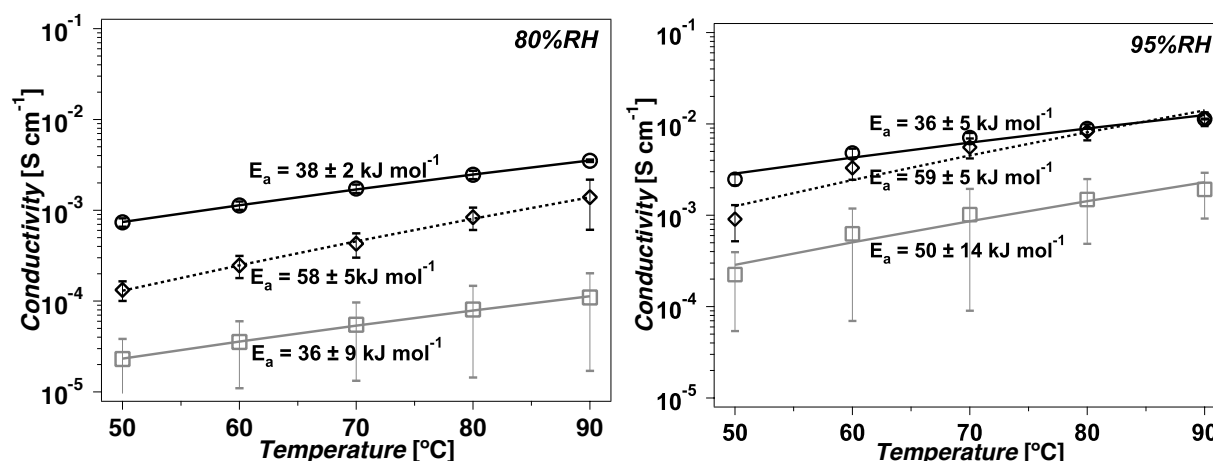
Figure 3.6: Conductivity of PFMA (circle), PFTMBA (diamond), PFEA (square) at a.) 80%RH and b.) 95%RH vs. temperature. The markers represent the experimental data and the lines represent the Arrhenius fit used to calculate activation energy.

polymer, followed by the trimethylbenzyl and ethyl ammonium. Conductivity increased with increasing ion exchange capacity at both humidities (Figure 3.7). The activation energies calculated for the PFQA materials ranged from 35-60 kJ mol^{-1} (Table 3.1). These activation energies are very high compared to reported the activation energies for Nafion™ that range from 5-20 kJ mol^{-1} [57, 58] and those for other anion exchange membrane, 10-25 kJ mol^{-1} [43, 58]. The high activation energies for the PFQA membranes, even at high humidities, may suggest the

percolation network generated in hydrated PFSA [44, 59, 60] membranes does not extend fully for the anion exchange membranes tested.
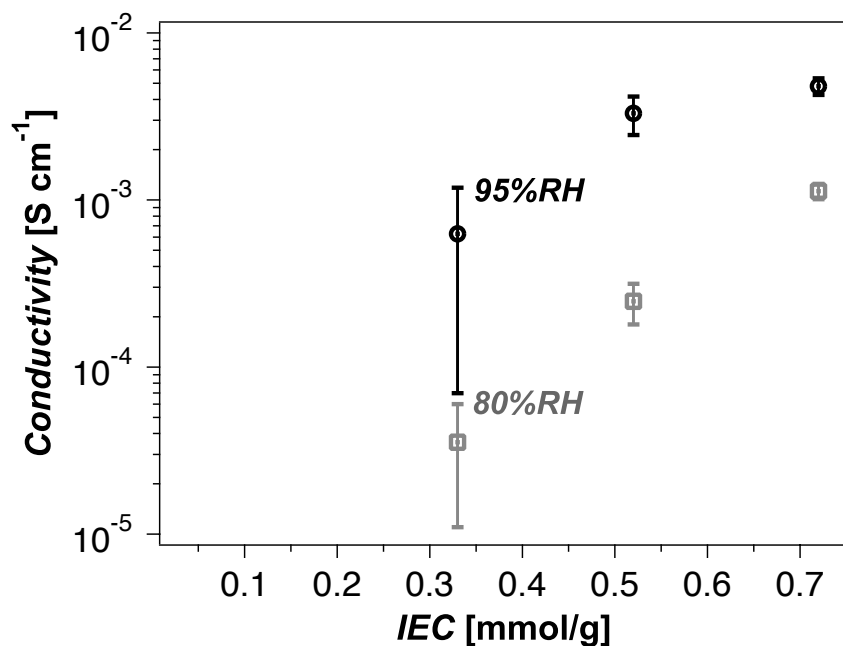
Figure 3.7: Conductivity as a function of ion exchange capacity, all measurements are at 60°C, the data sets are for 80%RH and 95%RH.

PFG-NMR was performed on the methyl ammonium polymer to determine the diffusion of water through the membrane. The calculated diffusion coefficient was plotted vs. the time between gradient pulses, (Δ), to evaluate the restriction of diffusion in the membrane along different length scales (Figure 3.8). The calculated diffusion coefficient decreased as the time between gradient pulses was increased indicating restriction to diffusion in the membrane. By regression of the diffusion coefficient to a Δ of zero the free diffusion coefficient D_0 was determined to be 2.5×10^{-5} cm^2 s^{-1} which is slightly larger than the free diffusion coefficient of liquid water [61, 62], suggesting this data overestimates the free diffusion coefficient of water in the membrane. The bulk, or infinite, diffusion coefficient is taken as the diffusion coefficient at the largest Δ and was equal to 1.6×10^{-5} cm^2 s^{-1}. These values are relatively high compared to diffusion coefficients reported for Nafion™ which are generally $<1 \times 10^{-5}$ cm^2 s^{-1} [63-66]. The

36

high diffusion through the membrane may indicate a different long range ordering in the quaternary ammonium membranes compared to PFSA membranes. The relatively low ionic conductivity observed in the PFQA membranes compared to the high diffusion suggests the ionic transport mechanism is different from the water transport mechanism for the membrane in the chloride form.
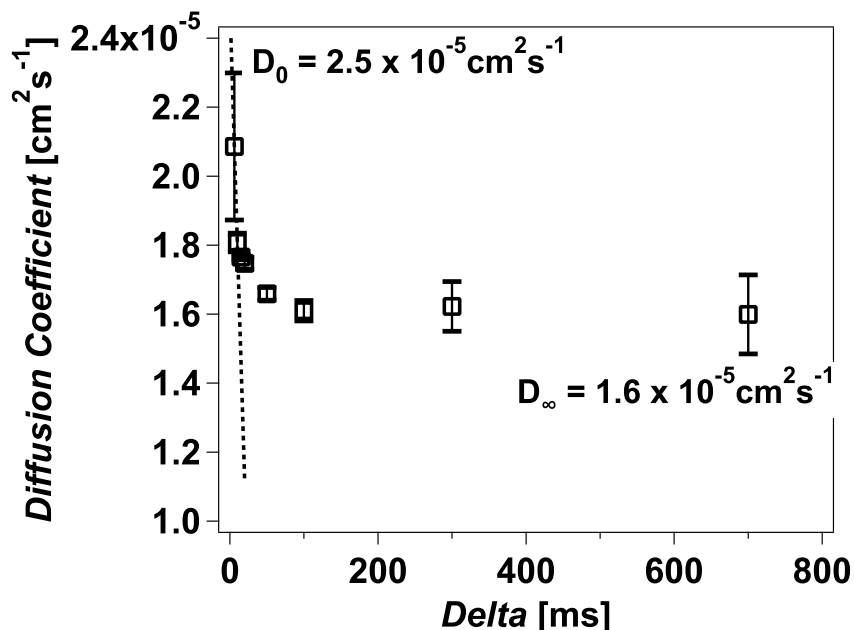
Figure 3.8: Calculated self diffusion coefficient of water through the methyl ammonium membrane at different Δ values, the time between the gradient pulses.

WU in the membrane was measured gravimetrically in a dynamic vapor sorption apparatus (Figure 3.9). WU was greatest for the methyl ammonium material with a maximum water uptake of about 8 wt%, followed closely the trimethylbenzyl and ethyl ammonium polymers. This level of WU is significantly lower than that of PFSA membranes. The trend of water uptake values corresponds with the IECs and performance of the membranes in conductivity experiments, however, the difference in water uptakes is less than expected given the significant difference in IECs. The hydration level (Figure 3.10) has a reverse trend from the water uptake measurements. The ethyl ammonium material showed the largest number of

37
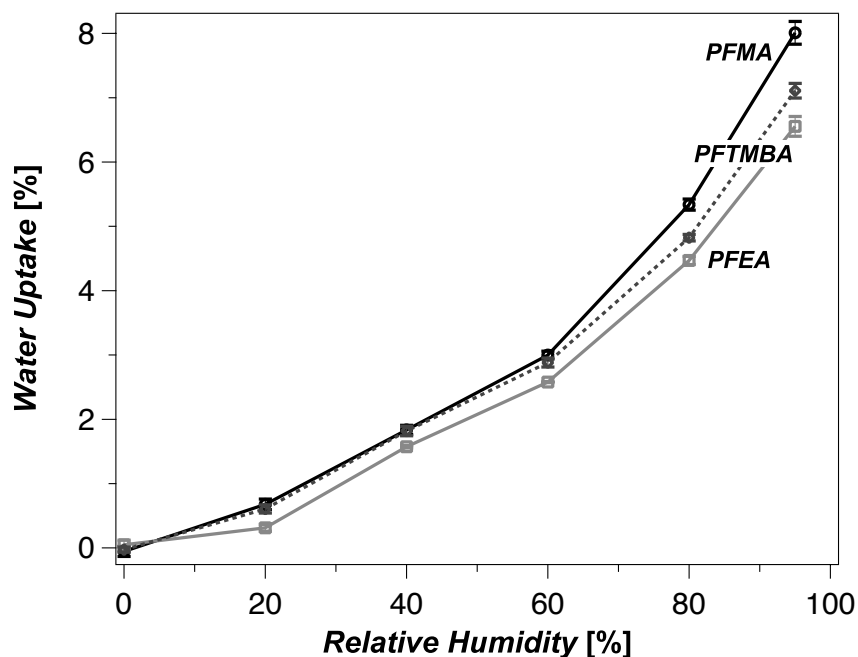
Figure 3.9: Water uptake for PFQA membranes at relative humidities between 0-95%RH, lines are just for clarity.
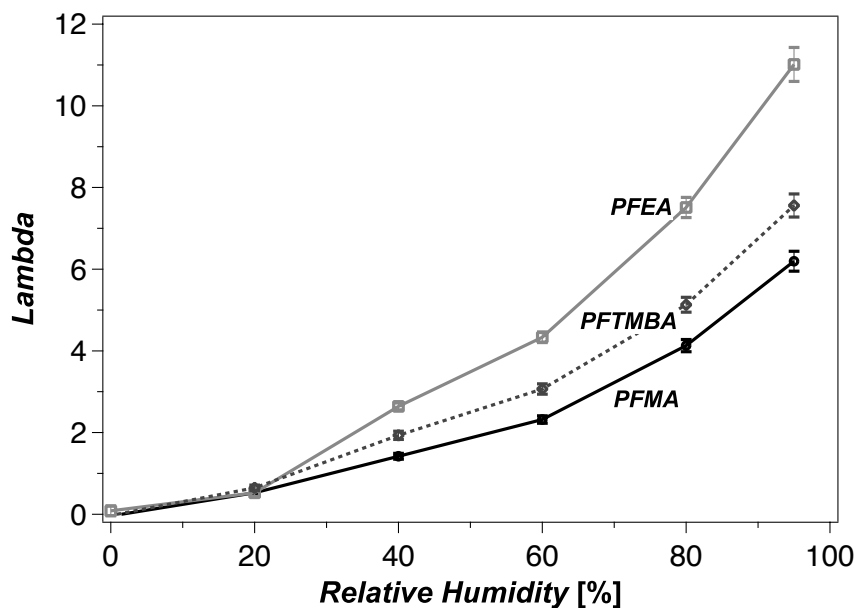
Figure 3.10: Hydration level of the PFQA membranes at relative humidities from 0-95%RH, lines are just for clarity.

coordinating waters, $\lambda = 11$ at 95%RH, followed by the trimethylbenzyl and methyl ammonium

materials, $\lambda = 8$ and 6 respectively. The similar water uptake but different hydration levels based

on cation suggest the solvation structures of the cations are different.

38

Morphology and membrane swelling were characterized using small angle X-ray scattering. The dominant feature of the SAXS spectra for the PFQA materials is a peak around 0.15 Å-1 (Figure 3.11). This feature is similar to the "ionomer peak" of PFSA materials that corresponds to the ionic aggregates of the polymer where water will be contained for swollen membranes [59, 60, 67]. This peak in the PFQA materials is larger for the dry membranes about 40 Å, compared to PFSA materials about 30 Å [37, 68]. The peak shifts to lower q as the humidity is increased due to the expansion of the ionic domain with water. Membrane swelling of the ionic region did not depend on cation species with all membranes having a 4 - 5 Å increase of the ionic region from a dry to humidified state (Figure 3.12). The increase in size of the ionic region in the PFQAs is low compared to PFSAs, which generally have a 10 - 15 Å increase in size from a dry to humidified state [37, 68]. The lower swelling of the PFQA membrane is expected given the low water uptake of these membranes. Although all the samples
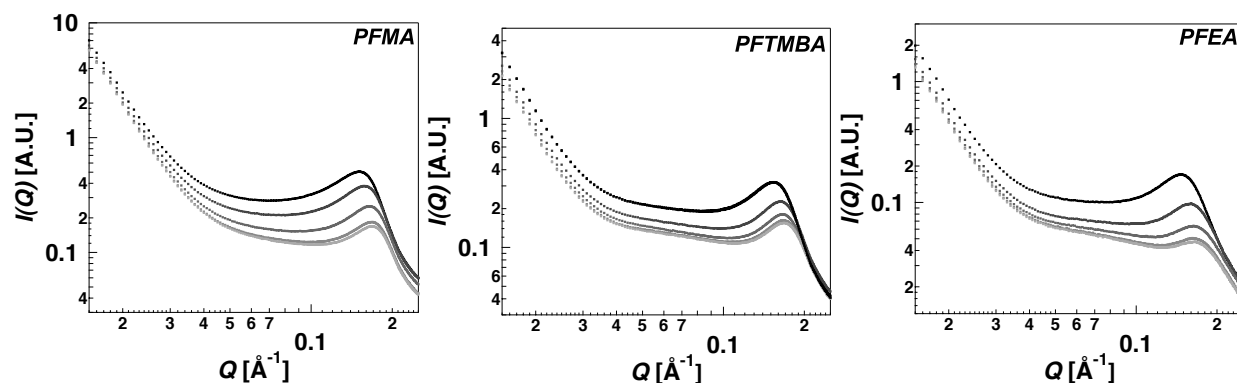
Figure 3.11: SAXS spectra for the PFQA membranes, a.) PFMA, b.) PFTMBA, c.)PFEA, the black data represent the humidified membranes at 95%RH with the colors getting lighter as humidity is decreased to 75%, 50%, 25% and finally 0%RH as the lightest grey data.

showed a slight shift in peak position, the shape and features of this region remained constant indicating no major structural reorganization of the ionic aggregates; this could contribute to the low ionic conductivity of the PFQA membranes. The position of the SAXS spectra upturn

between 0.03 - 0.04 Å-1 differed with respect to the functionalized cation species and suggested different long polymer ordering in the membranes with cation species (Figure 3.12).
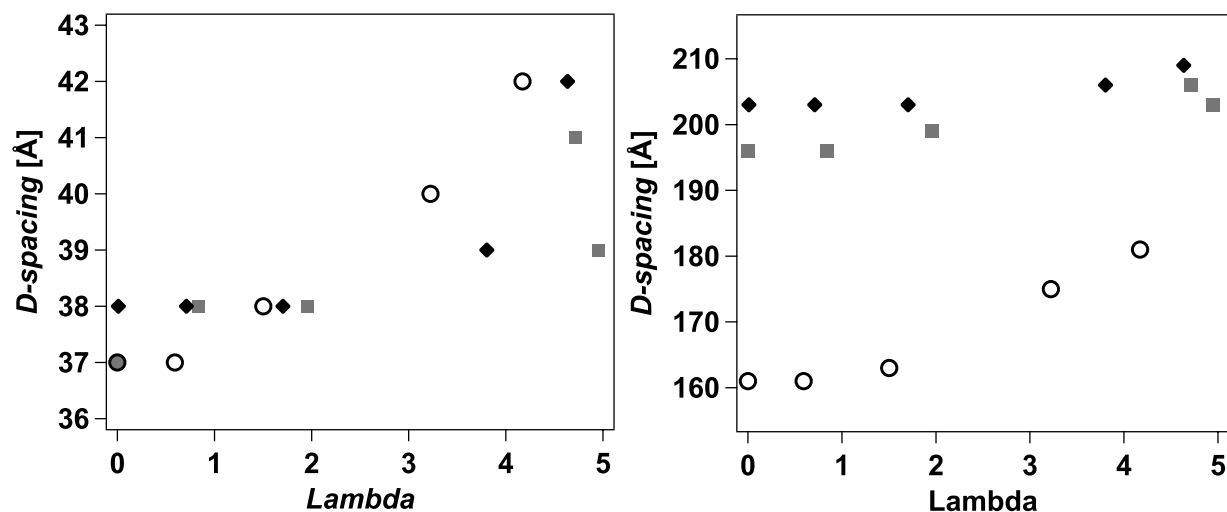
Figure 3.12: D-spacing of the a.) ionomer peak and b.) SAXS upturn with respect to the hydration level of the membranes at the different humidities evaluated during the SAXS experiments. PFMA (circle), PFTMBA (diamond), PFEA (square).

3.5 Conclusions

In this work, a perfluorinated polymer was functionalized with different quaternary ammonium cation species and the resultant PFQAs evaluated as potential AEMs. Acid-base titration and conductivity in the hydroxide form indicated all polymers suffered chemical degradation by hydroxide, eliminating the cation species from the polymer. Although reaction conditions were maintained constant for all polymers, the degree of functionalization varied with cation species resulting in different ion exchange capacities. Larger cation species had lower degrees of quaternization owing to steric hindrance during the alkylation reaction, highlighting the need to consider cation species and synthetic route during AEM development. Conductivity was shown to be highly dependent on cation species and IEC, and the activation energy for ion conduction was relatively high compared to PFSAs and other AEMs. The smallest cation species, methyl ammonium, reacted to the fullest and had the highest conductivity so it was the focus of

additional study. Diffusion of water through the methyl ammonium membrane showed restriction over different diffusion times. Overall, the fast diffusion of water in the membrane may indicate the water transport mechanism is different than the ionic conduction mechanism for the PFQA systems in the chloride form. WU was generally low for the PFQA materials and hydration level varied based on cation species suggesting different solvation structures. Small-angle scattering experiments suggested ionic aggregation in PFQA materials similar to PFSA membranes that did not depend on the cation species, but other SAXS features suggested slight differences in long-range order with cation species. The significant differences in membrane conductivity, WU, and morphology based on functionalized cation species highlights the importance of considering cation species when developing an AEM. The PFQA membranes suffered significant degradation from hydroxide signifying the need for development of more stable cation species and chemical linkage to the polymer before a perfluorinated AEM could be commercialized. Future study will focus on developing a different chemical attachment of the cation to the sulfonyl group and different cation species to improve polymer stability.

3.6 Acknowledgements

CHAPTER 4 : MECHANICAL CHARACTERIZATION OF ANION EXCHANGE MEMBRANES BY EXTENSIONAL RHEOLOGY UNDER CONTROLLED HYDRATION

This chapter is modified from a paper published in

Journal of The Electrochemical Society[9]

Melissa A. Vandiver[10], Benjamin R. Caire[11], Jordan R. Carver[12], Krysta Waldrop[13],

Michael R. Hibbs[14], John R. Varcoe,[15] Andrew M. Herring[16], and Matthew W. Liberatore[17]

4.1 Abstract

Alkali anion exchange membrane (AEM) based devices have the potential for electrochemical energy conversion using inexpensive catalysts and a variety of fuel types. Membrane stability and anion transport must be improved in AEMs before these devices can be fully realized. Mechanical failure of the membrane can contribute to failure of the device, thus membrane durability is critical to overall system design. Here, a study of the mechanical properties of three well-established AEMs uses a modified extensional rheometer platform to simulate tensile testing using small membrane samples. Mechanical properties were tested at 30 and 60°C under dry or water saturated gas conditions. Water in the membrane has a plasticizing effect, softening the membrane and reducing strength. PEEK membrane reinforcement limits swelling producing negligible softening and only a 9% decrease in strength from dry to hydrated conditions at 30°C. Higher cation concentration increases water uptake resulting in significant

softening, a 57% reduction in Young's modulus, and a 67% reduction in strength when hydrated at 30°C. In a working electrochemical device, AEMs must maintain integrity over a range of temperatures and hydrations, making it critical to considering mechanical properties when designing new membranes.

4.2 Introduction

Polymer electrolyte membrane fuel cells and electrolyzers are potentially disruptive technologies that will replace traditional heat engines such as internal combustion engines for transportation applications, portable electronics, and are scalable to larger energy storage facilities. Polymer electrolyte membrane fuel cells are suitable for transportation applications due to their low temperature start-up and operation, high power density, and quick refueling [3, 6, 69]. Proton exchange membranes (PEMs) have dominated polymer electrolyte membrane fuel cell development in the last several decades, resulting in the development of relatively stable, well performing membranes [3, 6, 19, 69]. Current PEM fuel cells remain cost prohibitive due to high catalysts costs, as well as long-term durability issues [2, 6, 7]. Anion exchange membranes (AEMs) can also be utilized in polymer electrolyte membrane devices and have several potential benefits over PEMs. AEM fuel cells benefit from increased kinetics in an alkali media allowing more complex fuels then hydrogen and have the potential to utilize non-platinum catalysts to reduce costs [8, 9, 11, 18, 70]. However, a number of challenges must be overcome before AEMs reach the performance and durability necessary for fuel cells and other electrochemical energy conversion devices. Hydroxide present in the AEM degrades many of the proposed cationic groups and some polymer backbones, making development of chemically stable AEMs difficult [8, 17, 70]. Additionally, transport of hydroxide in AEMs is inherently slower than protons in PEMs [15], to compensate, the concentration of ionic groups is often increased in

AEMs [9]. Increasing ion concentration in AEMs increases water sorption in the polymer and can result in significant dimensional swelling, which can alter the mechanical integrity of the membrane. Thus, simultaneous studies of ionic transport, water sorption, and mechanical durability are necessary to develop an optimized AEM. Research efforts primarily focus on improving ionic transport and water sorption, while mechanical stability of AEMs is often a secondary consideration. The lower transport efficiency of AEMs makes thin membranes critical to minimize area specific resistance, however, maintaining mechanical integrity of thin membranes is difficult [18]. Considering mechanical properties of new AEMs and tailoring membrane design towards robust, thin films is critical for the realization of AEM energy conversion devices in the future.

Fuel cell lifetime is often determined by the ability of the membrane to resist mechanical degradation.[6, 7, 27, 71, 72] Mechanical degradation of the membrane occurs through a combination of physical and chemical stresses present in the fuel cell [26]. A working fuel cell has a dynamic temperature and humidity environment resulting in changes in membrane hydration. Sorption and desorption of water can produce significant swelling and hygrothermal stresses in the membrane [6, 7, 26]. As the membrane is constrained in the membrane electrode assembly (MEA), dimensional swelling of the membrane results in stresses on the assembly and membrane. The hygrothermal stresses experienced by the membrane due to swelling and contraction can lead to pinhole and crack formation [27]. These defects weaken the membrane, leading to mechanical failure, and allowing crossover in electrochemical energy conversion devices. Crossover results in radical formation that can further degrade the membrane chemically [26]. Decoupling the effects of chemical and mechanical degradation is difficult in *in-situ* fuel cell tests, particularly over the short time-span of traditional testing, making it critical to develop

44

ex-situ, accelerated test methods to gauge mechanical degradation. Thorough studies have been performed on the mechanical strength, durability, and failure mechanisms of PEMs [6, 7, 25], and this information can be used to guide AEM development and testing. *Ex-situ* durability tests to gauge membrane lifetime of PEMs include rapid humidity cycling while monitoring gas crossover [28], pressurized blister tests [29], and mechanical fatigue testing by dynamic mechanical analysis [71]. These tests have been shown to accurately predict relative membrane lifetimes. Traditional tensile tests are a less accurate predictor of membrane lifetime in a fuel cell, but remain the standard characterization for comparing mechanical properties of polymer films [3, 6, 69]. Additionally, measurement of tensile properties at a range of temperature and humidity conditions is an important screening tool to gauge membrane potential as membranes become brittle and fragile at low hydrations [3, 6, 7, 19, 69].

Increasing durability of the polymer membrane is necessary for application in fuel cells [2, 6, 7, 18, 70], particularly in AEMs where thinner films are needed. A number of design factors can influence membrane strength and durability. Polymer chemistry is responsible for the basic mechanical properties of the membrane [8, 9, 11, 18, 70]. Block copolymer AEMs offer the opportunity to tailor mechanical properties by selecting the polymer chemistry of the hydrophobic block to tune desired properties. Since a chemically stable AEM with sufficient durability is not commercially available, many polymer chemistries are under investigation, and screening these polymers for mechanical properties will lead to the development of durable membranes. PEM research has shown that a higher degree of crystallinity can improve mechanical properties [8, 17, 19, 70]. Increasing polymer crystallinity can be achieved by altering polymer chemistry, such as reducing the side chain length in perfluorosulfonic acid (PFSA) PEMs [15, 20], or through various annealing techniques. Crosslinking is another

common technique to improve membrane strength [9, 19, 22]. Chemically crosslinking polymer chains increases the modulus and strength, however the method of crosslinking may reduce the ionic concentration and a high degree of crosslinking may cause membrane embrittlement. Physical reinforcement of membranes with a nonconductive, porous polymer film can also significantly improve durability, as long as it is also chemically stable to hydroxide [18, 23]. Porous polytetrafluoroethylene (PTFE) membranes and fibers have been incorporated into PFSAs to improve mechanical durability [6, 7, 19, 24, 27, 71, 72]. Reinforcing an ion exchange membrane also helps resist dimensional swelling, increasing stability between dry and hydrated states and prolonging membrane lifetime [7, 26, 72]. While physical reinforcement can strengthen the membrane and resist changes with hydration, the addition of a nonconductive material lowers the ion exchange capacity of the membrane. While a number of design factors can impact the mechanical durability of an AEM, consideration of these factors early in AEM research is important to develop satisfactory fuel cell membranes.

The mechanical behaviors of Nafion[®] and similar PFSAs have been studied in detail at a wide range of temperature and humidity conditions [6, 7, 25, 26, 73]. However, because AEM development is still preliminary, basic mechanical testing is not standardized and comparing mechanical properties of AEMs is difficult. In this study, the extensional properties of three well-studied AEMs were investigated under different temperature and humidity conditions. The AEMs used in this study are the industrially produced polyetheretherketone (PEEK) reinforced Fumasep[®] FAA-PEEK membrane from Fumatech [27, 74], an aminated tetramethyl polyphenylene (ATMPP) developed at Sandia National Laboratory [26, 31, 75, 76], and a radiation grafted poly(ethylene-co-tetrafluoroethylene)-based quaternary ammonium AEM developed at the University of Surrey [6, 7, 25, 42, 77]. The three membranes were chosen as

46

they have all been produced consistently in multi-gram quantities, the first under industrial quality control standards, the second in large research batches over multiple years, and the third from an industrially produced precursor film. This study compares the mechanical properties of these AEMs at a range of temperature and humidity conditions using a modified extensional rheometer system to simulate traditional tensile tests, and relates these properties to water uptake and swelling of the membranes.

4.3 Experimental

4.3.1 Materials

Three AEM membranes were tested: Fumasep® FAA-PEEK (Fumatech), an aminated tetramethyl polyphenylene (ATMPP) with benzyltrimethylammonium functionalities, and a poly(ethylene-co-tetrafluoroethylene) membrane radiation grafted with poly(vinylbenzyl trimethylammonium) groups (ETFE-g-PVBTMA) The Fumasep® FAA-PEEK membrane is a PEEK reinforced anion exchange membrane with a dry thickness of 110 μm and an IEC of 1.5 mmol/g. The chemistry of Fumasep FAA-PEEK was not disclosed, but literature has suggested a polysulfone or perfluorinated backbone with quaternary ammonium functionalities [28, 78, 79]. The Fumasep® membrane was in a dry state in the Cl⁻ form and was tested as received. The ATMPP membrane was fabricated as previously reported by Hibbs [29, 31, 75]. The ATMPP membrane had a dry thickness of 80 μm and an IEC of 2.5 mmol/g. The ATMPP membrane was received in the Br⁻ form and stored in liquid water. The ATMPP membrane was dried at ambient conditions prior to mechanical testing. Membranes were tested in their as-received counter-ion form to be comparable to literature, however additional mechanical testing of the ATMPP in the Cl⁻ form was performed for consistency and to guarantee counter-ion association did not significantly change mechanical properties. The ETFE-g-PVBTMA membrane was fabricated as

47

previous described by the University of Surrey group [42, 71, 77]. The ETFE-g-PVBTMA had a dry thickness of 80 μm and an IEC of 1.8 mmol/g. The membrane was received in a dry state in the Cl⁻ form and tested without further treatment.

a.   b.
Figure 4.1: Chemical structures of the a) ATMPP and b) ETFE-g-PVBTMA polymers.
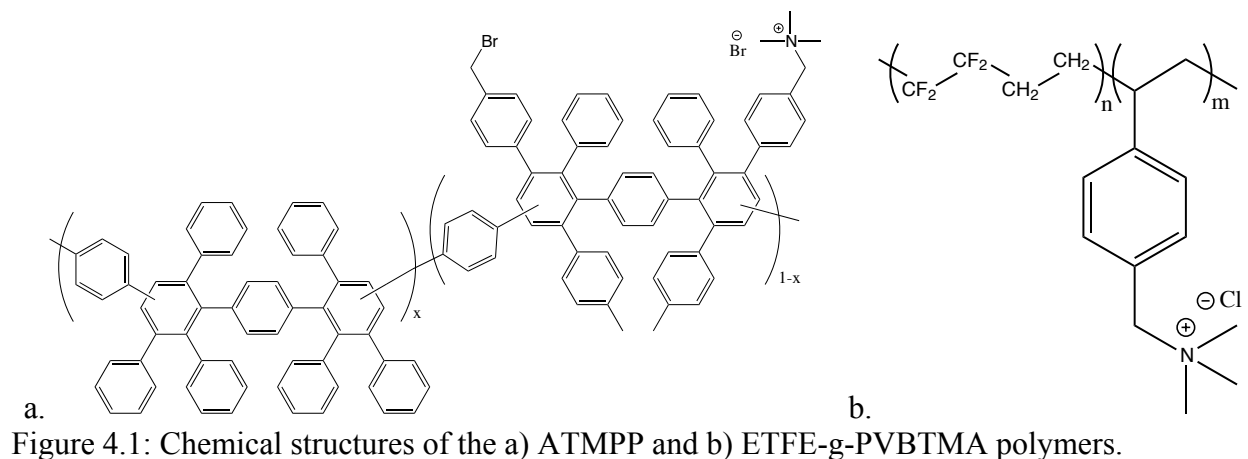
4.3.2 Water Uptake

Water uptake and saturation equilibration times were determined using a dynamic vapor sorption apparatus (SMS DVS Advantage 1). The mass of a membrane sample, about 4 mm^2, was measured gravimetrically under different humidity conditions. The water uptake (WU) of the membrane was calculated based on Equation (4.1)

$$WU = \frac{m_{\%RH} - m_{dry}}{m_{dry}} \times 100 \qquad\qquad (4.1)$$

where $m_{\%RH}$ is the mass of the sample at the given relative humidity and m_{dry} is the mass of the dry sample. The mass of the dry membrane was taken as the measured mass at the end of an initial three-hour drying period. Given the water uptake at saturated conditions and the known ion exchange capacity of the membrane, the hydration level, λ, which is the number of waters per cation functional group, can be calculated using Equation (4.2)

$$\lambda = \frac{WU}{m(H_2O) \cdot IEC} \qquad\qquad (4.2)$$

where $m(H_2O)$ is the molar mass of water.

48

4.3.3 Dimensional Swelling

Dimensional swelling of the AEM films with water was calculated by measuring film area and thickness dried at ambient conditions compared to films soaked in water at room temperature for two days. In-plane length and width measurements were made using a Marathon electronic digital caliper (0 − 150 mm, with 0.01 mm accuracy) and through-plane thickness measurements were made using a Marathon electronic digital micrometer (0 − 25 mm, with 0.002 mm accuracy). Wet membranes were removed from water and blotted to remove surface water; measurements were made as quickly as possible to prevent drying. Swelling was calculated with respect to the percent change of in-plane area and through-plane thickness of the film.

4.3.4 Conductivity

Ionic conductivity was calculated by measuring membrane resistance with electrochemical impedance spectroscopy. Impedance spectra were obtained over a frequency range of 1 to 10^6 Hz using a four-electrode test cell and multi-channel potentiostat (BioLogic VMP3, Knoxville, TN). The membrane resistance was defined as the low frequency intercept of the Nyquist impedance plot and used to calculate conductivity based on Equation (4.3)

$$\sigma = \frac{l}{R \cdot t \cdot w} \qquad\qquad (\,4.3\,)$$

where R is membrane resistance, l is the length between electrodes, and t and w are the membrane thickness and width respectively. The test cells were kept in a controlled environment (TestEquity Model 1007H, Moorpark, CA) to maintain relative humidity and temperature.

4.3.5 Tensile Tests

Mechanical tests were performed using a Sentmanat Extensional Rheometer (SER) fixture[38] (Xpansion Instruments) on an ARES G2 rheometer platform (TA Instruments). The

SER fixture suspends the membrane across two counter rotating drums. The rheometer controls the rotation of the drums, which stretch the sample to failure. The stress on the membrane sample is measured by the rheometer during film extension. The SER fixture is generally used to measure the elongation viscosity of polymers in their melt state, but has been shown to accurately measure tensile properties in the solid state [38]. The stress vs. strain data is used to determine the elastic modulus, ultimate strength, and elongation of the film. The modulus is defined as the slope of the stress vs. strain curve in the initial liner region that corresponds to elastic deformation. The engineering stress at break is defined as the stress measured immediately prior to break, based on the initial film dimensions. The elongation of the membrane is the percent increase in film length as determined by the strain at break.

Polymer films were cut into strips of 25 mm(L) x 3 mm(W), about 5 – 10 mg, for testing. The SER drums were wrapped in double-sided high temperature tape to prevent slipping of the films. Silicon coated screw-down pins secured the film to the drum surface; additionally tape was place over the outer edges of the film, outside the sample area. The Hencky strain rate at which the films were stretched was based on the ultimate elongation: $0.0033s^{-1}$ (0.021mm/s) for elongations less than 20%, $0.0167 \ s^{-1}$ (0.106 mm/s) for elongations between 20 and 100%, and $0.33 \ s^{-1}$ (2.12 mm/s) for elongations greater than 100%. These strain rates were calculated based on ASTM D882-12 for tensile testing of thin plastic sheeting, but modified to account for the predefined sample distance between the drums. Samples were tested under dry airflow at 30°C and 60°C. Dry test conditions were achieved using the forced convection oven (FCO) built into the ARES rheometer. Samples were allowed to equilibrate at temperature for 10 min before the tensile tests. Samples were also tested under saturated gas conditions at 30°C and 60°C. Humidified gas was supplied by a combination of dry and wet gas flows controlled by to two

mass flow controllers (10,000 cm^3/min capacity, MKS 1179A). The wet gas was passed through a humidity bottle (FCT, Inc.) with 10 m of Nafion$^®$ tubing to saturate the air with water. The wet and dry gas flows were combined and delivered to the ARES sample chamber through heated lines, to prevent condensation in the tubing. A humidity probe (Vaisala HMT 337) measures the dew point in the sample chamber and provides real time humidity conditions. Humidified samples were allowed to equilibrate (and take up water) for 40 min, except the ATMPP membrane that equilibrated for 1 h. These equilibration times were determined by separate dynamic vapor sorption experiments (described earlier), during which the gravimetric change in mass of polymer is measured with respect to humidity.

4.4 Results and Discussion

The charged nature of an AEM causes sorption of water into the polymer from surrounding vapor or liquid. Water uptake has a significant impact on ion transport, mechanical properties, and membrane performance. Water is critical to maintain ionic conductivity to facilitate ion diffusion and allow for Grotthuss charge hopping [18]. Sorption of water into the polymer can have a plasticizing effect on the membrane, which is quantified by increases in elasticity and elongation as well as a reduction in membrane strength [25, 73]. Generally, water uptake is proportional to IEC, and the water uptake can be translated to the number of water molecules associated with each cationic group. Accurately measuring water uptake at different relative humidities is critical to understanding how mechanical properties change under different environmental conditions.

Water uptake was measured for each AEM at 30°C and 60°C to determine the time required to reach full saturation in the film and relate changes in mechanical properties to relative humidity, Figure 4.2. The FAA-PEEK membrane has the lowest water uptake of the

AEMs, 4.8% and 7.2% at 30°C and 60°C respectively, corresponding to lambda equal to 1.8 and 2.7 respectively. The low water uptake of the FAA-PEEK membrane is a result of its low IEC and PEEK reinforcement that restricts dimensionally swelling. Due to its high IEC, the ATMPP membrane had the highest water uptake of 14% (lambda of 3.1) at both temperatures tested. This water uptake is lower than literature values for liquid water uptake (64 - 72%) [75] and gas phase water uptake with 1 h humidity steps (27%) but similar to the gas phase water uptake with 20 min humidity steps (17%) [76]. The ETFE-g-PVBTMA had moderate water uptake of 6.2% at 30°C and 10.4% at 60°C, corresponding to lambda equal to 1.9 and 3.2 respectively. These water uptakes are lower than literature values for uptake from liquid water (40%) [42]. The level of water uptake and hydration number will be related to the mechanical behavior of hydrated films described below.
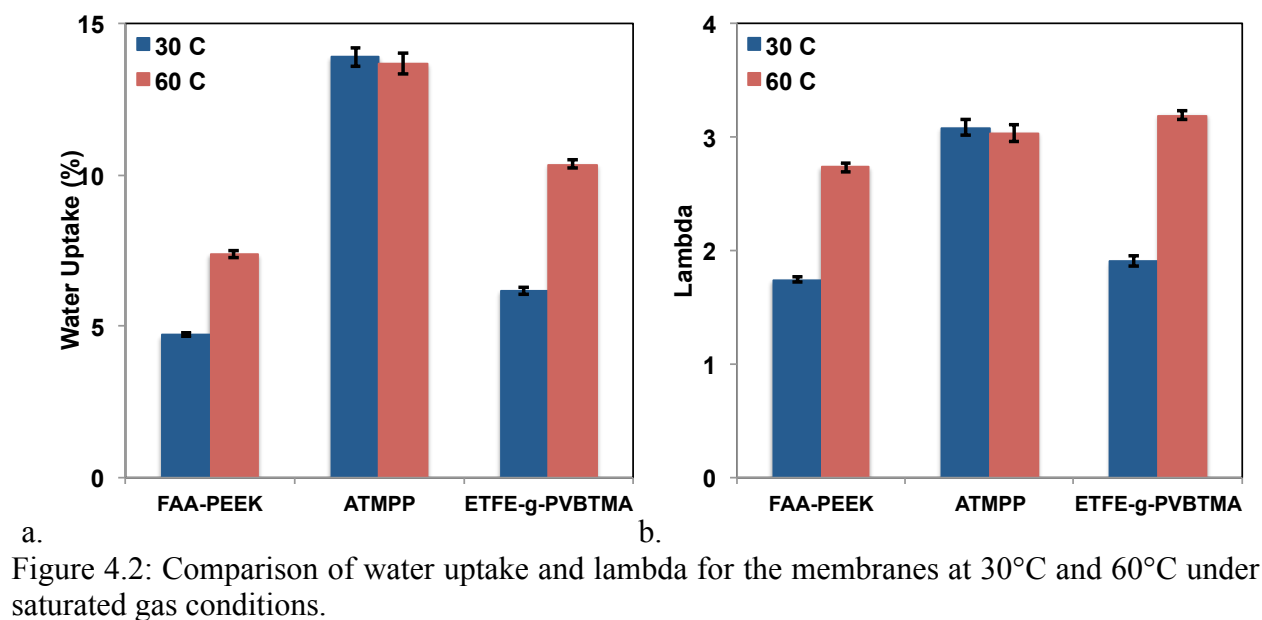
Figure 4.2: Comparison of water uptake and lambda for the membranes at 30°C and 60°C under saturated gas conditions.

Dimensional swelling was measured with respect to the in-plane area and through-plane thickness of the film (Figure 4.3). As expected, the FAA-PEEK membrane showed the lowest swelling due to its low water uptake and PEEK reinforcement. The FAA-PEEK membrane is the
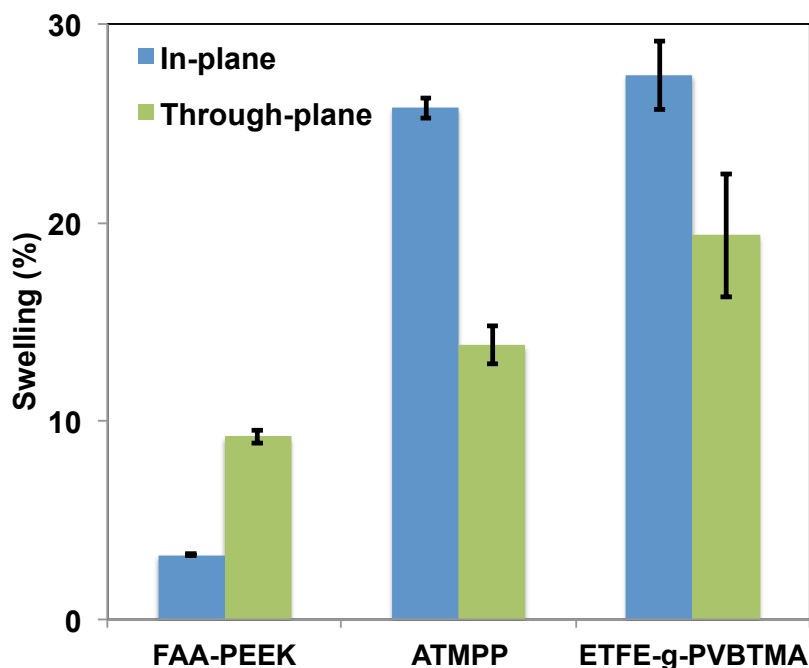
Figure 4.3: Dimensional swelling of AEM films soaked in liquid water compared to dry films at ambient conditions.

only AEM to have a larger through-plane swelling, 9%, compared to in-plane swelling, 3%, due to the PEEK reinforcement preventing swelling in the in-plane direction. The ATMPP and ETFE-g-PVBTMA films show a similar amount of swelling, with in-plane swelling being higher, 26 − 27%, compared to 14 − 19% in the through-plane direction. Dimensional swelling can be problematic in AEM based devices because the membrane is constrained by bipolar plates, and excessive dimensional changes could lead to delamination of the catalyst layers as well as mechanical failure of the membrane. Membrane elasticity must be adequate to allow swelling and deswelling without developing cracks or holes in the membrane. Maintaining adequate hydration and ion conduction while limiting dimensional swelling will improve the lifetime of an AEM based devices.

The ionic conductivity of the AEMs was measured to establish the relationship between ion conduction with IEC and water uptake. Conductivity in the halide form, chloride for FAA-

PEEK and ETFE-g-PVBTMA and bromide for ATMPP, was measured for all membranes at saturated relative humidity and 60°C. The FAA-PEEK film had the lowest conductivity of 11.6 ± 0.8 mS/cm as a result of its low IEC and relatively low water uptake compared to the other films. The ATMPP film, which had the highest IEC and water uptake of all films tested, had a conductivity of 20 ± 2 mS/cm. This value is similar to ATMPP bromide conductivities reported in literature, 10 - 38 mS/cm [75, 76]. The ETFE-g-PVBTMA had the highest conductivity of 47 ± 3 mS/cm, which is higher than through-plane carbonate or bicarbonate conductivities reported in literature (17 - 25 mS/cm) [42, 77]. Ion transport is significantly influenced by IEC and water sorption in the membrane and these factors will also have a large impact on mechanical performance.

At the lower temperature (30°C) and dry conditions all AEMs tested were stiff, having a Young's modulus of at least 425 MPa. While sample elongation on the SER is in one dimension, the strain is not truly uniaxial, because the sample is forced to bend around the SER drum. This makes comparison of SER measurements with traditional tensile tests difficult, particularly for stiff samples where bending may contribute to failure. The stiff nature of the AEM films caused some samples to fail at the attachment pins, however the measured properties (stress, elongation, and modulus) were statistically the same as samples that failed in the middle so all tests were included when calculating average properties and the associated error. All reported properties are the averages of at least five replicate experiments at each temperature and humidity condition, error bars represent one standard deviation.

The mechanical behavior of all three membranes at 30°C and dry conditions are compared in Figure 4.4. The ATMPP membrane is the stiffest film, represented by the steepest initial slope in the stress strain curve, due to the rigid nature of the branched polyphenylene

backbone. The ATMPP film also has a higher yield point, with the yield strain around 15% and yield stress around 65 MPa. The FAA-PEEK and ETFE-g-PVBTMA films both have a lower yield point, around 10% strain and 35 MPa. Due to its stiffer nature and higher yield point, the ATMPP film withstands the highest stress at failure (75 MPa). The FAA-PEEK and ETFE-g-PVBTMA withstood lower stresses, 60 MPa and 47 MPa respectively. Film elongation at dry conditions was low, between 22 and 29%. The modulus and strength of the AEMs at 30°C and dry are reasonable, however film elongation is a concern as the membranes need to withstand swelling and contraction with humidity cycling in a fuel cell.
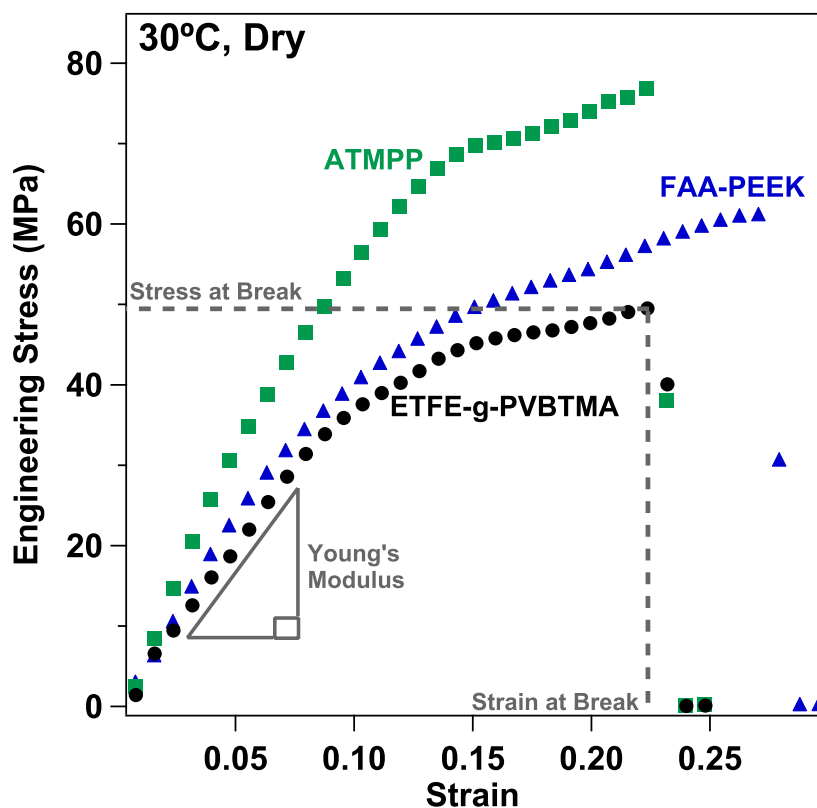
Figure 4.4: Representative stress vs. strain curves of the AEMs at 30°C under dry conditions. The linear region used to determine Young's Modulus and the defined stress and strain at break are labeled for the ETFE-g-PVBTMA film.

Increasing the testing temperature from 30°C to 60°C is expected to reduce the elastic modulus and stress at break, and increase the elongation of the polymer. However, the thermal

responses of the benchmark AEMs tested resulted in a range of responses. Exposing the AEMS to humidity allows the polymer to uptake water, which has a plasticizing effect [73, 75, 80]. The water plasticizer generally reduces the elastic modulus, increases elongation, and decreases the stress to break. The change in mechanical properties due to humidity is dependent on the amount of water taken up by the polymer. Table 4.1 summarizes the water uptake and mechanical properties measured for each membrane at the different sample conditions and compares available literature data at similar conditions.
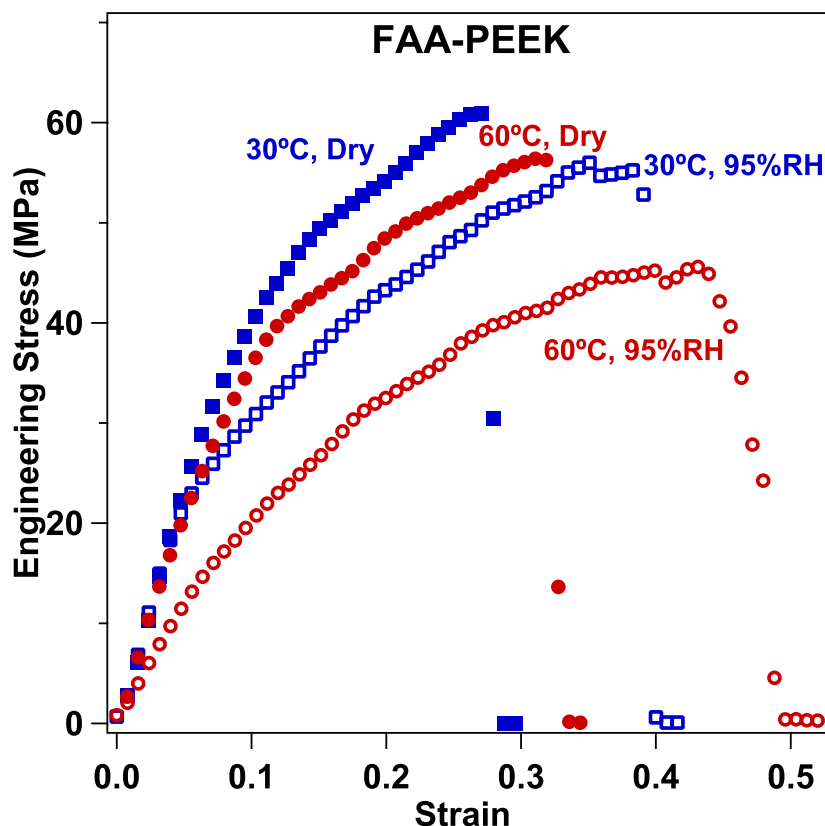
Figure 4.5: FAA-PEEK representative stress vs. strain curves at range of temperature and humidity conditions.

The FAA-PEEK film has a narrow range of mechanical changes over the range of conditions tested (Figure 4.5). The PEEK reinforcement increases membrane strength and durability because PEEK has a very high modulus (~4500 MPa) and tensile strength (~100 MPa)

Table 4.1: Water uptake and mechanical properties from current tests and the literature (italics refer to literature data).

	Water Uptake (%)	In-plane Swelling (%)[a]	Conductivity (mS/cm)	Young's Modulus (MPa)	Ultimate Strength (MPa)	Elongation (%)	Reference
FAA-PEEK							
30°C, Dry				440 ± 30	60 ± 5	29 ± 2	
60°C, Dry				400 ± 40	56 ± 4	33 ± 7	
30°C, 95%RH	4.7 ± 0.1	3.3 ± 0.1		440 ± 30	55 ± 5	41 ± 3	
60°C, 95%RH	7.4 ± 0.1		11.6 ± 0.8	240 ± 20	42 ± 3	44 ± 4	
PEEK				*4500*	*80 - 120*	*20 - 50*	*[81, 82]*
ATMPP							
30°C, Dry				580 ± 30	75 ± 6	23 ± 6	
50°C, 10%RH					*50*	*27*	*[75]*
60°C, Dry				470 ± 40	73 ± 9	26 ± 6	
[Cl⁻] 60°C, Dry				460 ± 50	60 ± 6	25 ± 5	
30°C, 95%RH	13.9 ± 0.3	26 ± 1		250 ± 40	25 ± 3	46 ± 13	
50°C, 90%RH	*70 ± 6[b]*		*37 ± 5[b]*		*20*	*80*	*[75]*
60°C, 95%RH	13.7 ± 0.3		20 ± 2	230 ± 20	22 ± 2	56 ± 6	
[Cl⁻] 60°C,95%RH				240 ±30	19 ± 1	68 ±7	
Polyphenylene				*1900*	*70*	*6*	*[83]*
ETFE-g-PVBTMA							
30°C, Dry				370 ± 40	47 ± 2	22 ± 2	
60°C, Dry				310 ± 60	27 ± 4	10 ± 3	
30°C, 95%RH	6.2 ± 0.1	27 ± 2		140 ± 40	32 ± 3	130 ± 10	
RT, hydrated	*40 ± 4[c]*		*21.7 ± 0.8[c]*		*14 -19*	*45 – 75*	*[42]*
60°C, 95%RH	10.4 ± 0.1		47 ± 3	80 ± 10	22 ± 2	210 ± 30	
ETFE film				*520 - 570*	*150 - 200*	*350 - 550*	*[84]*
Nafion® N115							
23°C, 50%RH				*249*	*43*	*225*	*[85]*
23°C, water soaked				*114*	*34*	*200*	*[85]*

a. Swelling measurements were at room temperature from liquid water.
b. Literature values for ATMPP water uptake was at 30°C from liquid water and conductivity was in the Br⁻ form at 80°C.
c. Literature values for ETFE-g-PVBTMA water uptake was in the OH⁻ form from liquid water at room temperature and conductivity was in the CO_3^{2-} form in liquid water at 50°C.

[81, 82]. The Young's moduli, represented by the initial slope of the stress vs. strain curves, are similar at 30°C (dry and hydrated) and 60°C/dry, being between 400 and 440 MPa. The decrease in slope at 60°C and saturated conditions corresponds to a lower modulus, 250 MPa, indicating a softening of the film due to the plasticizing effect of water. Elongation increases with temperature and humidity as expected, but has a relatively narrow range, from 29% to 44%. Similarly, increases in temperature and humidity correspond to decreases in stress at break, from 60 MPa at 30°C and dry to 42 MPa at 60°C and 95%RH. The relatively narrow range of

mechanical properties with respect to temperature and humidity is due to the PEEK reinforcement of the FAA-PEEK film that resists swelling and has no thermal transitions in this range [86].
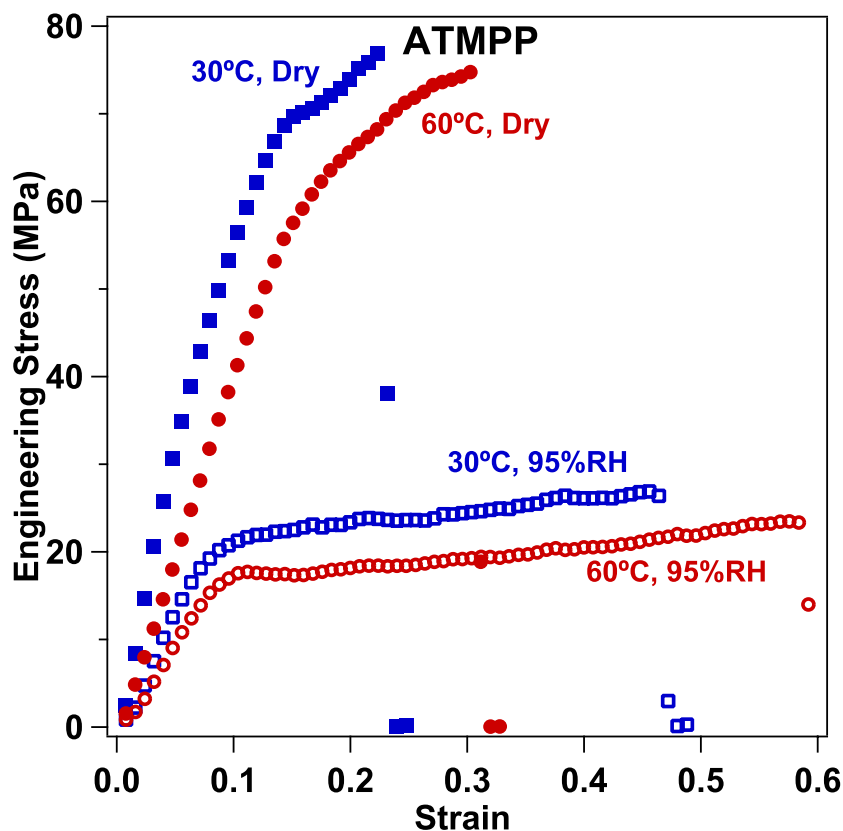
Figure 4.6: ATMPP representative stress vs. strain curves at range of temperature and humidity conditions.

The ATMPP film has a small response to temperature between 30°C and 60°C, but a large response to humidity (Figure 4.6). Compared to the ATMPP, a non-ionic, branched polyphenylene film was reported to have a much higher modulus (1900 MPa), similar strength (70 MPa) and lower elongation (6%) (Table 4.1), however these differences could be due in part to variations in molecular weight and slightly differing chemistries [83]. At dry conditions, increasing temperature from 30°C to 60°C results in a 19% decrease in modulus, from 580 MPa to 470 MPa, and negligible changes in stress at break (73-75 MPa) and elongation (23-26%). The

relatively large water uptake, 14%, by the ATMPP film results in dramatically different behavior at saturated conditions. At saturated conditions the material is softened, reducing the modulus to 250 MPa at 30°C and 230 MPa at 60°C. At saturated conditions film strength is reduced to approximately 33% of that at dry conditions, 22-25 MPa, and elongation approximately doubled, 46-56%. At saturated conditions the yield strain is relatively low, around 10%, compared to the final elongation while the yield stress, around 20 MPa, is similar to the stress at break. The ATMPP was also tested at 60°C in the Cl⁻ form with negligible changes in the measured properties. The dramatic reduction in modulus and strength at high hydration demonstrates the importance of testing AEM mechanical properties under operating conditions encountered in fuel cells and electrolyzers.

The ETFE-g-PVBTMA film responds dramatically to both temperature and humidity changes, Figure 4.7. Radiation grafting cations results in a reduction of all mechanical properties compared to the ETFE precursor film that has high modulus (520 - 570 MPa), strength (150 - 200 MPa), and elongation (350 - 550%) [84]. Increasing the temperature from 30°C to 60°C softened the film and resulted in lower stress at break and elongation. The modulus was reduced from 370 MPa at 30°C to 310 MPa at 60°C. Increasing temperature also lowered stress at break to 27 MPa compared to 47 MPa at 30°C, and the final elongation decreased to 10% from 22% at 30°C. The reduction in strength with increased temperature is expected, but the reduction in elongation is counterintuitive, and may be due to a disproportionate decrease in strength compared to modulus, resulting in earlier film failure. Adding water to the polymer under saturated conditions further softens the ETFE-g-PVBTMA film. At saturated conditions the modulus was reduced between 62% to 74%, to 140 MPa at 30°C and 80 MPa at 60°C. Humidified conditions also reduced the stress at break to 32 MPa and 22 MPa at 30°C and 60°C
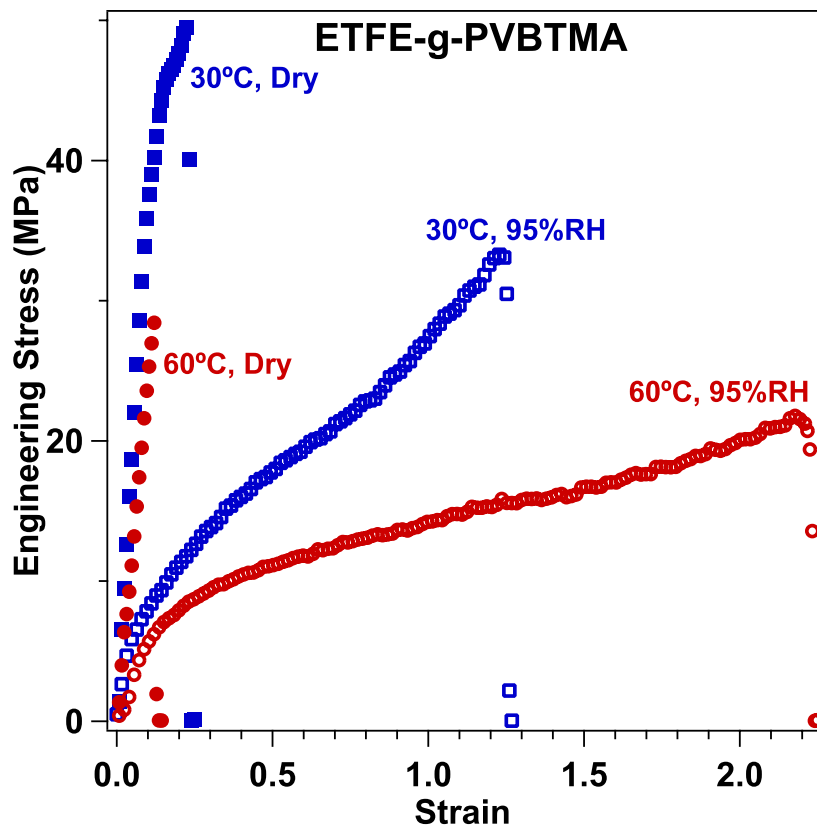
Figure 4.7: ETFE-g-PVBTMA representative stress vs. strain curves at range of temperature and humidity conditions.

respectively. Elongation is increased significantly when the ETFE-g-PVBTMA film is humidified. Elongation increases to 130% at 30°C and 210% at 60°C. Due to its low elongation at dry conditions, the ETFE-g-PVBTMA film may not be able to withstand the stresses associated with dimensional shrinking when the film undergoes drying. The drastic changes in the mechanical properties of the ETFE-g-PVBTMA under different temperature and humidity conditions could contribute to membrane failure [27].

The mechanical properties of the three AEMs are compared in Figure 4.8. All films are relatively stiff at dry conditions, i.e., having moduli between 310 and 580 MPa. The ATMPP film is the stiffest at dry conditions but undergoes softening under hydrated conditions. The FAA-PEEK is only softened at high temperature and humidity due to low water uptake at lower
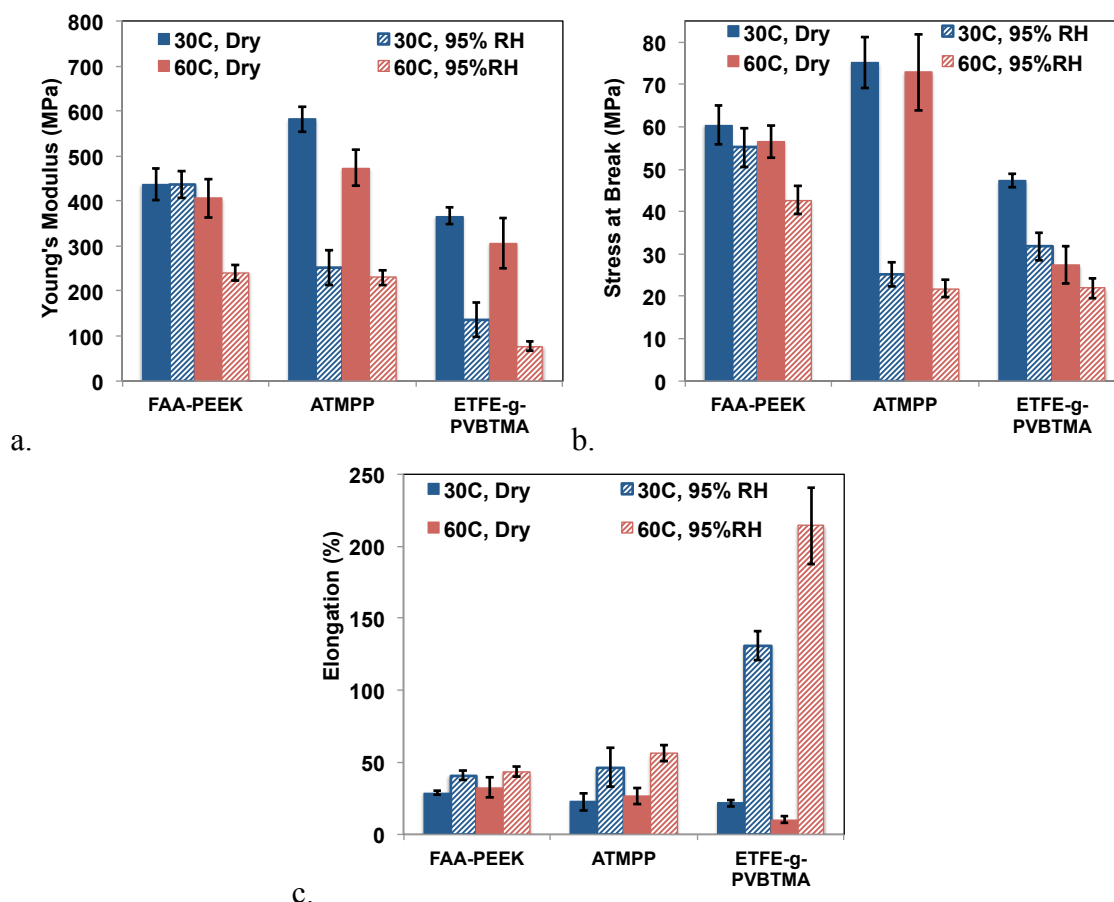
Figure 4.8: a) Young's modulus, b) Stress at Break, and c) Elongation of the three AEMs at 30°C and 60°C under dry and saturated conditions.

temperatures. The ETFE-g-PVBTMA membrane is softened by increases in temperature and humidity, and is consistently the most elastic film at all conditions tested. The highest stress at break is seen in the ATMPP film at dry conditions, however the ATMPP film significantly decreases in strength when humidified. The FAA-PEEK has the most consistent strength at all conditions tested, most likely due to PEEK reinforcement that is not effected by changes in humidity. All films had an increase in elongation under saturated conditions. The increase in elongation was least for the FAA-PEEK due to its lower water uptake and the reinforcing mesh. The highest elongations, 130% to 210%, were seen in the ETFE-g-PVBTMA film at saturated conditions, but the low elongations of the film at dry conditions could be problematic during humidity cycling. Ideally, a membrane would have high strength under both dry and humidified

61

conditions and sufficient elongation to account for dimensional changes with hydration level. Membrane reinforcement helps resist membrane changes with temperature and humidity, as shown with the FAA-PEEK film, however adding nonconductive reinforcement also lowers polymer IEC and limits water uptake that may be critical for efficient ion transport. The interplay between ionic conductivity, water uptake, and mechanical integrity makes designing an optimal anion exchange membrane extremely challenging, but considering all of these criteria in the early stages of development will lead to a robust, well performing anion exchange membrane.

4.5 Conclusions

Testing the mechanical performance of common AEMs provided baseline properties for membrane development for electrochemical energy conversion devices and highlights what properties need improvement. The mechanical properties of three common AEMs were investigated at a range of relevant temperature and humidity conditions. The three membranes tested had different chemical and physical properties, so mechanical responses to temperature and humidity varied greatly. The Fumasep FAA-PEEK film is reinforced by a PEEK mesh that restricts water uptake, which means that hydration has a negligible affect on Young's modulus at 30°C and produces only a 40% reduction at 60°C. Similarly, the hydrated strength decreases by only 9% and 24% at 30°C and 60°C respectively. The ATMPP film had the highest IEC, resulting in large water uptake and significant softening, a 51 - 55% reduction in modulus, and a 70% weakening of the film at saturated conditions. The ETFE-g-PVBTMA film responded to both temperature and humidity, having the largest increase in elongation at saturated conditions, over 200% when hydrated at 60°C. The ETFE-g-PVBTMA film may have difficulty maintaining membrane integrity during humidity cycling because the dimensional swelling exceeds the elongation at dry conditions. Ionic groups of the AEM facilitate water uptake, which is critical to

ion transport through the membrane, however water sorption leads to dimensional swelling and variation of mechanical properties. An AEM must be mechanically stable at a range of hydration levels to operate in a fuel cell, electrolyzer, or other electrochemical energy conversion device. Thus, mechanical durability, along with ionic conductivity and chemical stability, should be a fundamental design criterion for new AEM development to achieve robust device membranes.

4.6 Acknowledgments

CHAPTER 5 : DURABILITY AND PERFORMANCE OF POLYSTYRENE-B-POLY(VINYLBENZYL TRIMETHYLAMMONIUM) DIBLOCK COPOLYMER AND EQUIVALENT BLEND ANION EXCHANGE MEMBRANES

This chapter is modified from a paper published in

Journal of Applied Polymer Science[18]

Melissa A. Vandiver[19], Benjamin R. Caire[20], Zach Poskin[21], Yifan Li[22],

Sönke Seifert[23], Daniel M. Knauss[24], Andrew M. Herring[25], Matthew W. Liberatore[26]

5.1 Abstract

Anion exchange membranes (AEM) are solid polymer electrolytes that facilitate ion transport in fuel cells. In this study a polystyrene-b-poly(vinylbenzyl trimethylammonium) diblock copolymer was evaluated as potential AEM and compared with the equivalent homopolymer blend. The diblock had a 92% conversion of reactive sites with an IEC of 1.72 ± 0.05 mmol g^{-1}, while the blend had a 43% conversion for an IEC of 0.80 ± 0.03 mmol g^{-1}. At 50°C and 95% relative humidity, the chloride conductivity of the diblock was higher, 24-33 mS cm^{-1}, compared to the blend, 1-6 mS cm^{-1}. The diblock displayed phase separation on the length scale of 100 nm, while the blend displayed microphase separation (~10 μm). Mechanical characterization of films from 40 to 90 microns thick found that elasticity and elongation decreased with the addition of cations to the films. At humidified conditions, water acted as a

plasticizer to increase film elasticity and elongation. While the polystyrene-based diblock displayed sufficient ionic conductivity, the films' mechanical properties require improvement, i.e., greater elasticity and strength, before use in fuel cells.

5.2 Introduction

Low temperature fuel cells are promising, clean energy conversion technology for portable applications including automobiles and portable electronics [3, 4, 69]. Alkali fuel cells (AFC) were first developed by Bacon in the 1930s and later implemented on the NASA Apollo orbiter spacecraft using pure hydrogen and oxygen [3, 4, 8, 69]. Traditional AFCs utilize a liquid potassium hydroxide electrolyte to transport hydroxide ions from cathode to anode. The alkali nature of AFCs allows favorable electrode kinetics with the potential for non-precious medal catalysts and more versatile fuel utilization [11]. Unfortunately, exposure to carbon dioxide in the oxidant stream converts the hydroxide ions in the liquid electrolyte to carbonates that form solid precipitates fouling the electrodes and requiring circulation of the electrolyte to filter out the carbonate solids. The superior power density of proton exchange membrane fuel cells (PEMFC), without requiring a CO_2 free oxidant stream, prevented commercial development of the liquid AFC, allowing PEMFCs to dominate low temperature fuel cell research and development.

PEMFCs employ a solid acidic polymer to transport protons from anode to cathode. PEMs have been researched heavily the past several decades resulting in durable, thin films with high proton conductivity. Commercial development of PEMFCs remains difficult due to the high cathode catalysts cost, performance optimized for hydrogen fuel, and membrane lifetime [2, 6]. The limitations of PEMFCs have led recent research to focus on developing a solid polymer anion exchange membrane as the electrolyte in AFCs [9]. These anion exchange membranes

65

(AEM) fuel cells maintain the kinetic benefit of the alkali system, but tethering of the cation species, often ammonium, guanidinium, or phosphonium, to the polymer backbone prevents the formation of solid precipitates, even if the hydroxide counter-ions are converted to carbonates [8, 9, 18]. Chemical degradation is a concern with AEMs as both the cation species and polymer backbone are susceptible to attack by hydroxide. For this reason, many AEM polymer chemistries are under investigation, including perfluorinated AEMs that resemble PFSAs, polysulfone and polyphenylene based AEMs, and precast films (FEP/ETFE) irradiated to generate cation functionalities grafted on the polymer [30, 42, 45, 58, 76, 87, 88]. Various cation species, including quaternary phosphonium, tertiary sulfonium, and guanidinium based compounds, are being studied for alkali stability [70]. Vinylbenzyl trimethylammonium is the most common AEM cation of study, due to ease of functionalization and adequate alkali stability on short time scales [70]. The mobility of hydroxide ions is lower than protons in acidic systems [15], making it necessary to use thin membranes to reduce ionic resistance in the cell. The inherent limitations of AEM performance makes the development of thin, mechanically robust films critical to successful application in alkali anion exchange membrane fuel cells.

Development of high performance, mechanically robust thin films require a combination of suitable polymer chemistry and controlled film processing. The ability of block copolymers to self-assemble into phase-separated morphologies has created great interest in both PEM and AEM development. The phase separation generated in block copolymers allows pathways for ion transport while maintaining mechanical integrity of the film [89, 90]. Block copolymers for ion exchange membranes generally consist of a hydrophobic block that provides mechanical durability and prevents extreme swelling and a hydrophilic block of conductive polymer that provides the ionic transport pathway in the film. The chemically dissimilar blocks encourage

66

phase separation in the system, generating polymer morphologies that include spherical, cylindrical, lamellar, and bicontinuous [91]. Polystyrene based block copolymer AEMs have been synthesized and characterized previously, however the mechanical performance of these membranes is unknown [92, 93]. Tsai et al., synthesized polystyrene-block-poly(vinyl benzyl trimethylammonium) membrane at a range of IECs by sequential monomer addition using atom transfer radical polymerization. These polymers had well defined block lengths leading to distinct spherical, cylindrical, and lamellar morphologies that greatly influenced ion conduction through the membrane [92]. The polystyrene diblock of this study was previously blended with poly(phenylene oxide) and studied with respect to morphology, hydroxide conductivity, and mechanical properties; however dropcast films of the pure diblock were not robust enough to study [94]. Through controlled film casting, pure polystyrene diblock films were fabricated for this study. While transport pathways can be generated by the chemical nature of the diblock, controlled film processing ensures film uniformity that is essential for consistent conductive performance and mechanical durability.

While the majority of current AEM research has focused on the development of stable polymer chemistries with high ionic conductivity, consideration the membrane mechanical properties is also necessary. While perfluorinated sulfonic acid (PFSA) membranes have dominated PEMs due to their high ionic conductivity and suitable chemical and mechanical durability [2, 5], the lifetime of a PEM fuel cell is often defined by mechanical failure of the membrane. Polymer electrolyte fuel cells experience a range of humidity conditions during operation causing the membrane to swell and shrink. At high hydrations, the membrane experiences dimensional swelling, and desorption of water at low humidities causes the membrane to contract, leading to significant stresses [6, 25, 26]. Humidity cycling causes

repeated swelling and contraction of the membrane that can generate pinholes and cracks, which lead to eventual catastrophic mechanical failure. Mechanical durability and membrane lifetime can be gauged by rapid humidity cycling of the membrane to the point of gas crossover [28] or pressurized blister test that simulate the hygrothermal stress developed in constrained membrane [29]. It is more difficult to predict membrane lifetime from traditional tensile tests, however tensile measurements remain a basis for comparison between polymer systems. Measurement of mechanical properties under different hydration levels and after humidity cycling is critical to development of robust AEMs for long-term use in fuel cells.

In this study, a diblock copolymer of polystyrene-b-poly(vinylbenzyl trimethyl-ammonium) was evaluated as a potential anion exchange membrane for fuel cells, and compared with blend films of commercially available homopolymers. Polymer films were prepared in solution, functionalized, and characterized. Conductivity, morphology, and mechanical properties of the polymer films were investigated at a range of humidity conditions. While the two polymer systems have the same initial chemical composition, significant differences in stability, phase separation, and transport were observed for the block copolymer and blended membranes.

5.3 Experimental

5.3.1 Materials

The polystyrene-b-poly(vinylbenzyl chloride) (PS-b-PVBC) block copolymer was synthesized as previously described [94] with a total molecular weight of 85,700 g mol^{-1} and molecular weight distribution of 1.85. The diblock copolymer was prepared with the composition of 32 wt% PVBC block and 68 wt% PS block.

The homopolymers were purchased from Sigma-Aldrich and used without additional treatment. The polystyrene was in the form of beads with an average M_w of 192,000 g mol^{-1}. The poly(vinylbenzyl chloride) was a mixture of 3- and 4-isomers and was a powder with an average M_w of 100,000 g mol^{-1}. Homopolymers were mixed to obtain the same weight ratio, PS/PVBC, as the diblock copolymer.

5.3.2 Film Formation

The polymers in a powder form, or beads for polystyrene, were mixed with toluene at a concentration of 0.3 g mL^{-1} in a round bottom flask. The solution was heated at 80°C with magnetic stirring until the polymer was completely dissolved as a homogeneous solution, typically 1 h. The warm solution was pipetted on to a glass substrate and drawn across the substrate with a micrometer adjustable film applicator. The film applicator was drawn at a constant speed between 15-90 mm/s using a film coater (MTI Corporation's MSK-AFA-III, Richmond, CA). The solution was allowed to evaporate for about 4 h, after which the dried polymer film was covered with methanol and the edges of the film were peeled from the substrate, using a razor blade until the film released. The gap height of the micrometer adjustable film applicator was used to control film thickness and consistency. Blade heights ranged from 100 to 500 μm and final film thickness ranged from 40 to 90 μm.

Conversion of the polymer films to the conductive form was performed by soaking in 25wt% trimethylamine solution in water for 2 days. The films were then removed and washed repeatedly with deionized water to remove excess amine. Films were then soaked in 1 M sodium chloride solution overnight to ensure all anions in the film were chloride. Films were washed repeatedly over a period of two days to remove excess salts from the film. Films were stored in bags with a small amount of water due to their brittleness when dry. Some films were left in the

neutral form for mechanical comparison; these films were stored in bags with a small amount of methanol to prevent film cracking. Films were tested in the chloride form for mechanical testing, as the rheometer cannot be sealed to prevent exposure to carbon dioxide that would exchange hydroxide ions to carbonate and bicarbonate.

5.3.3 Ion exchange capacity

The ion exchange capacity (IEC) of the material was determined by an acid/base titration. Membranes were exchanged to the hydroxide form by soaking the film in 1 M sodium hydroxide solution for 2 days at room temperature followed by repeated washes to remove excess ions. The hydroxide form of the membranes were then soaked in 1 M sodium chloride solutions for 48 hours and the hydroxide ions in solution were titrated using standardized hydrochloric acid and continuous pH monitoring. Two inflection points were seen on the titration curve of pH vs. titrant volume, the first around a pH of 8 and the second at a pH of 5. The two inflection points suggest the hydroxide ions reacted with atmospheric carbon dioxide to form carbonate and bicarbonate ions in solution. The end point for the titration was defined as the second inflection point to correspond with the equivalent molar quantity of hydroxide ions before conversion.

Due to the possible sensitivity of the quaternary ammonium cations to hydroxide, the IEC was verified by titration of the chloride ions in solution after soaking chloride form membranes in 1M sodium bicarbonate solutions for 48 hours. Standardized silver nitrate solution, 0.0235 M, was used to titrate the membrane solutions with a potassium chromate indicator. The end point for the titration was defined as the point where permanent rust colored precipitates were seen in solution.

5.3.4 Water Uptake

Water uptake was characterized using a dynamic vapor sorption apparatus (SMS DVS Advantage 1, Allentown, PA). A membrane sample, about 4 mm^2, was placed on a glass weigh plate and the change in mass was measured gravimetrically under different humidity conditions. The water uptake (WU) of the membrane was calculated based on Equation (5.1)

$$WU = \frac{m_{\%RH} - m_{dry}}{m_{dry}} \times 100 \qquad (\ 5.1\ )$$

where $m_{\%RH}$ is the mass of the sample at the given relative humidity and m_{dry} is the mass of the dry sample. The mass of the dry membrane was taken as the measured mass at the end of the initial four-hour drying period. Given the water uptake at saturated conditions and the known ion exchange capacity of the membrane, the hydration level, λ, which is the number of waters per cation functional group, can be calculated using Equation (5.2)

$$\lambda = \frac{WU}{m(H_2O) \cdot IEC} \qquad (\ 5.2\ )$$

5.3.5 Small angle x-ray scattering

Small angle x-ray scattering experiments were performed at the X-ray Sciences Division, beamline 12-ID-B, at the Advanced Photon Source at Argonne National Lab. Measurements were taken in a transmission geometry using a Pilatus 2M SAXS detector with an acquisition time of 1 s at a beam energy of 12 keV and incoming x-ray wavelength of 1 Å. The 2D scatter was radially integrated to obtain data of intensity versus scattering vector q. The transmission intensity was normalized to exposure time and flux of the direct beam through the sample. Swelling of the samples prevents absolute thickness measurement so the atomic density cannot be determined in-situ and the intensity units become arbitrary. A custom built four-sample oven controlled the humidity and temperature of the samples during scattering experiments [95, 96].

Typical experiments contained three membrane samples and one empty compartment so a background pattern could be obtained throughout the scattering experiment. The humidity of the sample environment was controlled using a combination of wet and dry nitrogen that were mixed in a helical mixing tube before entering the sample oven. A humidity probe positioned in the sample oven provided real time humidity readout. Based on the humidity measurement gas flows were adjusted to achieve the desired temperature and humidity condition.

5.3.6 Optical Microscopy

A Thermo Scientific™ Nicolet iN10™ Infrared microscope with a permanently aligned 15X objective lens was used to collect optical images. A reflection electronic light-emitting diode illuminator was the light source. Visual images were captured using a built-in high-resolution 1/3-inch color digital camera (USB2 with 1024 x 768 low noise CCD). A dry membrane sample, about 5 mm^2, was positioned on a glass slide ensuring the sample was flat for even illumination. All images were collected under ambient conditions.

5.3.7 Conductivity

The in-plane conductivities (σ) of the membranes were calculated using electrochemical impedance spectroscopy to measure membrane resistance as given by Equation (5.3) below.

$$\sigma = \frac{l}{R \cdot w \cdot t} \tag{5.3}$$

Where R is the membrane resistance, l is the distance between the sense electrodes, w is the width of the membrane samples, and t is the thickness of the sample. Impedance spectra were obtained over a frequency range of 1 to 10^6 Hz using a four-electrode test cell connected to a multi-channel potentiostat (BioLogic VMP3, Knoxville, TN). Measurements were made in an environmental chamber to control sample temperature and humidity (TestEquity Model 1007H, Moorpark, CA). The resistance of the membrane was determined from the low frequency

intercept of the Nyquist impedance plot. All samples were in the chloride form and experiments were performed at constant relative humidity of 95%RH, varying temperature from 50 to 90°C.

5.3.8 Mechanical Characterization

Mechanical properties of the films were measured using an ARES G2 rheometer (TA Instruments, New Castle, DE) with a Sentmanat Extension Rheometer (SER) fixture (Xpansion Instruments, Tallmadge, OH) [38]. The SER fixture has two counter rotating drums that uniaxially stretch the polymer film suspended between the drums. The separate motor and transducer of the ARES G2 rheometer allows for strain controlled operation during which stress is measured by the rheometer. Polymer films were cut into strips of about 7mm(W) x 20mm(L) with the length being along the draw direction of the film. During initial testing, the polymer film was adhered to the SER drums at elevated temperature, 130–155°C, using the force convection oven (FCO) of the ARES. After adhesion the temperature of the oven was reduced to 100°C, below this temperature films would release from the drums, and the polymer film was stretched at a Hencky strain rate of 0.01 s^{-1}. The films are stretched to the point of failure, and the stress at failure is defined as the magnitude of the stress applied to the film just prior to break. The percent elongation is the percent increase in film length. The Young's modulus is a measure of the elastic nature of the film and was determined by the slope of the stress vs. strain curve in the elastic region, the linear region at very low strains. Initial mechanical characterization was performed on the cation functionalized diblock and blend films as well as the neutral precursors.

New SER drums were manufactured with a flat pin secured to the drum surface by screws at the top and bottom. This drum design allowed films to be loaded and stretched at lower temperatures [97]. A thin piece of silicon rubber was added to the inside of the pins to prevent membrane slipping during testing. In ambient air the films were positioned between the pin and

the drum surface and the screws were tightened to hold the membrane suspended between the two drums. The cationic diblock and blended films were stretched at a Hencky strain rate of 0.01 s^{-1} at 60°C under dry and humidified, 95%RH, conditions. The 60°C dry conditions were achieved using the FCO airflow prebuilt into the ARES. Humidified, 60°C, conditions were achieved using a combination of dry and wet gas streams supplied to the FCO chamber through a secondary port. Flow of the wet gas stream through two humidity bottles (Fuel Cell Technologies, Albuquerque, NM) in series saturated the wet gas stream. The wet and dry gas streams were controlled with two MKS RS-485 mass flow controllers and the streams were premixed and delivered in a heated line to the FCO chamber. A Vaisala HMT337 humidity probe provided real time humidity feedback to LabView software where the gas flows are controlled.

5.4 Results and discussion

5.4.1 Ion Exchange Capacity

The ion exchange capacities of the functionalized polymer films were determined by acid/base and Mohr titrations. By acid/base titration the IEC of the PS-b-PVBTMA diblock copolymer was 1.72 ± 0.05 mmol/g corresponding to a 92% conversion of the vinylbenzyl chloride sites based on the theoretical maximum IEC of 1.87 mmol/g. Acid/base titration was unsuccessful on the PS/PVBTMA homopolymer blend, the pH of the chloride solution that the hydroxide form film was soaked in did not increase significantly, being just higher than neutral. It is expected that the homopolymer blend suffered degradation upon exposure to hydroxide and the ions were subsequently washed away prior to titration. All subsequent testing of the polymer films was performed in the chloride form so hydroxide degradation was not a concern.

A Mohr titration of chloride ions was performed on the films to confirm the IEC without hydroxide effects. By chloride titration, the diblock film had a measured IEC of 1.73 ± 0.05

74

mmol/g, within the error of the IEC determined by acid/base titration, suggesting the diblock is stable in hydroxide (1 M NaOH for 2 days) compared to the homopolymer blend. The IEC of the homopolymer blend by chloride titration was 0.80 ± 0.03 mmol/g, which corresponds to incomplete, 43%, conversion of the vinylbenzyl chloride groups or loss of cations sites due to instability after conversion.

Functionalization of the PVBC homopolymer with cations results in a water-soluble polymer and it is possible some of PVBTMA would wash out of the film following quaternization. However, the high concentration of the solution used to draw the film is expected to provide adequate entanglement of the polymer chains to prevent loss of the PVBTMA. During functionalization no noticeable turbidity was observed, indicative of polymer dissolution, in the trimethylamine solution or the subsequent wash solutions. Additionally, no measureable decrease in dry film weight or thickness was detected after functionalization to the cationic form. Attempts to fully convert the homopolymer blend were made by soaking the films in trimethylamine for 4 and 10 days at ambient conditions and using a pressurized cell at 50°C and 30 bar pressure for 10 days. These attempts did not increase the measured IEC, and even lowered conversion in some cases, suggesting unstable cation attachment or dissolution of the PVBTMA as functionalization is increased. The lower IEC of the blend polymer compared to the diblock will be reflected in the remaining membrane characterization including water uptake, conductivity, and mechanical performance.

5.4.2 Water Uptake

Water uptake in the cationic diblock and blend films was measured gravimetrically using dynamic vapor sorption. Maximum water uptake at 60°C was $23.4 \pm 0.1\%$ for the diblock and $11.6 \pm 0.1\%$ for the homopolymer blend. The lower water uptake of the blend film reflects the

lower IEC of the polymer compared to the diblock. These water uptakes correspond to λ values of 7.5 ± 0.2 and 8.0 ± 0.3 for the diblock and blend, respectively. The λ values are lower than PEMs (14 to 22) [98-100], and other AEMs (12 to 25) [75, 101, 102]. The relatively low water uptake of these polymers is likely due to the stiff, hydrophobic nature of the polystyrene in the glassy state at 60°C.
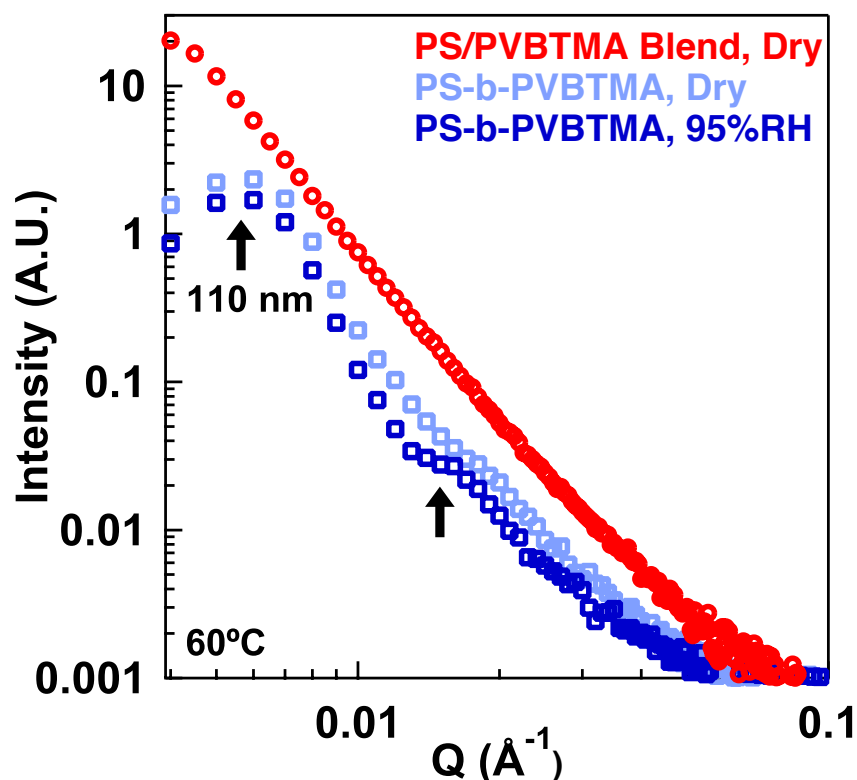
Figure 5.1: Small angle x-ray scattering patterns for the diblock copolymer membrane under dry (light blue) and humidified (dark blue) conditions and the homopolymer blend membrane under dry conditions (red). The arrows indicate the features of the diblock scattering pattern that correspond to primary d-spacing of 110 nm.

5.4.3 Polymer Morphology

Morphology of the diblock copolymer and homopolymer blend were investigated using small angle x-ray scattering (SAXS) under dry and wet conditions at 60°C (Figure 5.1). At both dry and wet conditions, the diblock membrane has a peak at q equal to $5.7×10^{-3}$ $Å^{-1}$ corresponding to a d-spacing of 110 nm. Under humidified conditions, the diblock film's

scattering has an additional shoulder at q equal to 1.5×10^{-2} Å^{-1} that corresponds to a d-spacing of 42 nm. The absence of this shoulder under dry conditions suggests that this size domain is dependent on water uptake by the polymer. The nanometer scale phase separations of the diblock membrane when humidified will likely facilitate ion conduction through the film. The homopolymer blend film has no features over the SAXS q-range because its phase separation is on a much larger length scale.
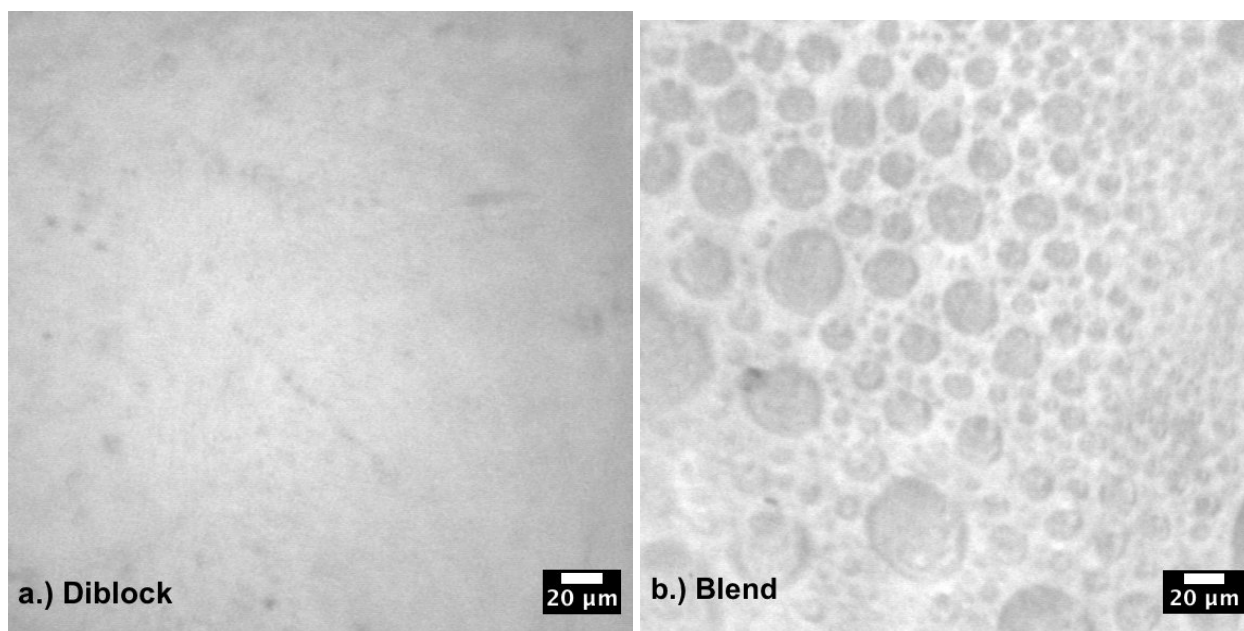
Figure 5.2: Optical microscope images of the a.) diblock copolymer membrane and b.) the homopolymer blend membrane. The homopolymer blend has isolated regions ranging between 5 and 50 μm.

Optical images of the functionalized diblock and blend membranes were taken at ambient conditions to observe surface morphology and phase separation (Figure 5.2). The diblock membrane shows no distinguishable characteristics on this micrometer size scale. In contrast, the homopolymer blend membrane has distinct spherical features, indicative of phase separation of the two homopolymers, on the micrometer scale. These spherical regions appear throughout the membrane and range in size between 5 to 50 μm. This scale of phase separation into isolated spherical regions is not favorable for ion conduction, which relies on interconnected pathways

77

through the film. The micrometer scale phase separation that occurs in the homopolymer blend membrane will likely correlate with relatively low ionic conductivity.

5.4.4 Ionic Conductivity

Ionic conductivity of the polymer films in the chloride form were measured at saturated relative humidity and temperatures between 50 and 90°C. The energy of activation for ion conduction was determined over this temperature range using an Arrhenius relationship. Three nominal film thicknesses were tested for both the diblock and homopolymer blend: 40 μm, 70 μm, and 90 μm (Figure 5.3).
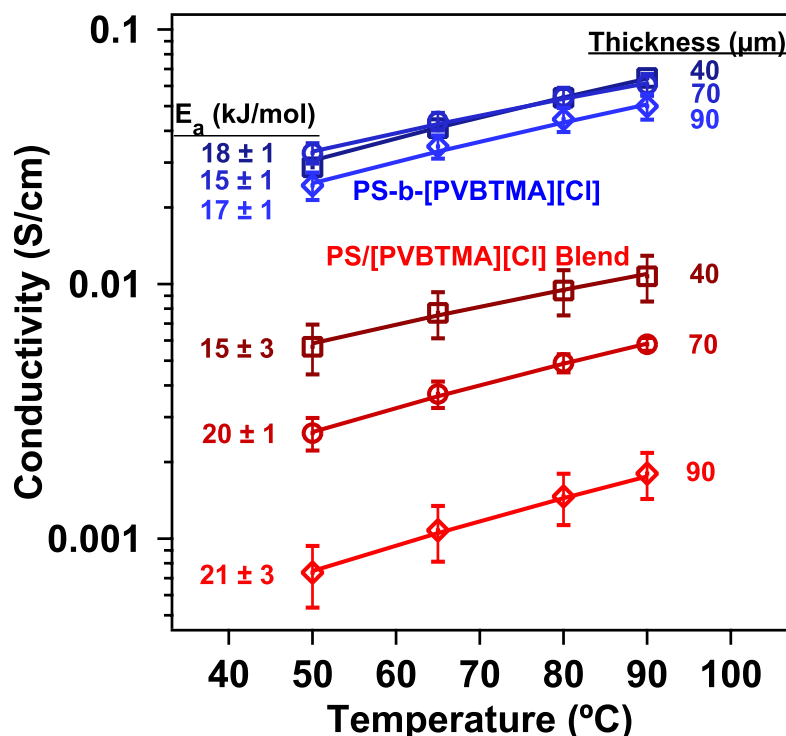
Figure 5.3: Chloride conductivity of the diblock, PS-b-PVBTMA[Cl], shown in blue and the homopolymer blend, PS/PVBTMA[Cl], shown in red. The darkest of each color corresponds with the thinnest, 40 μm, films transitioning to the lightest colors corresponding to the thickest, 90 μm, films. Lines show Arrhenius fits leading to the activation energies listed on the left side of the figure.

Conductivities were an order of magnitude higher for the diblock copolymer compared to the blend. At 50°C the conductivities of the diblock films were 24-33 mS cm^{-1}, comparable to

other AEMs [8, 18, 103], while the conductivities of the blend films were only 0.7-6 mS cm[1].

The higher conductivity of the diblock compared to the blend is expected due to its higher IEC

and nanometer scale phase separation. The conductivities of both the diblock and blend films

were highest for the thinnest, 40 μm, films and lowest for the thickest, 90 μm, films. The

activation energy for ion conduction was similar, between 15 and 21 kJ mol^{-1}, for both the

diblock and blend systems across all thicknesses. These activation energies for ion conduction

are similar to other AEMs [43, 58] and higher than PFSAs, typically 5 – 10 kJ mol^{-1} [57, 58].

The higher conductivity of the diblock copolymer is a result of its higher IEC as well as more

favorable morphology (discussed earlier) for ion conduction compared to the homopolymer

blend film. The increased conductivity of thin, diblock films highlights the importance of

reducing film thickness while maintaining integrity and ensuring interconnected pathways for

ion conduction.
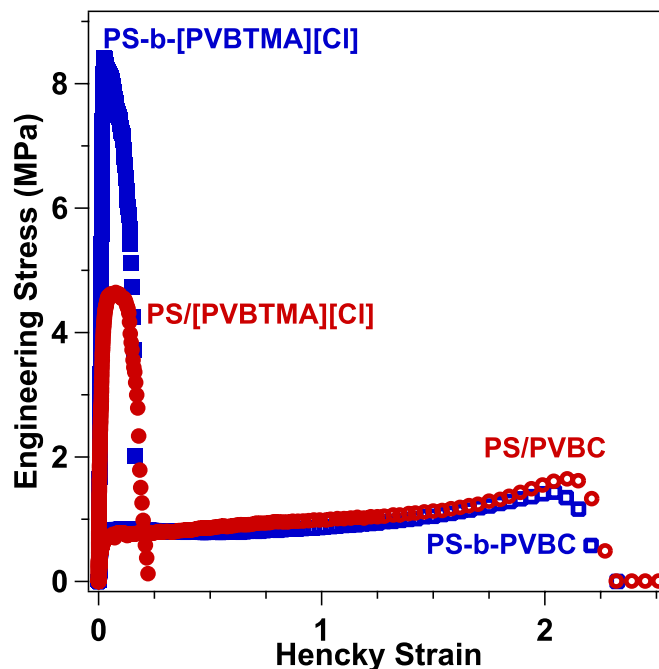
Figure 5.4: Typical stress vs. strain curve for the four types of films tested: cationic diblock (solid blue), neutral diblock (open blue), cationic blend (solid red), and neutral blend (open red).

5.4.5 Mechanical Properties

The mechanical properties of the diblock and blended films in both neutral and cationic forms were evaluated by stretching the films to their breaking point at 100°C, under dry air flow. Typical stress-strain curves (Figure 5.4) allow the determination of stress at break, percent elongation, and Young's (elastic) modulus. Films were tested at same nominal thicknesses (40 μm, 70 μm, and 90 μm) as the conductivity measurements for both the neutral and cationic forms.

The Young's modulus, which is the measure of elasticity in the film, increases for all films upon conversion to the cationic form indicating a stiffening of the film with cation addition (Figure 5.5). The moduli for the films ranged from 4 to 100 MPa for the neutral films and 150 to 450 MPa for the cationic films. Addition of cations to the polymer increases ionic interaction among the polymer chains decreasing elasticity. The moduli did not have an easily defined dependence on film thickness, however the thinnest (40μm) were slightly stiffer (i.e., larger Young's modulus) in most cases.
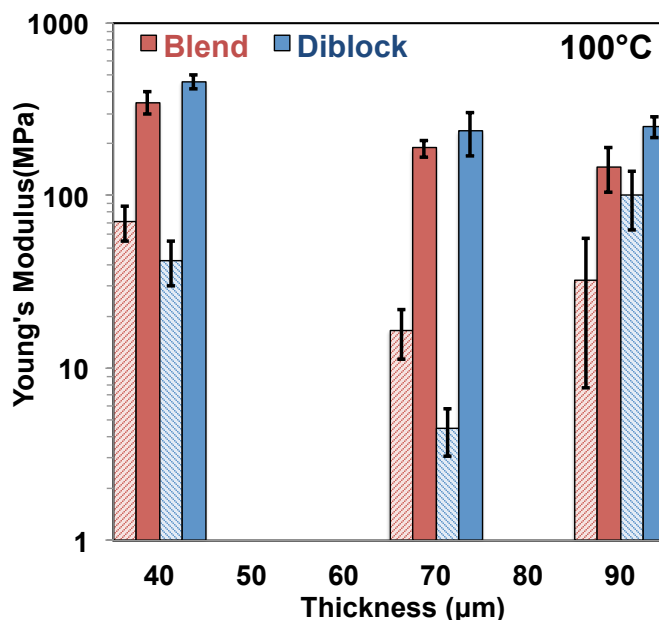
Figure 5.5: The Young's modulus is displayed for the four polymer chemistries: neutral blend (red dashed), cationic blend (solid red), neutral diblock (dashed blue), cationic diblock (solid blue).

The increased stiffness of the cation functionalized films resulted in an increase in stress at break. Stress at failure ranged from 0.7 – 2.6 MPa for the neutral films and 1.8 – 9.9 MPa for the cationic films (Figure 5.6). The cationic diblock films consistently withstood the highest stress at break, up to 10MPa, however this strength is likely too low for sustained use in a fuel cell (e.g., Nafion has a tensile strength 25-43 MPa) [85].
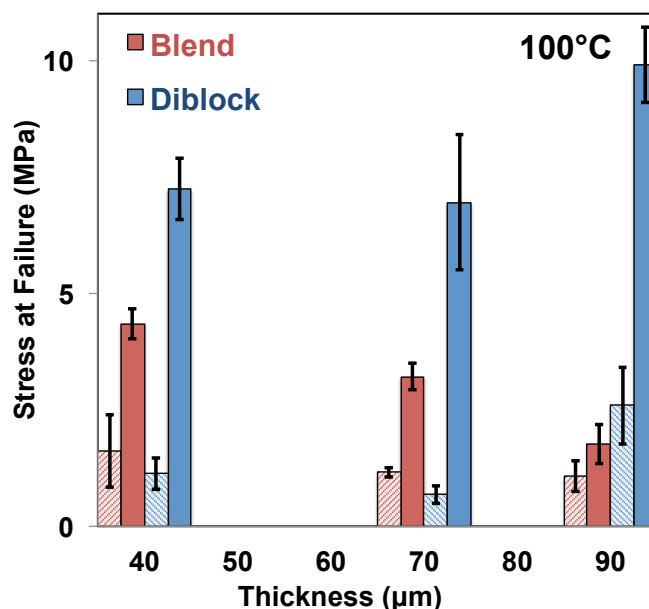
Figure 5.6: The stress at failure is displayed for the four polymer chemistries: neutral blend (red dashed), cationic blend (solid red), neutral diblock (dashed blue), cationic diblock (solid blue).

The higher elasticity of the neutral films correlated with significantly larger elongations compared to the cationic forms. Percent elongation ranged from 200 to 280 % for the neutral films and only 8 to 57 % for the cationic films (Figure 5.7). The larger elongations of the neutral films correlate with smaller stresses at break (Figure 5.6). The low level of elongation in the cationic films would be problematic in a fuel cell where the constrained membrane must be elastic enough to withstand swelling and shrinking that occurs due to humidity changes during operation.
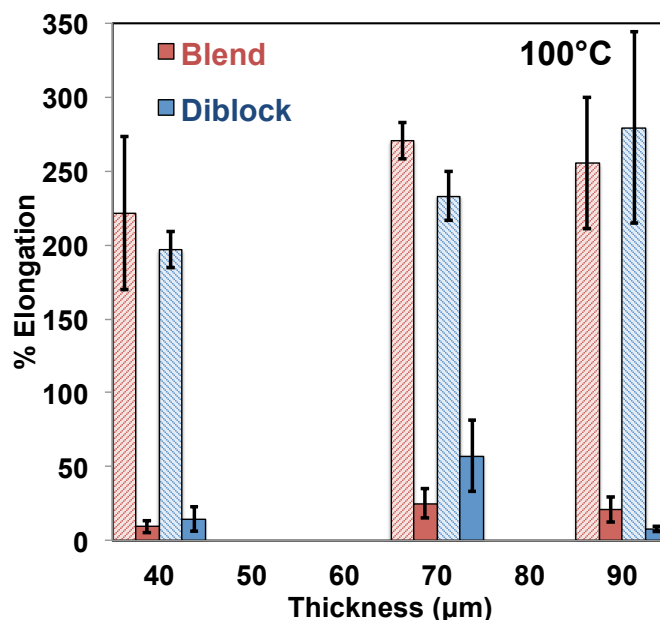
Figure 5.7: The percent elongation is displayed for the four polymer chemistries: neutral blend (red dashed), cationic blend (solid red), neutral diblock (dashed blue), cationic diblock (solid blue).

Functionalization of the films with cations caused an increase in stress at failure but severely decreased percent elongation and elasticity. The stiffening of the polymer films when cations are present decreased the mechanical integrity of the films. The loss of mechanical integrity of the polymer film with the addition of cations is discouraging, but highlights the importance of considering mechanical properties when designing AEM polymers.

In addition to the mechanical testing of the films in the neutral and cationic forms at different thicknesses, the cationic films were tested at 60°C under dry and humidified conditions to determine the effect of water sorption on mechanical properties (Figure 5.8). Films tested at dry and humidified conditions had a nominal thickness of 55 μm. Generally, for ion exchange membranes, water taken up by the polymer acts as a plasticizer, i.e., increasing fluidity, decreasing the modulus and stress, and increasing elongation [75, 104]. The Young's modulus for both the diblock and blend films decreased significantly, from between 515 – 625 MPa to between 200 – 275 MPa, when the films were humidified verifying that the plasticizing nature of

82

the water increases film elasticity. Elongation increases significantly for the diblock film, from 2% at dry conditions to 43% at 95%RH. Elongation of the blend films did not change significantly with water uptake; this could be a result of the low water uptake of the blend film or the difference in phase separation in the blend. The stress at break for the diblock decreased only slightly, to 8 MPa, from the dry state (9 MPa). The brittleness of the dry polymer films resulted in visible crack formation that contributed to the failure of the membrane in the dry state. Maintaining water in the film reduced crack formation allowing greater elongation of the polymer. The blend membrane showed little difference in stress at break between dry and humidified conditions similar to its elongation behavior, likely due to its low water uptake. Unfortunately, while the diblock displayed mechanical improvement with water sorption in terms of elongation and elasticity, better mechanical properties are still needed to be comparable to PEMs [6, 25, 73, 105] and other AEMs [22, 75, 97].
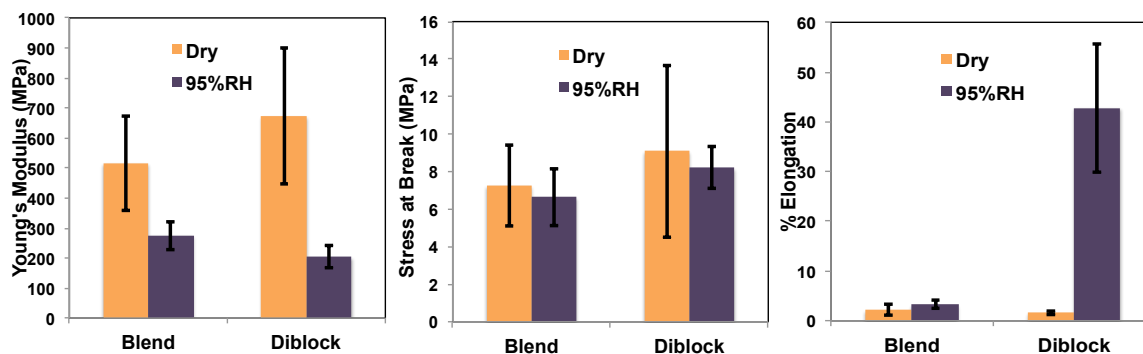
Figure 5.8: a) Stress at break, b) % Elongation, and c) Young's Modulus for the blend and diblock cationic films at 60°C under dry and humidified conditions.

5.5 Conclusions

The chemical and mechanical properties of a diblock copolymer composed of a hydrophobic, polystyrene block and a hydrophilic, conductive poly(vinylbenzyl trimethylammonium) block were compared to an analogous homopolymer blend. SAXS of the diblock suggested nanoscale size ordering that was dependent on water uptake by the polymer.

Nanoscale features were absent for the homopolymer blend due to the phase separation on the order of 10 μm. The nanometer phase separation of the diblock is favorable for ion conduction, while the micrometer scale phase separation of the homopolymer blend hinders ion conduction. Conductivity of the diblock was comparable to other leading AEMs and was an order of magnitude higher than the homopolymer blend, due to its higher IEC and nanometer scale phase separation. Mechanical integrity of the films was reduced when quaternary ammonium cations were present in the polymer. Percent elongation and elasticity were significantly lower for the cationic polymer films compared to their neutral counterparts. Water taken up by the polymer has a plasticizing effect on the films, increasing elasticity and elongation. The blend films displayed less mechanical response to humidity, likely due to their lower water uptake. While the nanoscale phase separation of the diblock copolymer produced good ionic conductivity, the high stiffness and low elongation of the films could lead to mechanical failure in an AEM fuel cell. Future work will replace the stiff polystyrene block with a more elastic hydrophobic polymer to improve mechanical properties of the AEM. This study highlights the importance of considering mechanical performance, as well as conductivity, when designing polymers for anion exchange membranes.

5.6 Acknowledgements

CHAPTER 6 : MECHANICAL PERFORMANCE OF POLYIOSOPRENE COPOLYMER
ANION EXCHANGE MEMBRANES BY VARYING CROSSLINKING METHODS

6.1 Abstract

Anion exchange membranes (AEM) are attractive electrolytes for alkali fuel cells and electrochemical devices due to facile kinetics and potential for non-precious metal catalysts. Fabrication of mechanically durable AEMs with high ionic conductivity is a challenge. Here, conductivity and mechanical properties of two random polyiosoprene based copolymers, crosslinked by various methods, were investigated across all hydration levels. Polymer chemistry and degree of crosslinking had significant affects on conductivity, swelling, and mechanical properties. The addition of polystyrene created a terpolymer with a higher ion exchange capacity (IEC), which could still be rendered insoluble by crosslinking. The higher IEC of the terpolymer resulted in higher chloride conductivity, 20 - 75 mS/cm at 50°C and 95%RH, compared to 4 - 17 mS/cm for the copolymer at the same conditions. At dry conditions films were stiff, having Young's moduli between 100 - 740 MPa, but hydration caused severe softening, reducing moduli by 1 - 2 orders of magnitude. The severe softening effect of hydration was confirmed by dynamic mechanical analysis. The AEMs studied did not have adequate mechanical durability at hydrated conditions, thus additional optimization of polymer chemistry and crosslinking are required to produce robust AEMs for fuel cells and electrochemical devices.

6.2 Introduction

Fuel cells are attractive energy conversion devices that utilize hydrogen to produce electrical energy that can power both stationary and transportation applications with the by-product being water [4, 6]. Electrolyzers utilize a similar principle to produce hydrogen from water using electrical energy. Fuel cells and electrolyzers both utilize a polymer electrolyte

membrane to separate the catalyst layers and efficiently transport ions, while limiting crossover of other species [3, 6]. Proton exchange membranes (PEM), specifically perfluorosulfonic acid polymers such as Nafion[®], have been utilized almost exclusively for current fuel cells, owing to their high proton conductivity and suitable chemical and mechanical stability [2, 19]. While PEM fuel cells have been widely researched and developed over the last few decades, anion exchange membrane (AEM) fuel cells offer potential advantages over PEMs [8, 9, 18, 70]. The alkali nature of AEMs improves kinetics allowing opportunities for non-precious medal catalysts [9, 70]. On going research seeks to develop robust, well performing AEMs for use in fuel cells, electrolyzers, and other electrochemical devices.

Anion exchange membranes must have a high ionic conductivity and be chemically and mechanically stable over the lifetime of the fuel cell [9, 70]. Chemical stability is a concern in AEMs as hydroxide ions present in the membrane have the potential to degrade the polymer backbone and cation functionalities [9, 49, 75]. Hydroxide transport is inherently slower than proton transport, to compensate the concentration of ion groups is often increased in AEMs. Increasing cation concentration in the polymer can significantly increase water uptake, causing dimensional swelling of the membrane and loss of mechanical integrity [70]. The membrane must be mechanically robust over a range of temperature and humidity conditions experienced in a working fuel cell [106, 107]. At high hydrations the membrane swells with water, but at lower hydrations, drying causes contraction of the membrane and produces significant hygrothermal stresses [7, 26, 106]. During repeated humidity cycles these hygrothermal stresses can cause pinholes and cracks in the membrane, which contribute to the eventual failure of the membrane. A membrane must be elastic enough to accommodate for swelling and contraction due to humidity changes, and strong enough to withstand the associated hygrothermal stresses [108]. A

successful AEM must combine high conductivity and mechanical durability, making simultaneous study of these two aspects critical for new AEM development.

One method to improve mechanical performance and durability of AEMs and reduce swelling is by crosslinking of polymer chains [109, 110]. Crosslinking can be applied to the inert portions of the polymer backbone or at the cation sites, and can be performed in solution or after the polymer is cast into a solid film. Crosslinking of noroborene monomers has produced high conductivity AEMs with good mechanical performance and limited swelling [111, 112]. Crosslinking utilizing diamines to produce dication functionalities between polymer chains has also been demonstrated for AEMs [113-116]. Use of more exotic cations, such as quaternary phosphoniums, can also be used as a crosslinker and have been shown to dramatically reduce membrane swelling [117]. Direct polymerization of quaternary ammonium cyclooctenes during membrane casting was used to produced mechanically stable crosslinked membranes with good ionic conductivity [22]. Crosslinking is a tunable method that can be applied to AEMs to improve mechanical stability and reduce swelling, while maintaining ionic conductivity.

In this study two polyiosoprene copolymers were crosslinked and evaluated in terms conductivity and mechanical performance at a range of hydrations. A random copolymer of polyiosoprene and poly(vinylbenzyl trimethylammonium) (PI-ran-PVBTMA) and a terpolymer of polyiosoprene, poly(vinylbenzyl trimethylammonium), and polystyrene (PI-ran-PVBTMA-ran-PS) were investigated. Conductivity of the two polymers were measured and correlated to extent of crosslinking and mechanical properties. Extensional properties of the membranes were measured with an extensional rheometer platform to simulate a tensile tester with small membrane samples. A tensile geometry allowed dynamic mechanical analysis with small amplitude oscillatory strain experiments to evaluate moduli changes over a range of temperatures.

87

Temperature and humidity were controlled during mechanical testing to determine the affect of hydration on membrane performance.

6.3 Experimental

The polyiosoprene copolymer was synthesized as previously reported [118] with and ion exchange capacity (IEC) of 1.5 mmol/g (Figure 6.1). The terpolymer was synthesized by a similar procedure: isoprene (24 ml, 240 mmol), 4-vinylbenzyl chloride (9 ml, 63.9 mmol) and styrene (1.85 ml, 16.1mmol) were transferred into a 50 ml Schlenk flask. 61.6 mg (0.159 mmol) SG1 BlockBuilder™ catalyst was added. The flask was immersed in an ice bath, and the contents of the flask were purged with nitrogen for 30 minutes. Reaction was initiated by immersing the reaction flask into an oil bath at 125°C. After 18 hours the reaction was quenched. Polymer was recovered by precipitating in excess methanol. Subsequent quaternization with trimethylamine (TMA) results in a terpolymer with an IEC of 2.3 mmol/g.
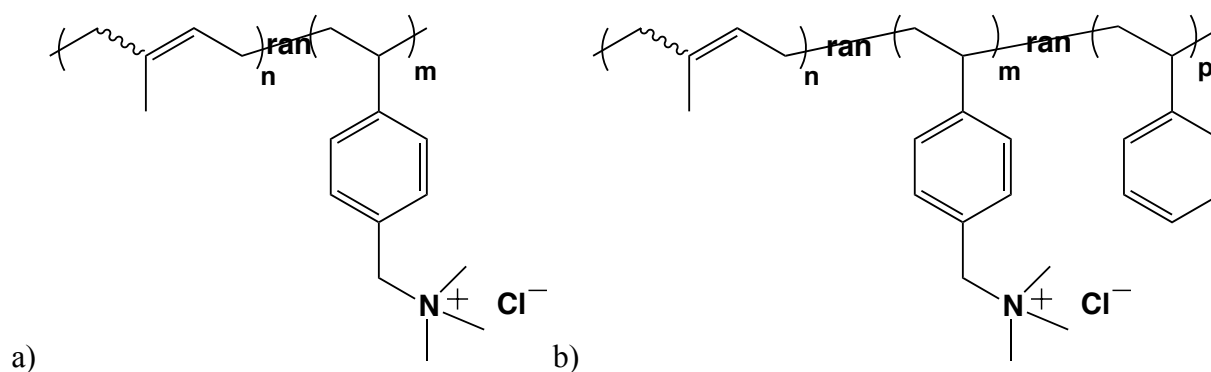
Figure 6.1: Chemistry of the a) copolymer and b) terpolymer prior to crosslinking.

6.3.1 Film preparation and crosslinking

For thermally crosslinked films, the polymers were dissolved in ethanol at 22wt%. The polymers were mixed at room temperature for 4 h, sonicated at 30°C for 1.5 h, and again stirred at room temperature for 1 h. The solution was poured on a Teflon substrate and a doctor blade

with a 500 micron gap height was traversed over the solution at 20 mm/s using an automatic film applicator (MTI Corporation's MSK-AFA-III, Richmond, CA). The films were allowed to dry overnight at a room temperature in a fume hood. To induce crosslinking, the films were placed in an oven at 145°C for a duration of 3 or 24 hours. After removal from the oven, the films were allowed to cool, removed from the Teflon substrate, and placed in water at room temperature to allow for dimensional swelling. The films were removed from the water after 1 h and allowed to dry at room temperature. Films were stored under dry conditions for further testing.

The photocrosslinked (UV) films had a photoinitiator and crosslinking agent added to the casting solution. The photoinitiator, 2-Hydroxy-4′-(2-hydroxyethoxy)-2-methylpropiophenone (Sigma Aldrich), was added to ethanol at 1.5wt%. The polymer was dissolved in the ethanol/initiator solution at the same concentration as the thermally crosslinked films (22wt%). The solution was mixed in the dark, at room temperature for 4 hours and sonicated at 30°C for 1.5 h. After sonication the crosslinking agent, 1,10 decanedithiol (Alfa Aesar), was added to the polymer solution and mixed for 1 h at room temperature, avoiding light exposure. Dithiol crosslinking agent was added in a 3:1 ratio to the number of 1,2 and 3,4 addition double bonds on the polyisoprene, as determined by ^{1}H NMR. The 1,2 and 3,4 addition double bonds are susceptible to chemical crosslinking with the dithiol. Addition of the photoinitiator and dithiol crosslinker lowers the polymer IEC because inert mass is added to the film. The copolymer IEC was reduced to 0.9 mmol/g and the terpolymer was reduced to 1.5 mmol/g. The polymer solution was casted using the automatic film applicator using the same method described for the thermally crosslinked films. After casting, the films were covered to prevent light exposure and allowed to dry at room temperature in a fume hood. The dry film was crosslinked by exposure to UV light using a F300 Series Fusion UV curing system with a P300MT power supply. The film

was passed through the curing system four times at a speed of 15 ft/min with a power of 300 W/in. After UV crosslinking the films were removed from the Teflon substrate, submerged in water for 1 h, and allowed to dry before subsequent testing.

6.3.2 Conductivity

Conductivity was measured by electrochemical impedance spectroscopy using a four-electrode in-plane conductivity cell. Impedance spectra were obtained over a frequency range of 1 to 10^6 Hz using a multi-channel potentiostat (BioLogic VMP3). A TestEquity sample chamber controlled temperature and humidity during data acquisition. Membrane resistance was defined as the low frequency intercept of the Nyquist impedance plot and conductivity was calculated based on equation (6.1).

$$\sigma = \frac{l}{R \cdot t \cdot w} \qquad (6.1)$$

Where R is the membrane resistance, l is the length between electrodes, and t and w are the thickness and width of the membrane sample, respectively. Reported conductivity data are the average of at least three separate membrane samples and multiple impedance spectra at each steady state temperature; error bars are one standard deviation.

6.3.3 Water Uptake

Water uptake was measured gravimetrically after soaking in liquid water for 24 h compared to samples dried under vacuum overnight at 40°C. Samples were weighed three times and averaged. Wet samples were removed from liquid water, blotted dry, and quickly weighed to prevent drying. Water uptake was calculated based on equation (6.2).

$$WU = \frac{m_w - m_0}{m_0} \times 100 \qquad (6.2)$$

Where m_w is the mass of the water soaked samples and m_0 is the dry mass of the sample.

6.3.4 Membrane Swelling

Dimensional swelling of the membrane was determined by measuring film dimensions in dry and wet states. Membrane samples were dried overnight in a vacuum oven at 50°C. In-plane dimensions were measured using a Marathon electronic digital caliper (0–150 mm, with 0.01 mm accuracy) and thickness measurements were made using a Marathon electronic digital micrometer (0–25 mm, with 0.002 mm accuracy). Membrane samples were placed in water at room temperature for 24 h to take up water. Samples were removed from water, blotted to remove surface water, and quickly measured to prevent drying. Percent swelling was calculated with respect to in-plane and through-plane dimensions.

6.3.5 Extensional Testing

A Sentmanat extension rheometer (SER) (Xpansion Instruments) fixture on an ARES G2 rheometer (TA Instruments) was utilized for extensional testing. The SER fixture typically measures elongation viscosity of polymers in their melt state, but has also been shown to measure tensile properties of solid polymer films [38, 97]. The SER fixture has two counter-rotating drums that suspend the film. The drums rotate, stretching the film to its failure point, while the stress applied to the film is measured by the rheometer. The stress vs. strain curve is used to calculate Young's modulus, elongation, and ultimate strength. The Young's modulus is defined as the slope of the initial, elastic deformation region of the stress vs. strain curve, and is a measure of the film elasticity. Elongation and strength are defined by the strain and stress, respectively, at the film's failure point. Reported values (Young's modulus, strength, and elongation) were the average of at least five samples and corresponding error is one standard deviation.

A custom-built sample chamber was utilized to control temperature and humidity simultaneously. An aluminum sample chamber with electrical heaters was used to control sample temperature. Two mass flow controllers (10,000 SCCM, MKS 1179A) supplied wet and dry gas flows to the sample chamber. The wet gas line passed through a humidity bottle (FCT, Inc.) with 10 m of Nafion® tubing that saturated the gas stream with water. The gas was delivered to the sample chamber through heated lines to prevent condensation. Extensional tests were performed at 30°C and 60°C at dry and saturated conditions.

6.3.6 Dynamic Mechanical Analysis

The ARES G2 rheometer was used to perform DMA testing using a film/fiber rectangular tension geometry. The rectangular tension geometry has two screw-down clamps that hold the sample in tension while a small-amplitude oscillatory strain is applied to the film. DMA tests were performed under dry or saturated conditions while ramping temperature from 30°C to 70°C at 0.5°C/min. Samples were approximately 6 mm (W) by 25 mm (L), but were loaded at a starting gap height of 10 mm. A oscillatory strain of 0.1% was applied at a frequency of 1 Hz. Samples were maintained at minimum axial tension force of 0.008 N and the axial force was set to be at least 20% greater than the oscillatory strain force applied to the film. Under hydrated conditions the films were extremely soft and maintaining tension on the sample resulted in significant sample elongation as temperature was ramped. Films were loaded at ambient conditions, for saturated humidity tests the samples were allowed to equilibrate and take up water at 30°C and 90% relative humidity for 1 h prior to the start of the test. For dry tests the samples were allowed to equilibrate at 30°C and <10%RH for 10 min prior to the start of the test. DMA tests were repeated at least twice at each condition to confirm a consistent moduli response; tests were limited due to sample availability.

6.4 Results

Duration and method of crosslinking had a significant impact on film conductivity, water sorption, and mechanical performance. Increased crosslinking reduced water uptake and improved mechanical properties, but lowered ionic conductivity. Polymer chemistry and ion concentration also influenced membrane performance. Optimizing polymer chemistry, ion concentration, and crosslinking will improve AEM performance and durability.

6.4.1 Conductivity

In-plane conductivities of the copolymer and terpolymer films were measured as a function of temperature (50 - 90°C) at a constant relative humidity of 95% (Figure 6.2). Overall, the terpolymer had higher conductivity, ranging from 20 - 76 mS/cm at 50°C, compared to the copolymer, 4 - 17 mS/cm, as a result of the terpolymer's higher IEC. Crosslinking method and extent of crosslinking had a significant influence on membrane conductivity. The UV crosslinked films have IECs reduced from the parent polymer, due to the addition of the inert crosslinking agent. Decreasing the IEC results in lower conductivity for the UV crosslinked films. For example, the UV crosslinked copolymer film had 35% lower conductivity compared to the thermally crosslinked copolymer films. The UV crosslinked terpolymer has lower conductivity than the 3 hr thermally crosslinked film, but slightly higher conductivity compared to the 24 hr thermally crosslinked film. The short duration (3 hr) thermally crosslinked films had the highest conductivity in both the copolymer and terpolymer systems, due to the lower degree of crosslinking and higher swelling that allows better ion mobility. The 3 hr thermally crosslinked films could only be measured at lower temperatures; at higher temperatures the polymers became fluid-like and flowed out of the conductivity cell during testing. Three hours of thermal crosslinking was not enough to render the films insoluble at higher temperature conditions; this

hydration effect will be further explained in the mechanical properties study below. The 3 hr thermally crosslinked terpolymer film had measurable conductivity up to 80°C, while the copolymer was immeasurable after 65°C. The terpolymer has better film integrity at higher temperatures under hydrated conditions, despite the fact that the terpolymer has a higher IEC. The addition of glassy polystyrene to the polymer matrix improves film integrity allowing the higher IEC terpolymer to remain a solid film at higher temperatures when hydrated.
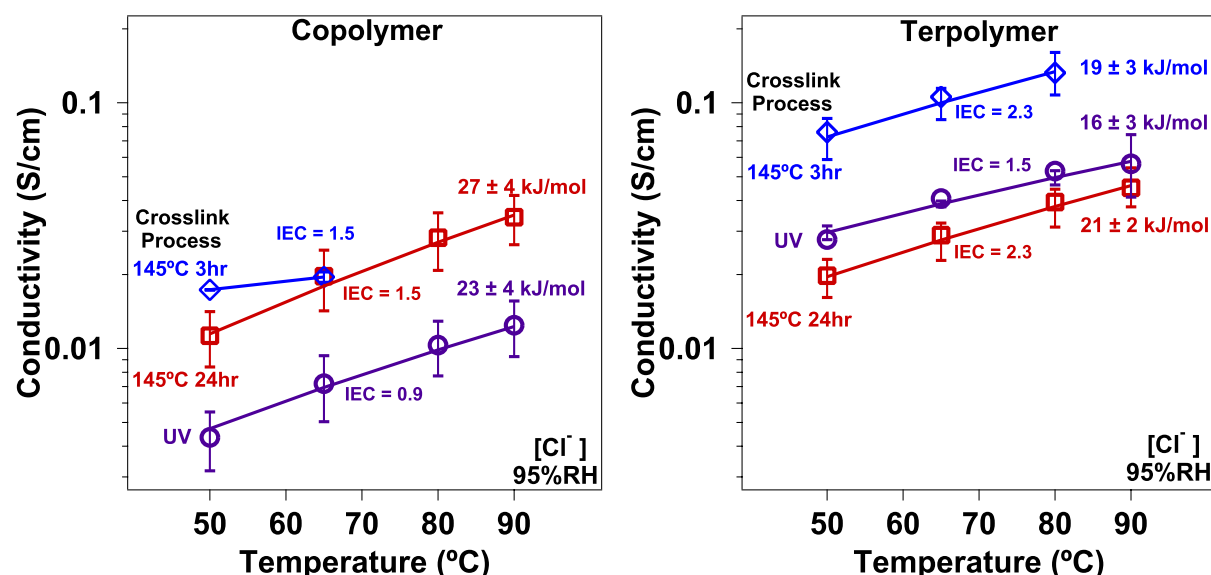
Figure 6.2: Conductivity of the copolymer and terpolymer films crosslinked either thermally at 145°C for 3 or 24 hrs, or UV crosslinked

6.4.2 Water Uptake

Water uptake was dependent on polymer chemistry and crosslinking method (Figure 6.3). A low degree of crosslinking (3 hr thermal) resulted in significant water uptake by the film, 830% and 450% for the copolymer and terpolymer, respectively. Increasing the degree of crosslinking (24 h thermal and UV) reduces the water uptake. Water uptake for the copolymer was reduced to 24% for the 24 h thermally crosslinked and 18% for the UV crosslinked films. The terpolymer films had higher water compared to the copolymer, 96% for the 24 h thermally crosslinked and 62% for the UV crosslinked. The copolymer has a higher percent of isoprene (87

94

mol%) compared to the terpolymer (71%), so more crosslinkable units are present in the copolymer. The large number of crosslinkable units, along with a high degree of crosslinking in the 24 hr thermally and UV crosslinked copolymer films prevents significant water uptake. The lower number of crosslinkable units in the terpolymer, along with its higher IEC, causes water uptake to be higher, even when degree of crosslinking is high (24 hr thermal and UV crosslinked). While water uptake is critical to maintain ion conduction, excess water uptake causes significant membrane welling and can weaken the film to the point of mechanical integrity loss.
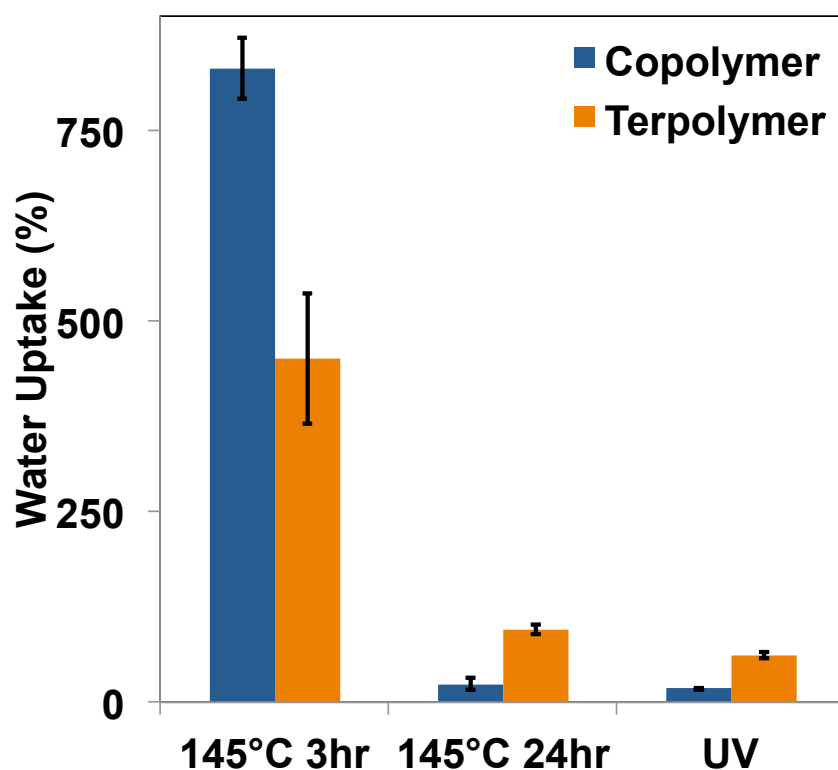
Figure 6.3: Water uptake of the copolymer and terpolymer as a function of on crosslinking method.

6.4.3 Membrane Swelling

The extent of crosslinking impacted initial dimensional swelling, when the cast films were soaked in water and subsequently dried. The films crosslinked for a short duration (3 hr)

had larger dimensional swelling and did not fully contract back when drying. This resulted in the 3 hr crosslinked films being significantly thinner (20-30 microns) compared to the 24 hr crosslinked films (60-70 microns) and UV crosslinked films (90-110 microns).

Dimensional swelling between dry and hydrated states can affect mechanical integrity of the membrane and assembly during operation. Dimensional swelling was influenced by polymer chemistry and crosslinking, and a directly related to measured water uptake (Figure 6.4). The 3 hr thermally crosslinked copolymer film had the highest degree of swelling at 118% in the in-plane direction, through-plane swelling was much lower at 16%. The other copolymer films (24-hr thermally and UV crosslinked) had significantly lower dimensional swelling, 12-15% in-plane and 5-6% through-plane. Compared to the copolymer, the terpolymer had a higher degree of swelling (excluding the high in-plane swelling of the 3 hr thermally crosslinked copolymer). The terpolymer had similar in-plane swelling for all films, 44% and 54% for the 3 hr and 24 hr thermally crosslinked respectively, and slightly less for the UV crosslinked at 34%. Through-plane swelling was highest for the 3-hr thermally crosslinked film at 58% and this was the only
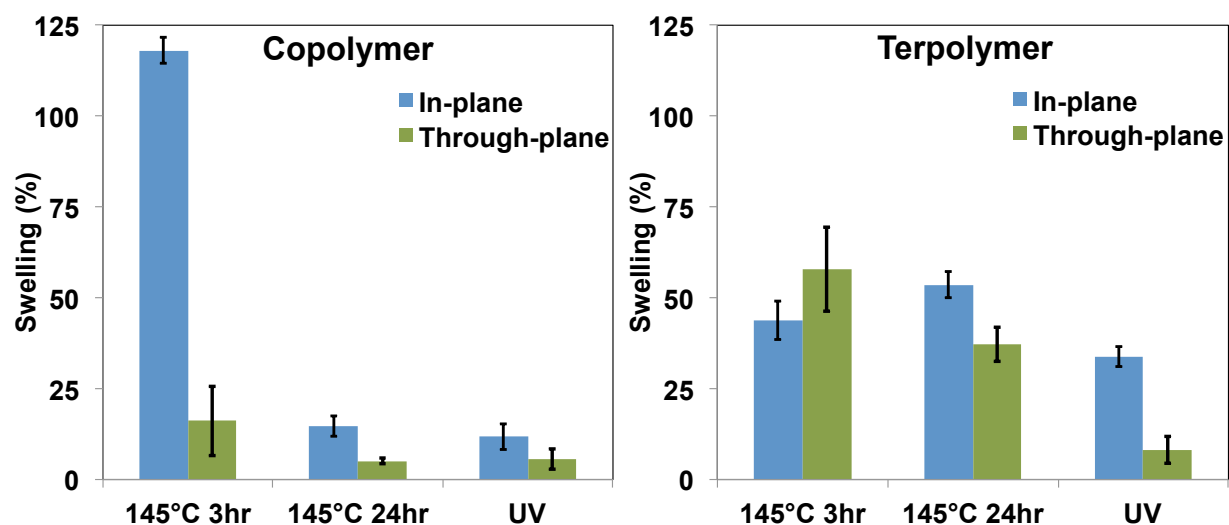
Figure 6.4: Dimensional swelling of the copolymer and terpolymer measured after soaking in water for 24 hrs compared to films vacuum dried at 50°C overnight.

film to have a higher through-plane swelling than in-plane swelling. Through-plane swelling was 30% lower compared to in-plane for the 24 hr thermally crosslinked terpolymer and 76% lower for the UV crosslinked terpolymer. Limiting dimensional swelling is important to prevent membrane degradation and assembly damage when a fuel cell undergoes humidity changes, and crosslinking is one technique to successfully reduce dimensional swelling.

6.4.4 Extensional Tests

Extensional tests were performed at 30°C and 60°C under dry and hydrated conditions. Films were extremely stiff at dry conditions and underwent severe softening when hydrated (Figure 6.5) causing films to become extremely weak. Under dry conditions, all films are stiff having moduli between 100 and 740 MPa; this is comparable to moduli reported for other AEMs [97, 119-121]. Generally, the terpolymer was slightly stiffer than the copolymer due to the addition of glassy polystyrene to the polymer matrix. A lower degree of crosslinking (3 hr thermal) resulted in softer films than those with a higher degree of crosslinking (24-hr thermal/UV). All films were severely softened at hydrated conditions due to the plasticizing effect of water in the film. At 30°C, the 24 hr thermally crosslinked films had the smallest decrease in moduli from dry to hydrated states, however reduction was still 76% for the copolymer and 90% for the terpolymer. The 3 hr thermally and UV crosslinked films all had at least a 95% reduction in modulus from dry to hydrated states. Humidifying the films at higher temperature, 60°C, caused several of the films to soften to the point that the measured stress was below the noise level of the instrument. Extensional properties were not measurable for the 3-hr thermally crosslinked films or the 24 hr thermally crosslinked copolymer at 60°C and saturated. The 24 hr thermally crosslinked terpolymer was measurable, suggesting that adding polystyrene to the polymer matrix improves mechanical durability when hydrated, despite the terpolymer's

higher IEC. Both UV crosslinked films were measurable at the 60°C and saturated conditions, however measured moduli were extremely low, being 11 MPa for the copolymer and 5 MPa for the terpolymer. These moduli values are low compared to working fuel cell membranes such as Nafion, which has a modulus of 114 MPa in water at 23°C [85].
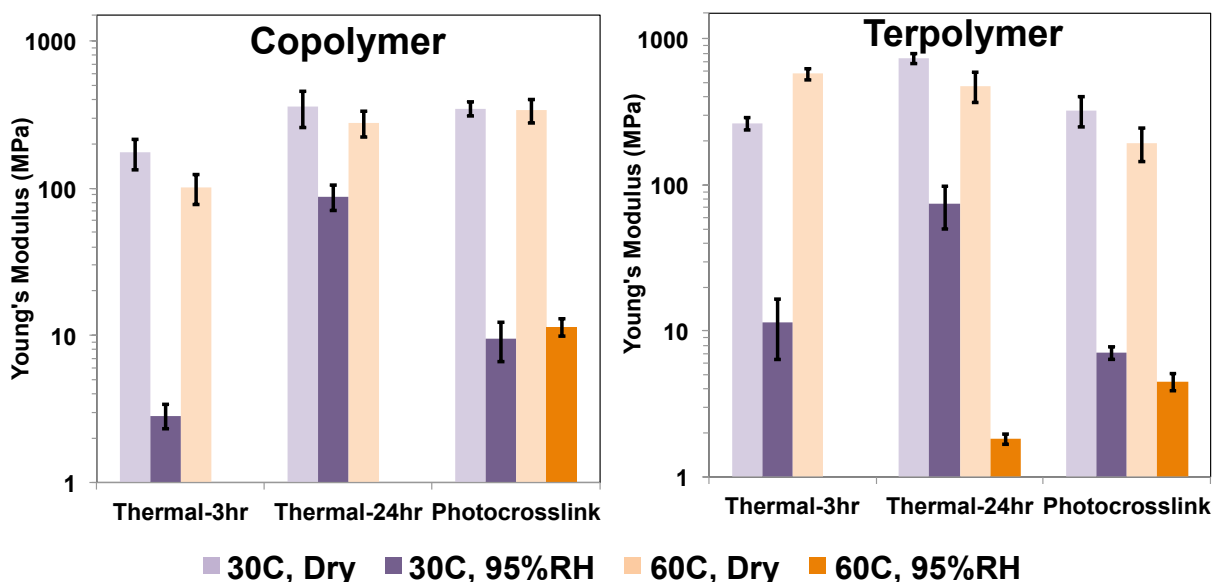
Figure 6.5: Young's Moduli (on a log scale) of the copolymer and terpolymer based on crosslinking technique.

While the moduli values of the films were fairly high at dry conditions, the stress to failure was low to moderate compared to other AEMs (5 - 70 MPa) [42, 75, 97], crosslinked AEMs (2 - 27 MPa) [22, 111, 112] and PEMs (20 - 50MPa) [19, 85] (Figure 6.6). At dry conditions the thermally crosslinked copolymer films had relatively low stress to break, between 3 to 6 MPa, while the thermally crosslinked terpolymer films had slightly higher stress to break, 7 to 15 MPa. The UV crosslinked films had consistently higher stress to break, 13 to 30 MPa for the copolymer and 19 to 20 MPa for the terpolymer. At dry conditions the copolymer had a slight decrease in strength from 30°C to 60°C, while the terpolymer had little to know change with temperature, likely due to the added polystyrene that is thermally stable within this temperature range. Hydrating the films causes significant reduction in strength due to the severe softening

discussed above. At 30°C film strength was reduced to between 1 MPa to 2.7 MPa, and at 60°C the maximum stress to break measured for any of the films was only 1.4 MPa. The strength of these films at hydrated conditions is insufficient and the extreme differences in mechanical properties between dry and hydrated states could cause membrane degradation and assembly failure.
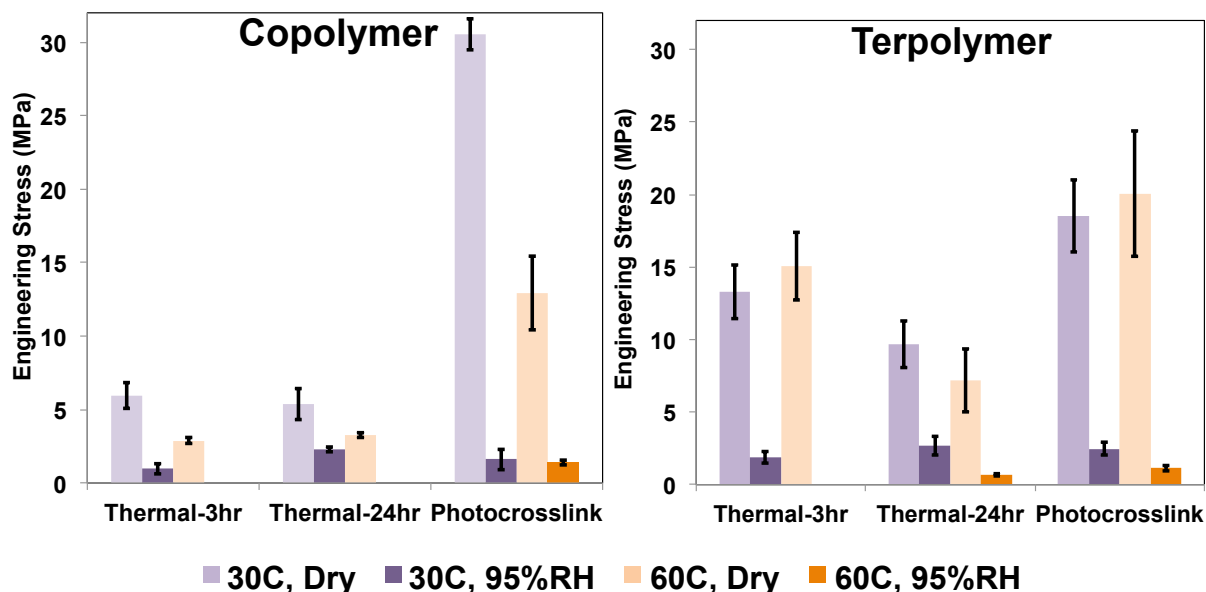
Figure 6.6: Engineering stress of the copolymer and terpolymer based on crosslinking technique.

Adequate film elongation is important to accommodate dimensional changes with swelling (Figure 6.7). At dry conditions the films have low elongation, and elongation decreases with crosslinking duration. The 3 hr thermally crosslinked films have dry elongations about 15%, except for the terpolymer at 60°C, while the 24 hr thermally crosslinked films have lower elongations between 2% to 3%. The UV crosslinked films have slightly higher dry elongations between 10% to 23%. The low degree of crosslinking in the 3 hr thermally crosslinked films causes elongation to increase dramatically when hydrated, up to 130% and 100% for the copolymer and terpolymer, respectively, at 30°C. Alternatively, the higher degree of crosslinking for the 24 hr thermally crosslinked films results in relatively small increase in elongation, up to

7% for both the copolymer and terpolymer at 30°C. Elongation of the UV crosslinked films is much more consistent across different temperature and hydration conditions, the copolymer film ranges from 10% to 19% while the terpolymer ranges from 21% to 31%. The narrow range of elongations of the UV crosslinked films suggests that UV crosslinking provides greater mechanical stability compared to the thermal crosslinking.
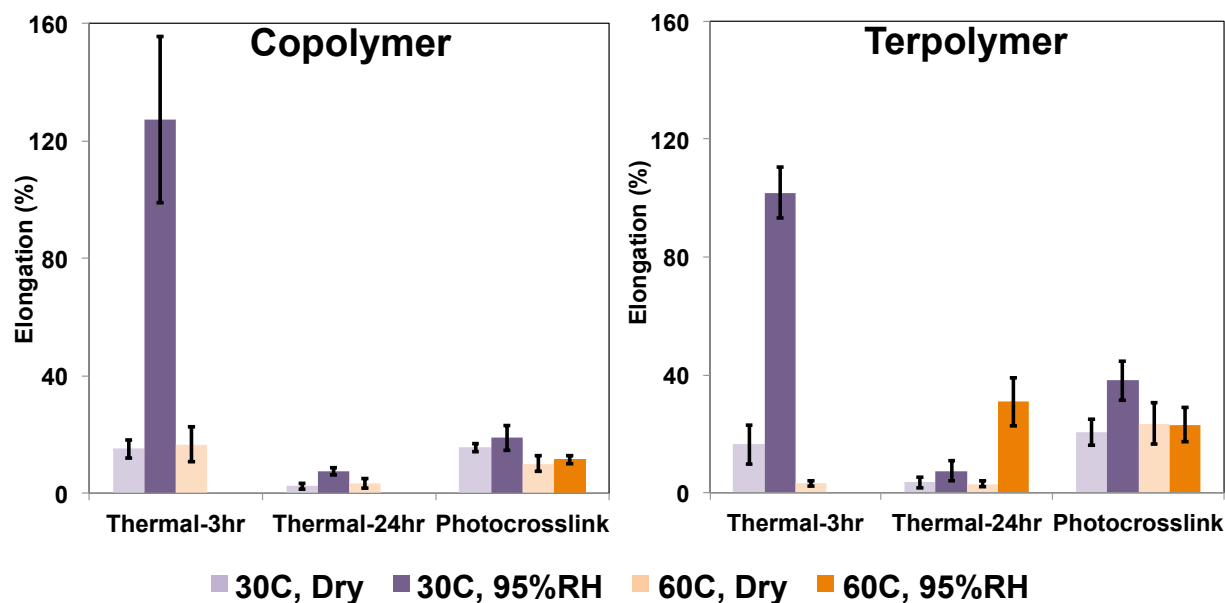
Figure 6.7: Elongation of the copolymer and terpolymer based on crosslinking technique.

Extensional tests revealed dramatic differences in the mechanical properties of the crosslinked polymer films from dry to hydrated states. The films were relatively stiff at dry conditions, particularly as the degree of crosslinking was increase by increasing crosslinking duration. While stiff, the films had relatively low strength and elongation at dry conditions. Hydrating the films caused severely softening and weakening of the films, to the point that at higher temperature some films were immeasurable and were deemed to have lost film integrity. Overall, the UV crosslinked films had better, more consistent, mechanical properties over the range of temperatures and hydrations tested. Ultimately, while crosslinking increased film stiffness, these films are too weak when hydrated for use in an electrochemical device. The

extreme disparity between dry and hydrated mechanical properties, and the fact that some films were immeasurable at high hydrations, warranted further study by dynamic measurements of mechanical behavior.

6.4.5 Dynamic Mechanical Analysis

Dynamic mechanical analysis observed moduli changes while ramping temperature from 30°C to 70°C at dry or saturated relative humidity conditions (Figure 6.8). DMA distinguished mechanical changes due to temperature compared to those due to hydration level. At dry conditions, little change in storage modulus was measured between 30°C and 70°C. The copolymer films had slightly different moduli based on crosslinking technique (750 - 1500 MPa at 30°C) that decreased little as temperature was ramped to 70°C. Alternatively, the terpolymer films moduli do not change with crosslinking method and are consistent over the 30°C to 70°C temperature range, having moduli around 1000 MPa for all films tested.
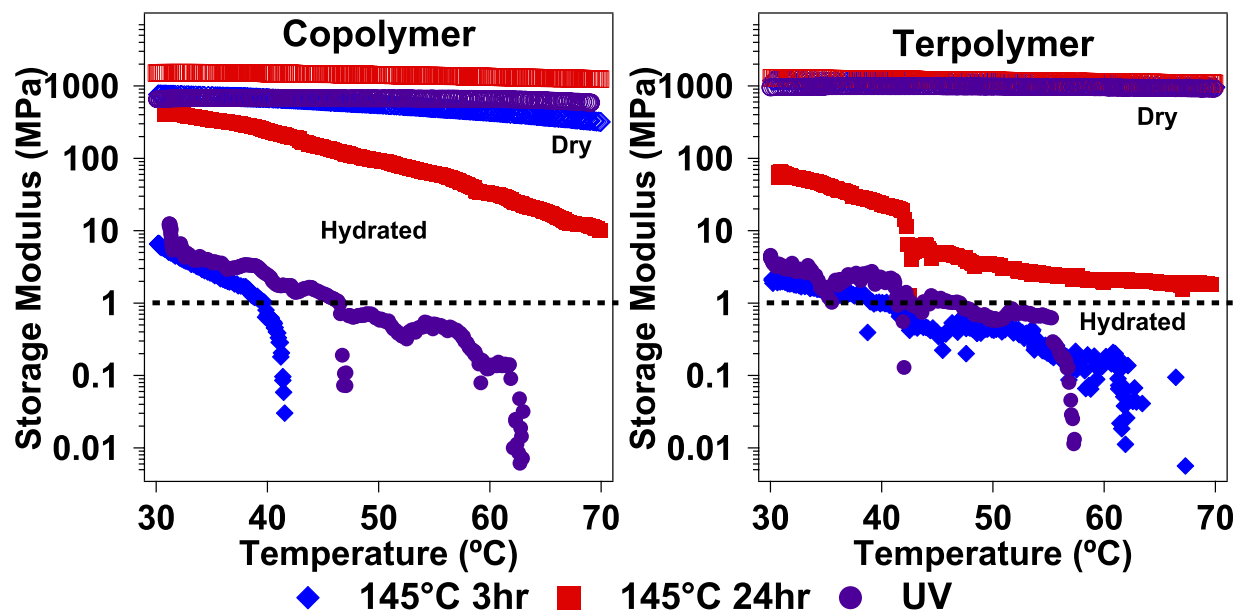
Figure 6.8: Storage modulus vs. temperature for the copolymer and terpolymer, solid points are at saturated relative humidity and the unfilled data points are at dry conditions. The dashed line shown is defined as minimum modulus for film integrity.

Compared to the narrow change in moduli with temperature at dry conditions, the response of the films at saturated conditions were significant, spanning orders of magnitude. The films had moduli one to two orders of magnitude lower than the dry films at 30°C. The 24 hr thermally crosslinked films were measurable over the entire temperature range, while the softer 3 hr thermally and UV crosslinked films became so soft as temperature increased that moduli became immeasurable. A sharp decrease in modulus, indicating severe softening, was observed for the 3 hr thermally and UV crosslinked films. While magnitude and change in moduli were consistent between tests, the temperature for the onset of modulus decrease varied slightly between runs (1 - 8°C), so rather than define film integrity loss by the onset of the modulus decrease we defined a modulus of minimum integrity as 1 MPa (dashed line in Figure 6.8). The temperature when the minimum modulus was reached, was independent of chemistry; both of the 3 hr thermally crosslinked films reached this minimum modulus at 40°C while the minimum moduli for UV crosslinked films were at 46°C for the copolymer and 47°C for the terpolymer. The modulus of the 24 hr thermally crosslinked films remained above the 1 MPa for the entire temperature range.

Overall, saturated humidity conditions lead to a sharp decrease in moduli, even to the point of being immeasurable, as temperature is increased. Conversely, a nearly constant moduli at dry conditions demonstrates the significance of membrane hydration to mechanical performance and membrane integrity. Anion exchange membranes must be mechanically stable over a large range of temperature and humidity conditions, the change in moduli by orders of magnitude from dry to saturated conditions makes these crosslinked films inadequate for a working fuel cell or electrochemical device.

6.5 Conclusions

In this work, two polyiosoprene based copolymers were crosslinked by various methods to render insoluble anion exchange membranes. The terpolymer of study had a small amount of polystyrene added to the polymer matrix in addition to the polyiosoprene and conductive vinylbenzyl trimethylammonium units. The addition of glassy polystyrene allowed higher ion concentrations and improved membrane integrity following crosslinking. Three crosslinking methods were investigated, thermal crosslinking at two durations (3 or 24 hrs) and UV crosslinking with a dithiol crosslinker. Reduction of IEC due to UV crosslinking led to lower conductivity. A shorter duration of thermal crosslinking increased conductivity, but films became fluid-like at higher temperatures when hydrated causing loss of solid film integrity. The copolymer films were more resistant to swelling due to the larger number of crosslinkable isoprene units and lower IEC.

Mechanical properties of the crosslinked films were highly dependent on hydration level. Dry films were stiff with relatively low strength and elongation. Hydrated films were extremely soft and even weaker, but had higher elongation. UV crosslinked films had more consistent mechanical properties than the thermally crosslinked films, but still suffered poor mechanical integrity at hydrated conditions that would be insufficient for a fuel cell. Dynamic mechanical analysis demonstrated the difference in mechanical properties was due to hydration not thermal transitions, i.e., the dry films were stable over the range of temperatures tested. Saturated conditions caused moduli to be reduced to the point of being immeasurable. While crosslinking rendered solution processed films insoluble, the extreme disparity of the films' mechanical properties between dry and hydrated states is unacceptable for fuel cell operations. Optimization of polymer chemistry and crosslinking is required to achieve the desired narrow range of

mechanical properties that can withstand dimensional swelling and hygrothermal stresses associated with humidity changes for sustained use in a fuel cell or electrochemical device.

6.6 Acknowledgements

CHAPTER 7 : EFFECT OF HYDRATION ON THE MECHANICAL PROPERTIES AND ION CONDUCTION IN A POLYETHYLENE-B-POLY(VINYLBENZYL TRIMETHYLAMMONIUM) ANION EXCHANGE MEMBRANE

7.1 Abstract

Anion exchange membranes (AEM) are promising solid polymer electrolytes utilized in alkali fuel cells and electrochemical energy conversion devices. AEMs must efficiently conduct ions while maintaining chemical and mechanical stability at a range of operating conditions. The ionic nature of AEMs tends to make membranes stiff and brittle under dry conditions, but water sorption at higher hydrations causes significant softening and weakening of the membrane. In this work, a new polyethylene-b-poly(vinylbenzyl trimethylammonium) polymer (70 kg/mol) was investigated that could be cast into large (300 cm^2), thin (12 ± 3 μm) membranes. These membranes exhibited improved elasticity over previously tested AEMs, minimal dimensional swelling, and decent ionic conductivity (5 ± 2 mS/cm at 50°C, 95%RH in the bromide form). Extensional testing indicated a 95% reduction in Young's modulus between dry and hydrated states. Further investigation of the complex modulus as a function of hydration, by dynamic mechanical analysis, revealed a sharp decrease in modulus between dry and hydrated states. Mechanical softening was reversible, but the location of the transition displayed hysteresis between humidification and dehumidification. Conductivity increased after membrane softening; suggesting bulk mechanical properties could be used to identify the hydration level required for improved ion transport. Understanding the relationship between ion conduction and mechanical properties will help guide AEM development and identify operating conditions for sustained performance.

7.2 Introduction:

Anion exchange membranes (AEM) can be utilized as solid polymer electrolytes for alkali fuel cells [9, 12, 70]. Compared to proton exchange membrane (PEM) fuel cells alkali AEM fuel cells benefit from facile kinetics and opportunities for non-precious metal catalysts [8, 11, 18]. As a relatively recent field of study, AEMs face a number of developmental challenges before commercial application can be realized. These challenges include chemical stability of the ionic group and polymer backbone, lower ion transport compared to PEMs, and mechanical strength and durability of the membrane. The alkali environment of an AEM fuel cell exposes the membrane to hydroxide ions that can attack the ionic group tethered to the polymer or the polymer backbone itself [12]. A significant amount of ongoing research is directed towards identifying alkali stable polymer chemistries and novel cation functionalities for chemically robust AEMs [49, 112, 122, 123]. Transport of hydroxide ions is inherently slower than protons in PEMs, and to compensate for this factor, ionic concentration is often increased in AEMs [9]. While increasing ion concentration in AEMs will improve ion conduction, a high ion concentration also increases water sorption in the membrane that can negatively impact mechanical integrity and durability [70]. Additionally, dimensional swelling resulting from water uptake can deform the membrane or cause delamination from catalyst layers. Repeated swelling cycles generate stresses inside the membrane that can create pinholes and cracks in the membrane [6]. A successful AEM must efficiently conduct hydroxide ions and be chemically and mechanically stable over the lifetime of the device, however the complex interplay between these properties requires new AEM development to simultaneously consider ion conduction, stability, water sorption, and mechanical properties.

AEMs require a polymer chemistry of dual functionality, often achieved using copolymers, where one section of the polymer is ionic and hydrophilic to promote ion conduction while the other is hydrophobic to maintain the solid integrity of the membrane. Block copolymers are of particular interest due to their ability to phase separate into organized morphologies that generate well-defined ion conduction paths. Polystyrene based diblocks have been synthesized previously that organized into various morphologies including spheres, cylinders, and lamellae depending on the ratio of the polymer blocks[92]. While polystyrene based diblocks have showed good ionic conductivity and ordered morphologies [92], the high T_g polystyrene in an cationic membrane results in stiff, brittle films that do not have adequate mechanical durability for use in electrochemical devices [124]. Replacing the hydrophobic block with a rubbery polymer, such as poly(methyl butylene), produced films with better elasticity and flexibility [118]. Similarly, polyethylene has been incorporated in AEMs. Ring-opening metathesis polymerization of ammonium functionalized cyclic olefins produced crosslinked and non-crosslinked polyethylene copolymer AEMs with good conductivity and mechanical durability [22, 125]. Polyethylene based AEMs with flexible ammonium groups in a crosslinked matrix synthesized by metallocene-mediated copolymerization displayed adequate swelling and exceptional conductivity [126]. Grafting vinylbenzyl chloride units on to polyethylene resin or free-standing films has generated AEMs with decent conductivity and chemical stability [127, 128]. While copolymer and grafted polyethylene AEMs show promising performance, the cationic functionalities are of a random nature, and do not benefit from the well-defined morphologies produced in block copolymer systems. This work investigates a polyethylene-based diblock AEM that will combine organized polymer morphology and good mechanical properties.

Fuel cells operate in a dynamic environment in terms of temperature and humidity resulting in a range of hydration levels in AEMs. At high humidities, water is taken up by the polymer causing dimensional swelling of membranes [7, 71]. Under dryer conditions, the membrane loses water causing film contraction and significant hygrothermal stresses in the polymer [24, 71]. With repeated humidity cycling, these hygrothermal stresses can generate pinhole and cracks in the membrane that contribute to catastrophic failure [26, 27, 71]. AEMs must have adequate elasticity and elongation at dry conditions to accommodate for dimensional swelling without damaging the membrane or causing plastic deformation [7]. Limiting the dimensional swelling of an AEM will improve mechanical durability [7], but the ionic nature of the polymer and the fact that water is required to facilitate ion conduction makes swelling inevitable. Functionalization of a polymer with cations reduces elasticity and elongation [129], making it difficult to produce AEMs that maintain adequate mechanical durability. Additionally, water sorption in AEMs can severely soften and weaken AEMs when they are hydrated, such as the crosslinked membranes discussed in Chapter 6. Producing AEMs that have sufficient elasticity and elongation at dry conditions and maintain adequate strength at hydrated conditions is a continued challenge. Characterization of mechanical properties over the complete range of operating temperatures and hydration levels is critical to the development of robust AEMs.

A polyethylene-b-poly(vinylbenzyl trimethylammonium) was synthesized by anionic polymerization and previously characterized in terms of basic morphology, conductivity, and mechanical properties as a function of block ratio [94]. This AEM polymer can be solution cast to produce large, thin films. In this study, a single block ratio was evaluated to determine mechanical properties as function of humidity and correlated to water content and ion conduction.

7.3 Experimental

The polyethylene-b-poly(vinylbenzyl bromide) (PE-b-PVBBr) polymer was synthesized as previously described [94]. Large area, thin films were fabricated and characterized with respect to ionic conductivity, water uptake, swelling, and mechanical properties.

7.3.1 Membrane Fabrication

For membrane casting the polymer was dissolved in xylene at a 10 wt% concentration, the solution was mixed at 90°C for 2 h. An automatic film applicator (MTI Corporation's MSK-AFA-III, Richmond, CA) with a micrometer adjustable blade was used to draw the polymer solution at a consistent speed and thickness. A temperature-controlled hotplate was placed over the existing vacuum chuck of the film applicator. A glass plate was positioned on the hotplate and heated to 80°C. The micrometer adjustable blade was kept in an oven at 80°C until immediately prior to casting. The blade was removed from the oven, placed on the glass substrate, the hot polymer solution was poured in front of the blade, and the solution was drawn to a thin wet film. The blade was set to a gap height of 200 microns and drawn at a speed of 50 mm/s. After casting, the hotplate was kept at 80°C for 30 min, after which the temperature control was turned off and the substrate allowed to cool. The film was allowed to dry overnight at room temperature in the fume hood. The next day, the polymer film was removed from the glass substrate. The film was further dried overnight in a vacuum oven at 80°C to remove residual solvent. Vinylbenzyl trimethylammonium cation functionalities were generated by soaking the film in 25 wt% trimethylamine solution at room temperature for 2 days. After functionalization the film was washed repeatedly to remove excess trimethylamine and dried overnight in a vacuum oven at 40°C. Films were characterized in the bromide counter ion form to avoid alkali degradation and mixed carbonates counter ions.

7.3.2 Ion Exchange Capacity

Ion exchange capacity (IEC), number of cations per mass of polymer, of the membranes was measured by Mohr titration. Films were converted to the chloride form by soaking in 1 M NaCl for at least 48 h, followed by rigorous washing to remove excess salt and drying in a vacuum oven. The chloride form films were soaked in 100 mL of 1 M $NaNO_3$ for 48 h. Aliquots of the $NaNO_3$ solution were titrated using a $AgNO_3$ solution with a K_2CrO_4 indicator. The end of the titration was defined by the presence of permanent rust colored precipitates in solution.

7.3.3 Ionic Conductivity

In-plane ionic conductivity was measured by electrochemical impedance spectroscopy using a multichannel potentiostat (BioLogic VMP3) and a TestEquity environmental chamber. Impedance spectra were obtained over a frequency range of 1 to 10^6 Hz. Membrane resistance was determined by the low frequency intercept of Nyquist plot and membrane conductivity was calculated based on equation (7.1)

$$\sigma = \frac{l}{R \cdot t \cdot w} \tag{7.1}$$

Where R is the membrane resistance, l is the distance between electrodes, and t and w are the thickness and width of the membrane sample. Conductivity was measured as a function of temperature between 50 and 90°C, at 95% relative humidity, to determine the activation energy for ion conduction. Conductivity was also measured as a function of humidity between 30 and 90%RH, at 60°C, to determine the effect of hydration on ion conduction.

7.3.4 Water Uptake

Water uptake was measured gravimetrically from liquid water at room temperature and from water vapor at 60°C. Liquid water uptake was measured by weighing samples dried overnight in a vacuum oven at 40°C compared to samples soaked in liquid water for 24 h.

Soaked samples were blotted to remove surface water and weighed immediate to prevent dehydration. All samples were weighed three times and averaged. Vapor water uptake was measured by using dynamic vapor sorption apparatus (SMS DVS Advantage 1, Allentown, PA). Samples were dried at a set point 0%RH (actual %RH was less than 1.7%) for 20 minutes to obtain the dry weight of the sample. After the initial drying period, the sample was equilibrated at 10%RH for 20 minutes to obtain a starting hydration level similar to mechanical testing. Following the equilibration period, humidity was ramped at 0.25%RH / min while the DVS instrument measures the gravimetric change in mass. The ramp rate was chosen to match dynamic mechanical experiments. Water uptake is calculated based on equation (7.2)

$$WU = \frac{m_{\%RH} - m_{dry}}{m_{dry}} \times 100 \qquad (7.2)$$

where $m_{\%RH}$ is the mass at the given relative humidity and m_{dry} is the dry sample weight. If the IEC is known then the number of waters per cation, λ, can be calculated with equation (7.3)

$$\lambda = \frac{WU}{m_{H_2O} \cdot IEC} \qquad (7.3)$$

where m_{H2O} is the molar mass of water and IEC is the ion exchange capacity of the film.

7.3.5 Dimensional Swelling

Dimensional swelling due to water sorption was characterized by measuring film dimensions in the dry and liquid water soaked state. Membranes were dried overnight in a 40°C vacuum oven and measured in terms of width, length, and thickness. Width and length measurements were performed using a Marathon electronic digital caliper (0–150 mm, with 0.01 mm accuracy). Thickness measurements were made using a Marathon electronic digital micrometer (0–25 mm, with 0.002 mm accuracy). All measurements were repeated at least three times for each dimension. Samples were soaked in liquid water for 24 h in liquid water at room

temperature. Samples were removed from the water, blotted to remove surface water, and quickly measured. In-plane and through-plane swelling were calculated based on the dimensional changes between the dry and wet states.

7.3.6 Extensional tests

Extensional mechanical testing was performed using a Sentmanat Extension Rheometer (SER) (Xpansion Instruments, Tallmadge, OH) fixture on an ARES G2 rheometer (TA Instruments, New Castle, DE). The SER has two counter-rotating drums; films are suspended between drums and stretched to failure. The SER fixture is typically used to measure extensional viscosity of polymer melts, but has also been shown to accurately measure tensile properties of solid polymers [38, 97]. The SER drums were modified to have screw down pins that would hold thin samples, a small amount of silicon rubber on the inside of the pin prevented film slip and generation of pinch points that would cause premature failure. Double sided tape was also placed on the drum surface to aid sample loading and further prevent film slip. Films were tested at Hencky strain rates that correspond to ASTM D882–12, for tensile testing of thin plastic sheeting, but rates were modified to account for the constant sample loading distance inherent to the SER fixture. Hencky strain rate is determined by final elongation and due to all samples having elongations larger than 100% a strain rate of 0.33 s^{-1} was used for all testing.

Samples were tested under dry and fully saturated air conditions at 60°C. A custom-built sample chamber was used to control temperature and humidity simultaneously. The insulated aluminum sample chamber has four electric cartridge heaters to control temperature. Humidity was supplied by a combination of dry and wet gas lines controlled by two mass flow controllers (10,000 SCCM, MKS 1179A, Andover, MA). The wet gas line passes through a humidity bottle (FCT, Inc., Albuquerque, NM) with 10 m of Nafion® tubing to saturate the gas stream with water.

112

The wet and dry gas lines were combined and delivered to the sample chamber through heated lines to prevent condensation. Temperature and humidity probes (Vaisala HMT 337, Boulder, CO) provided real time feedback of sample conditions into LabView software that also controlled gas flows and temperature set points.

7.3.7 Dynamic Mechanical Analysis

Dynamic mechanical testing was performed while ramping temperature, at constant dry or saturated relative humidity, and by ramping humidity, at constant temperature, to distinguish mechanical transitions due to temperature and hydration level. DMA test were performed on the ARES G2 rheometer with the film/fiber tension geometry. The unique Force Rebalance Transducer (FRT) of the ARES G2 allows small amplitude, up to 50 micron, oscillatory measurements in the axial direction. Temperature was ramped at a rate of 0.5°C/min from 30°C to 90°C, up and down for one complete cycle. At dry conditions, samples were loaded at a 5 mm starting gap and had an oscillatory strain of 0.1% at a frequency of 1 Hz. Dry tests used only dry gas flow and measured relative humidity was less than 10%RH over the entire temperature range. Due to reduced sample stiffness at hydrated conditions, saturated tests were loaded at a starting gap height of 1 mm and had an oscillatory strain of 0.5% at a frequency of 1 Hz. Saturated relative humidity tests utilized 4700 sccm wet gas and 300 sccm dry gas flow and had measured relative humidities above 85%RH over the entire temperature range.

Tests ramping humidity were performed at a ramp rate of 0.25%RH/min from 10%RH to 90%RH, up and down for two complete cycles. The sample was maintained at 90%RH for 1 h after the ramp up in humidity to ensure the sample was fully saturated before ramping humidity down. Humidity ramp tests were loaded at a starting gap height of 1 mm and had an oscillatory strain of 0.5% at 1 Hz. All tests had a minimum axial force setting of 0.01 N and were set to

maintain the axial force 30% higher than the oscillatory force on the sample. Sample tension (axial force) was maintained by automatic adjustment of the gap height, which caused sample elongation with increased temperature or humidity. Hydrated tests (temperature and humidity ramps) had total sample elongations up to 35%, which was within the elastic region based on extensional testing.
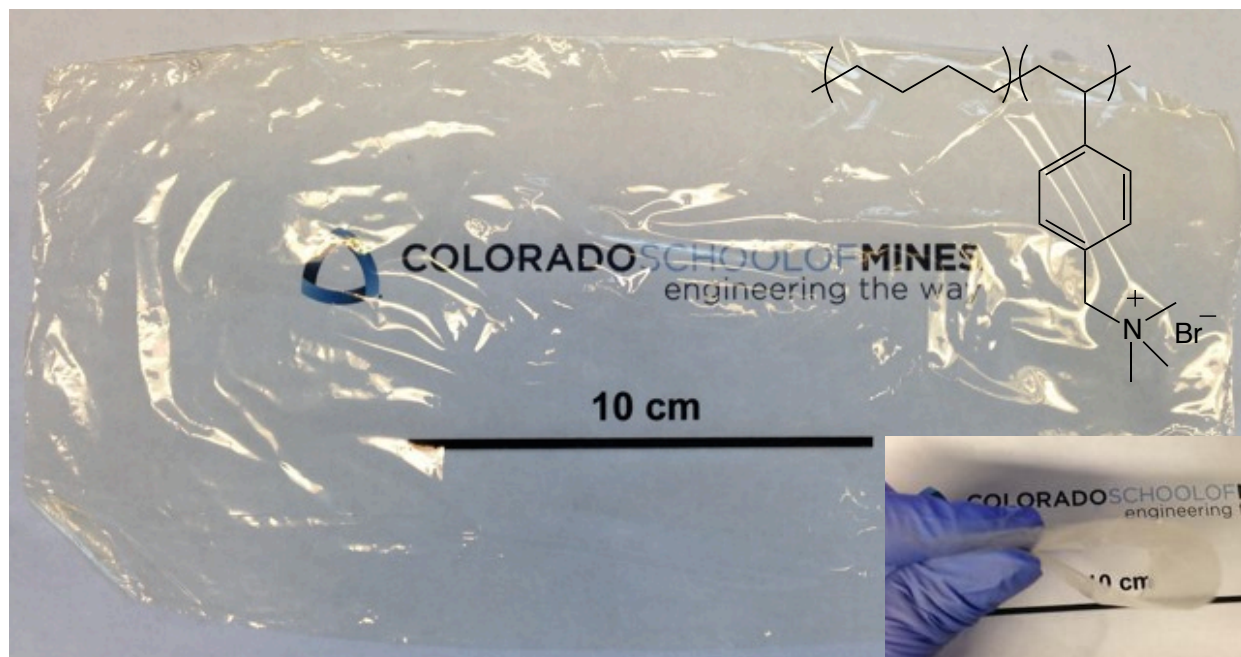
Figure 7.1: Photograph of PE-b-PVBTMA[Br] film after casting and functionalization. Film was pliable as shown by the folded film in the right lower inset.

7.4 Results

Casting the PE-b-PVBBr from xylene using the automatic film applicator resulted in large, ~300 cm^2, flexible films with a consistent thickness of 10-15 microns (Figure 7.1). Functionalization of the polymer with vinylbenzyl trimethylammonium cations was confirmed by titration. The theoretical IEC of the brominated polymer was 1.63 mmol/g based on the ^{1}H NMR spectra. The titrated IEC of the PE-b-PVBTMA was 1.21 ± 0.08 mmol/g corresponding to a 74% conversion of brominated sites. The incomplete conversion of brominated sites to cations

114

may be a result of low dimensional swelling (discussed later) of these films that would restrict transport of the trimethylamine into the polymer.

Ionic conductivity of the PE-b-PVBTMA polymer in the bromide counter ion form was measured as a function of temperature at saturated conditions (95%RH). Conductivity ranged from 5 mS/cm at 50°C to 15 mS/cm at 90°C and had an activation energy of 27 kJ/mol based on an Arrhenius fit (Figure 7.2). These conductivities are similar to other AEMs with similar IECs [43, 92, 124]. The activation energy of the PE-b-PVBTMA membrane is higher than standard PEMs [57] and similar to slightly higher than AEMs [43, 87].
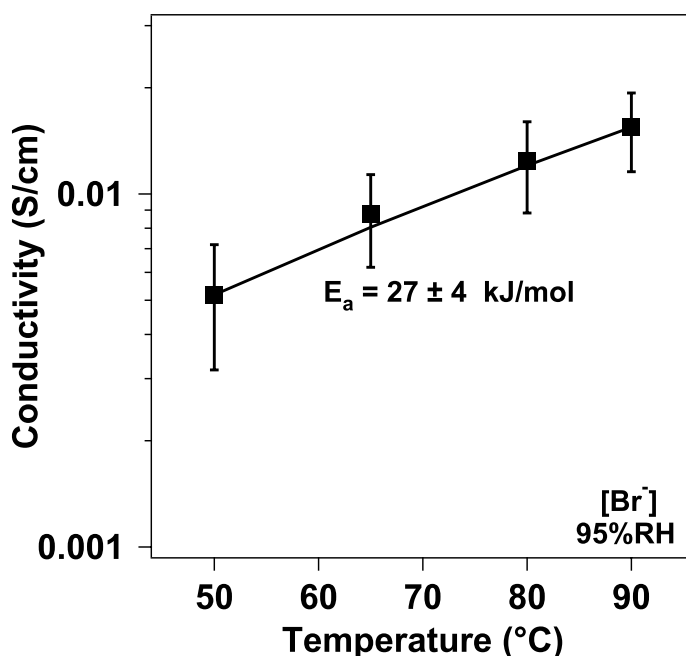
Figure 7.2: Ionic conductivity of the PE-b-PVBTMA[Br] polymer at 95%RH.

Liquid water uptake and swelling were measured to determine dimensional stability. Water uptake was relatively low for the PE-b-PVBTMA at $17 \pm 5\%$, corresponding to a lambda value of 8 ± 2. This water uptake is smaller than most other AEMs [58, 75, 130], due in part to its relatively low IEC. The low water uptake results in low dimensional swelling of the film. Dimensional swelling was $8 \pm 3\%$ in the in-plane direction, and $5 \pm 2\%$ in the through-plane

direction. A low level of dimensional swelling is beneficial to prevent significant hygrothermal stresses due to elongation and contraction of the membrane during humidity changes and reducing the chance of delamination or cracking of catalyst layers in the stack.

Extensional tests were performed to measure tensile properties of the PE-b-PVBTMA[Br] films under dry and saturated gas conditions at 60°C (Figure 7.3). When hydrated, water taken up by the polymer acts as a plasticizer, increasing elasticity and elongation and reducing strength. Water plasticization can be detrimental to the mechanical durability and performance of ion exchange membranes. Maintaining sufficient mechanical performance over a range of hydration levels is critical for long-term stability of AEMs. The PE-b-PVBTMA[Br] membrane had good strength at dry conditions, 28 ± 4 MPa, and strength was only reduced by 29% to 20 ± 4 MPa when fully saturated. The strength of the PE-b-PVBTMA is lower than
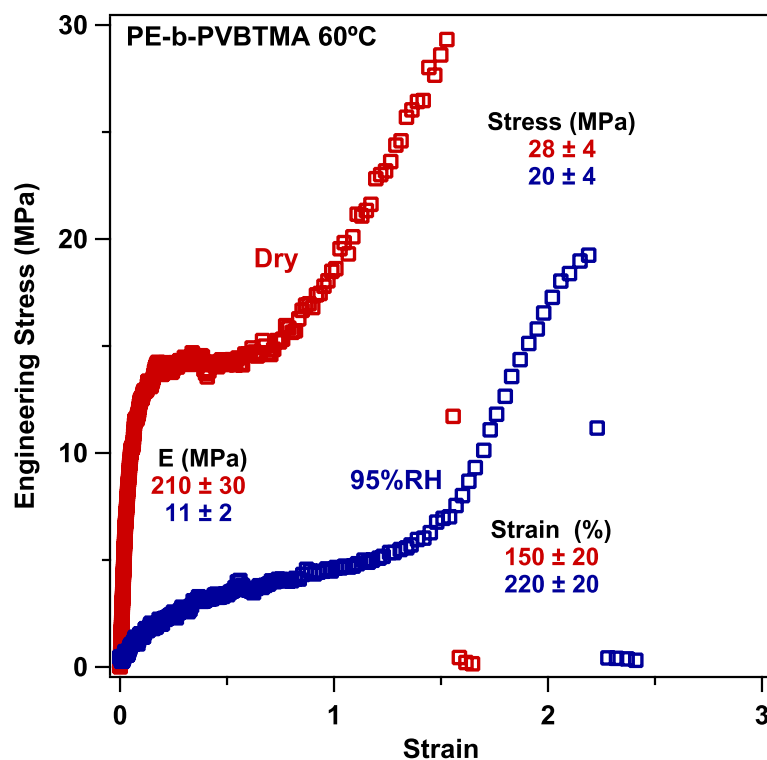
Figure 7.3: Representative stress vs. strain curves of the PE-b-PVBTMA[Br] films at dry (red) and 95%RH (blue) conditions. Average tensile properties of Young's modulus (E), stress, and elongation are shown inside the figure.

Nafion® [85], but better than many AEMs [22, 111, 112, 129], and the narrow change between dry to hydrated conditions is promising for stable performance in an electrochemical device. Elongation of the PE-b-PVBTMA[Br] film was 150 ± 20% at dry conditions and 220 ± 20% at saturated conditions. Elongation must be sufficient to accommodate dimensional swelling due to water uptake, and the elongation of the PE-b-PVBTMA is significantly larger than the dimensional swelling from liquid water discussed previously. At dry conditions the PE-b-PVBTMA polymer has a Young's modulus of 210 ± 30 MPa, similar to Nafion® [85], meaning the membrane is stiff enough to be dimensionally stable, but not brittle. However, when hydrated the membrane is severely softened, with the Young's modulus being reduced by 95% to 11 ± 2 MPa. This reduction in modulus is significant and may be a concern for stable mechanical performance. The severe reduction of modulus between dry and hydrated states warranted further study by dynamic mechanical analysis.

Dynamic mechanical analysis was performed while ramping temperature under dry or saturated relative humidity conditions to identify thermomechanical transitions within the fuel cell operating range (Figure 7.4). At dry conditions, the storage modulus has a fairly narrow range varying from 420 ± 120 MPa at 30°C to 210 ± 10 MPa at 90°C and shows no hysteresis between the heating and cooling. While the dry storage modulus changed by about 50% between 30 - 90°C, under hydrated conditions the change in modulus was more significant ranging from 43 ± 13 MPa at 30°C to 6 ± 1 MPa at 90°C (or a 86% decrease).

At hydrated conditions hysteresis in the storage modulus is observed. Upon cooling from 90°C to 30°C, the storage modulus measured only 21 ± 5 MPa, compared to 43 ± 13 MPa at the start of the test. This hysteresis could be due to different sorption kinetics during heating compared to cooling, incomplete saturation at the start of the test even after 1 h of equilibration,
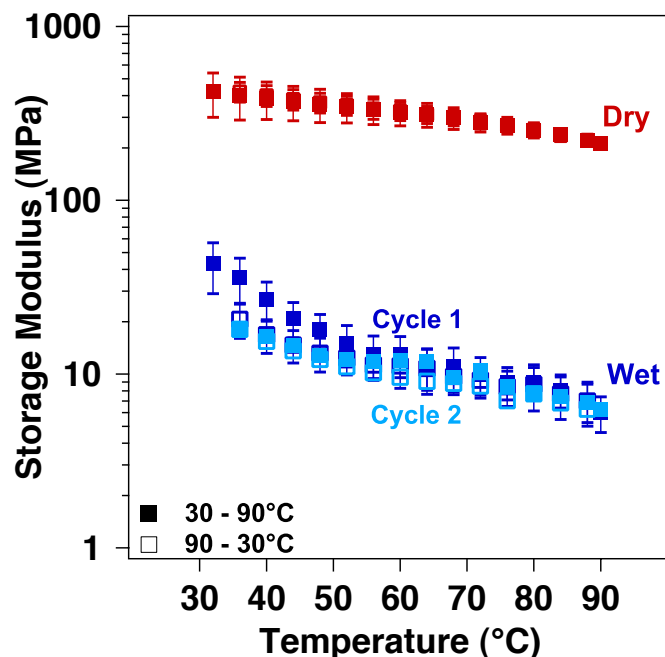
Figure 7.4: Storage modulus, measured by DMA, of the PE-b-PVBTMA[Br] membranes as a function of temperature under dry and saturated relative humidity conditions. Solid markers are during heating from 30 - 90°C and open markers are during cooling from 90 - 30°C. The light blue data is the second cycle of heating and cooling for one sample at saturated conditions.

or higher sample elongation during the initial heating ramp to maintain sample tension. During the initial heating ramp, the sample elongates between 15 - 25% in order to maintain tension on the sample, and upon cooling the sample contracts but not fully, remaining 5 - 15% elongated. This hysteresis was further investigated by allowing the sample to undergo a second cycle of heating and cooling. The second cycle showed no hysteresis between heating and cooling steps, so it is likely that incomplete hydration at the start of the test resulted in higher moduli at low temperatures for the initial heating compared to cooling and subsequent cycle. While the storage moduli decreased with increasing temperature at both dry and hydrated conditions, no major mechanical transitions were observed over this range of temperatures, suggesting the large difference in moduli between dry and hydrated states is result of hydration alone.

Mechanical transitions related to hydration (humidity), hygromechanical, were analyzed by performing DMA while ramping humidity from 10 to 90%RH and back to 10%RH, at a

constant temperature (Figure 7.5). Humidity testing was initially performed at 60°C to match extensional testing. During humidification, the storage and loss moduli remained relatively steady until a sharp decrease in moduli between 55 - 75%RH, when both moduli are reduced by an order of magnitude. Upon dehumidification, the moduli transitioned back to its stiffened state, but the location for the transition was shifted down to 35 - 50%RH. Returning to 10%RH the storage modulus was slightly larger, 350 ± 4 MPa, than the initial value, 200 ± 17 MPa, and the loss modulus decreased slightly, 16.5 ± 0.7 MPa, compared to the initial value of 24.5 ± 0.7 MPa. This hysteresis of the moduli at dry conditions is most likely due to initial stretching of the film during the first humidification, because hysteresis was not seen in subsequent cycles. The samples were humidified and dehumidified a second time to determine further hysteresis of the

Figure 7.5: Storage (E') and loss (E'') moduli of PE-b-PVBTMA[Br] as function of humidity. Solid markers are during humidification from 10 - 90%RH, open markers are during dehumidification from 90 - 10 %RH. Cycle 1 is shown in dark blue (E') and red (E''), cycle 2 is shown in light blue (E') and orange (E'').

membranes. The second cycle displayed the same softening transition during humidification and stiffening transition during dehumidification as the first cycle. At low humidities, the moduli values of the second cycle align with dehumidification values of the first cycle, further confirming that the low humidity hysteresis is due to initial sample elongation rather than differences of the kinetics between sorption and desorption.

The hygromechanical transition of the PE-b-PVBTMA membrane can be further confirmed by plotting Tan δ as a function of humidity (Figure 7.6). Error bars were removed from the Tan δ plot for clarity, but are included in the supplemental data. Tan δ exhibits clear peaks at 65%RH and 45%RH, for humidification and dehumidification, respectively. The magnitude of Tan δ decreases from the cycle 1 to cycle 2, as a result of the moduli hysteresis, but the shape of the Tan δ curves remains consistent between cycles.
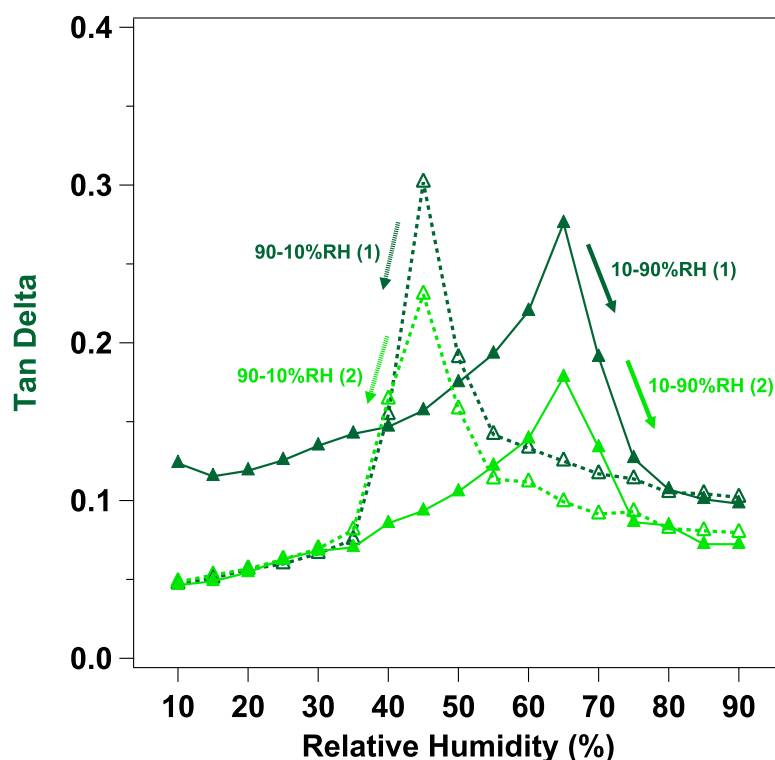
Figure 7.6: Tan δ vs. relative humidity, the solid markers are during humidification and open are markers are during dehumidification. Dark green corresponds to cycle 1 and light green to cycle 2.

The hysteresis of the hygromechanical transition from humidification to dehumidification could be a result of different kinetics of water sorption compared to desorption. Polymer sorption and desorption kinetics were investigated by measuring gravimetric water uptake, using DVS, at the same conditions (ramp rate and cycle conditions) as the DMA testing. A small hysteresis in water uptake is measured during humidification compared to dehumidification (Figure 7.7), resulting in slightly differences in lambda values, up to 1.5 differences, between humidification and dehumidification for the same relative humidity value.
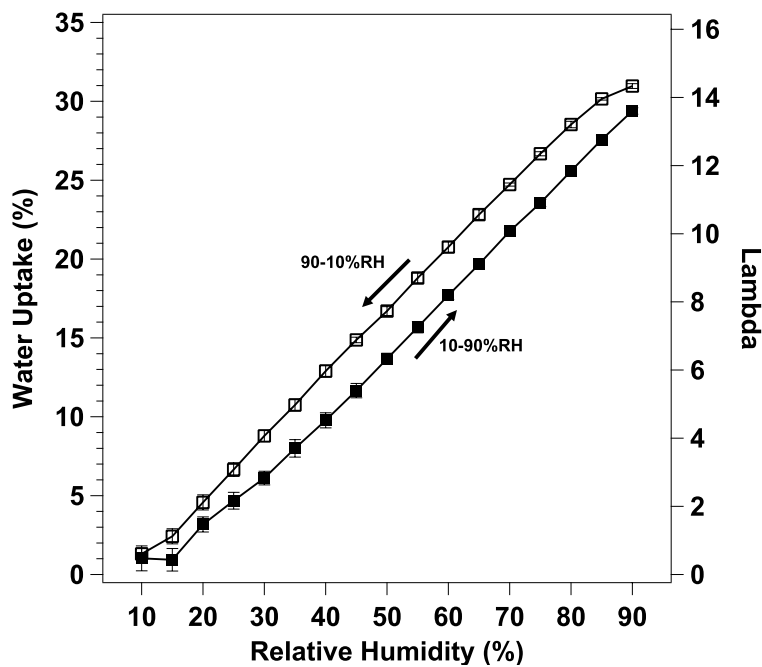
Figure 7.7: Water uptake and lambda vs. relative humidity. Solid markers are during humidification from 10 - 90 %RH and open markers are during dehumidification from 90 - 10%RH. There was no significant difference from cycle 1 to cycle 2 so data from the two cycles was averaged together.

The DMA measurements can be normalized to lambda (water content) to eliminate the effect of sorption/desorption kinetics (Figure 7.8). Normalizing the measured moduli by lambda causes the hygromechanical transition window to narrow, however hysteresis is still clearly present from hydration to dehydration. Hysteresis when the moduli have been normalized to

water content proves sorption/desorption kinetics are not responsible, rather the hysteresis is due to a different mechanical response during softening compared to stiffening. The hygromechanical transitions points, in terms of water content, can be identified by plotting Tan δ as a function of lambda (Figure 7.9). Based on the peak of Tan δ, the hygromechanical transition occurs at lambda approximately equal to 9 during humidification, but the reverse transition occurs at a lower lambda value of about 7 during dehumidification. Membranes are softened at high hydrations, but there is a delay in stiffening while water content is being reduced. Delayed restiffening could significantly influence membrane performance as environmental conditions change within the fuel cell.
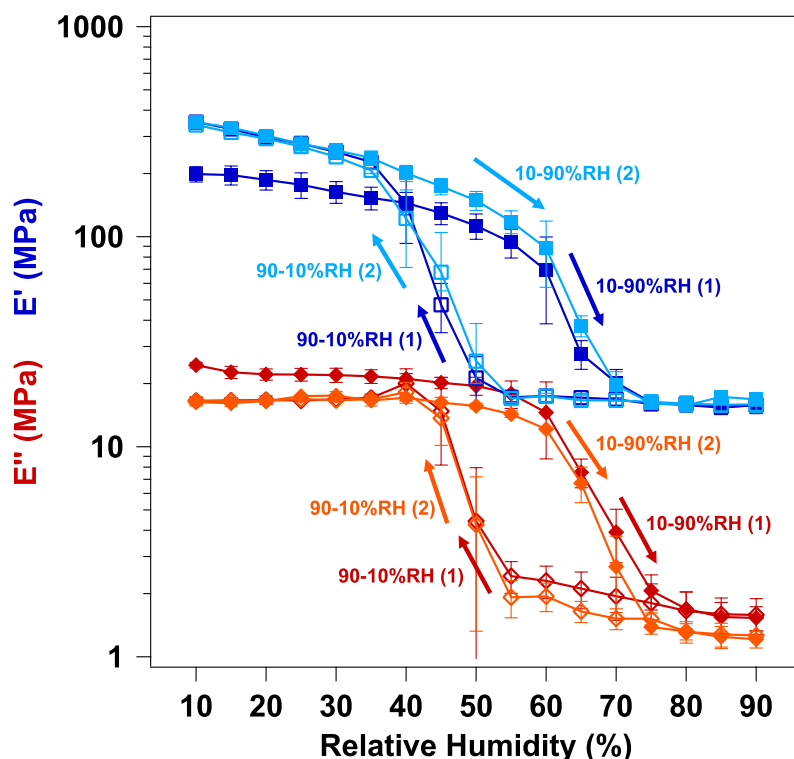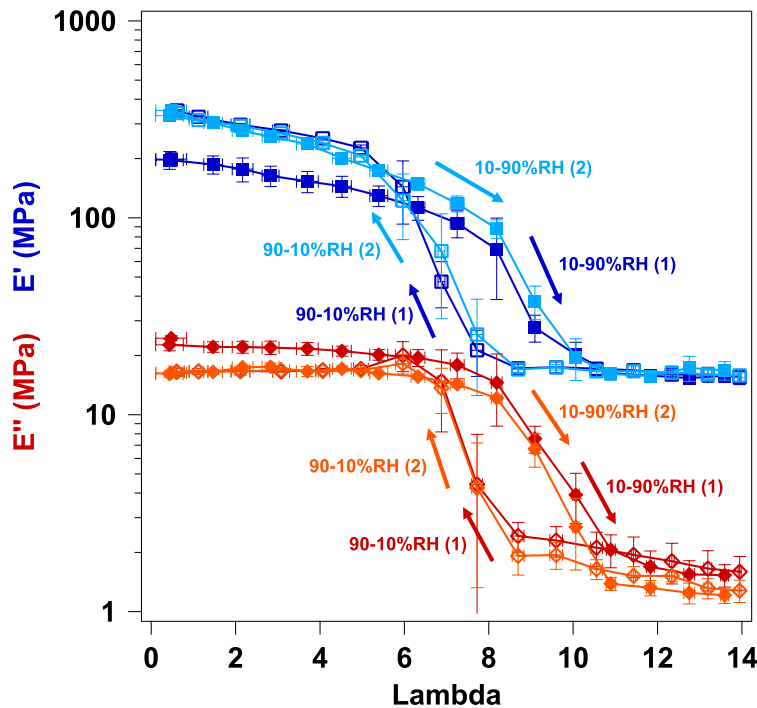

Figure 7.8: Storage (E') and loss (E'') moduli as a function of lambda. Solid markers are during humidification from 10 - 90%RH, open markers are during dehumidification from 90 - 10 %RH. Cycle 1 is shown in dark blue (E') and red (E''), cycle 2 is shown in light blue (E') and orange (E'').
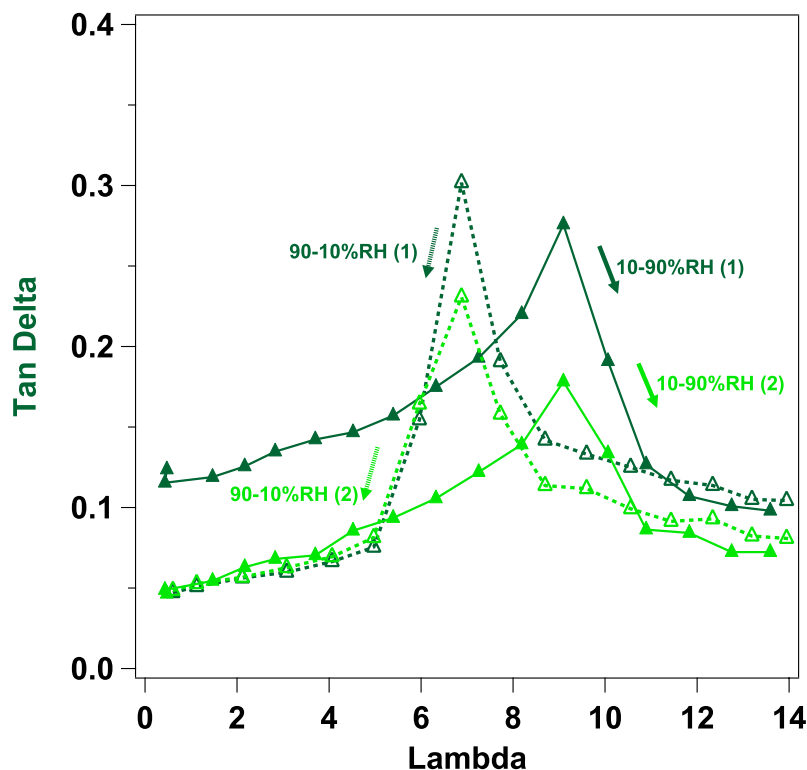
Figure 7.9: Tan δ vs. lambda, the solid markers are during humidification and open are markers are during dehumidification. Dark green corresponds to cycle 1 and light green to cycle 2.

The effect of mechanical softening on ionic transport was investigated by measuring conductivity as a function of humidity. Conductivity must be measured at steady-state conditions, given the nature and duration of the measurement, so humidity could not be ramped at the same conditions as DMA testing. Conductivity was measured at 60°C starting at 30%RH, increasing humidity in 10%RH steps, up to 90%RH and back down to 30%RH. Conductivity was measured for 30 min at each relative humidity set point after a steady RH was achieved. Conductivity showed no evidence of hysteresis between the increasing and decreasing humidity measurements so all measurements were averaged for a given relative humidity.

An increase in conductivity was measured following mechanical softening of the material at higher water contents (Figure 7.10). Conductivity is already dependent on hydration, but increased chain flexibility due to mechanical softening with hydration may also contribute to

enhanced ion transport. The relationship between ion conduction and mechanical softening is important to understanding AEM performance, and could help identify operating conditions for maintaining membrane and device performance. It may be beneficial to fully saturate the membrane at the start of operation, to ensure mechanical softening, and then maintain humidity above the stiffening transition for sustained ion transport.
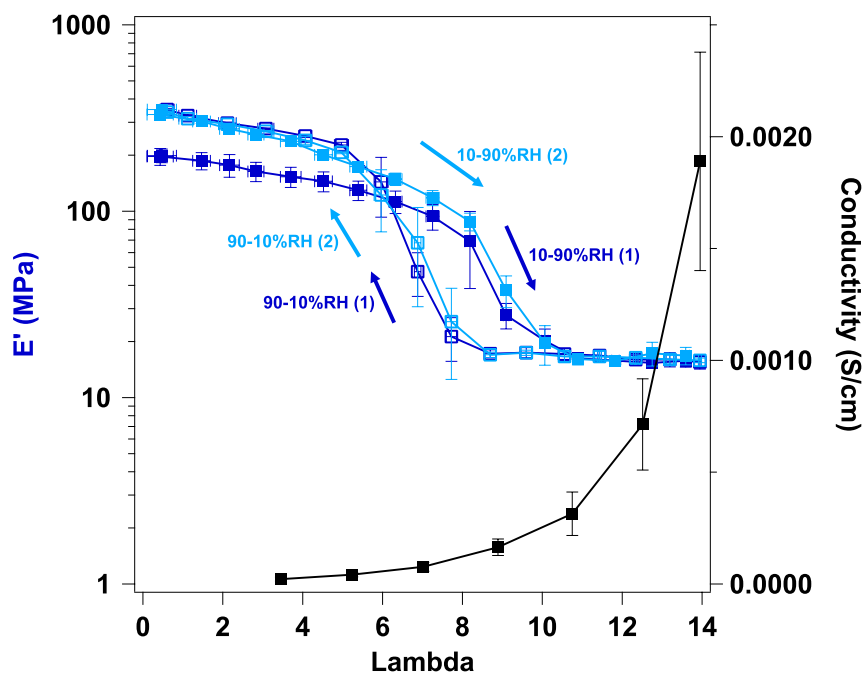
Figure 7.10: Storage modulus and ionic conductivity as a function of lambda.

In order to confirm that the hysteresis of the hygromechanical transitions was not exclusive to 60°C, the humidity DMA tests were repeated at 40°C and 80°C (Figure 7.11). Error bars were removed from the data for clarity, but can be seen in Appendix A. At 40°C, hygromechanical softening during humidification does not occur until very high humidities, between 70-85%RH, while the reverse transition during dehumidification is much lower, between 40-55%RH. Thus, reducing temperature to 40°C seems to increase the mechanical hysteresis between humidification and dehumidification. Alternatively, increasing the temperature to 80°C reduces hysteresis almost completely, so the transition occurs between 45 -

55%RH for both humidification and dehumidification. The modulus behavior at multiple temperatures could not be normalized by lambda, because dynamic vapor sorption was not available above 60°C, but attempts were made to normalize the data using absolute humidity and enthalpy of the air. Normalization by absolute humidity and enthalpy shifted the transition curves, but no additional trends were distinguishable (see Appendix A).

If ion transport is dependent on mechanical softening, the reduction of the transition point at higher temperatures suggests AEMs may successfully operate at lower humidity conditions at higher temperatures. While mechanical softening during humidification is dependent on temperature, mechanical stiffening, during dehumidification, is completed at the same relative humidity, 40%RH, regardless of temperature. The delay in mechanical stiffening may help maintain fuel cell performance, if the membrane is saturated initially (to induce softening), and then maintained at humidities above the stiffening transition. Identifying hygromechanical softening and hysteresis will help identify humidity conditions necessary to facilitate and maintain ion conduction in AEMs.

7.5 Conclusions

The polyethylene-b-poly(vinylbenzyl trimethylammonium) is a promising AEM material that can be processed into thin, well-performing, stable membranes. The PE-b-PVBTMA membrane has relatively low water uptake and dimensional swelling, and good ionic conductivity. Extensional tests showed the membrane displayed good strength and elongations at both dry and hydrated conditions. However, there was significant softening of the membranes from dry to hydrated conditions warranting further investigation.

a)

b)
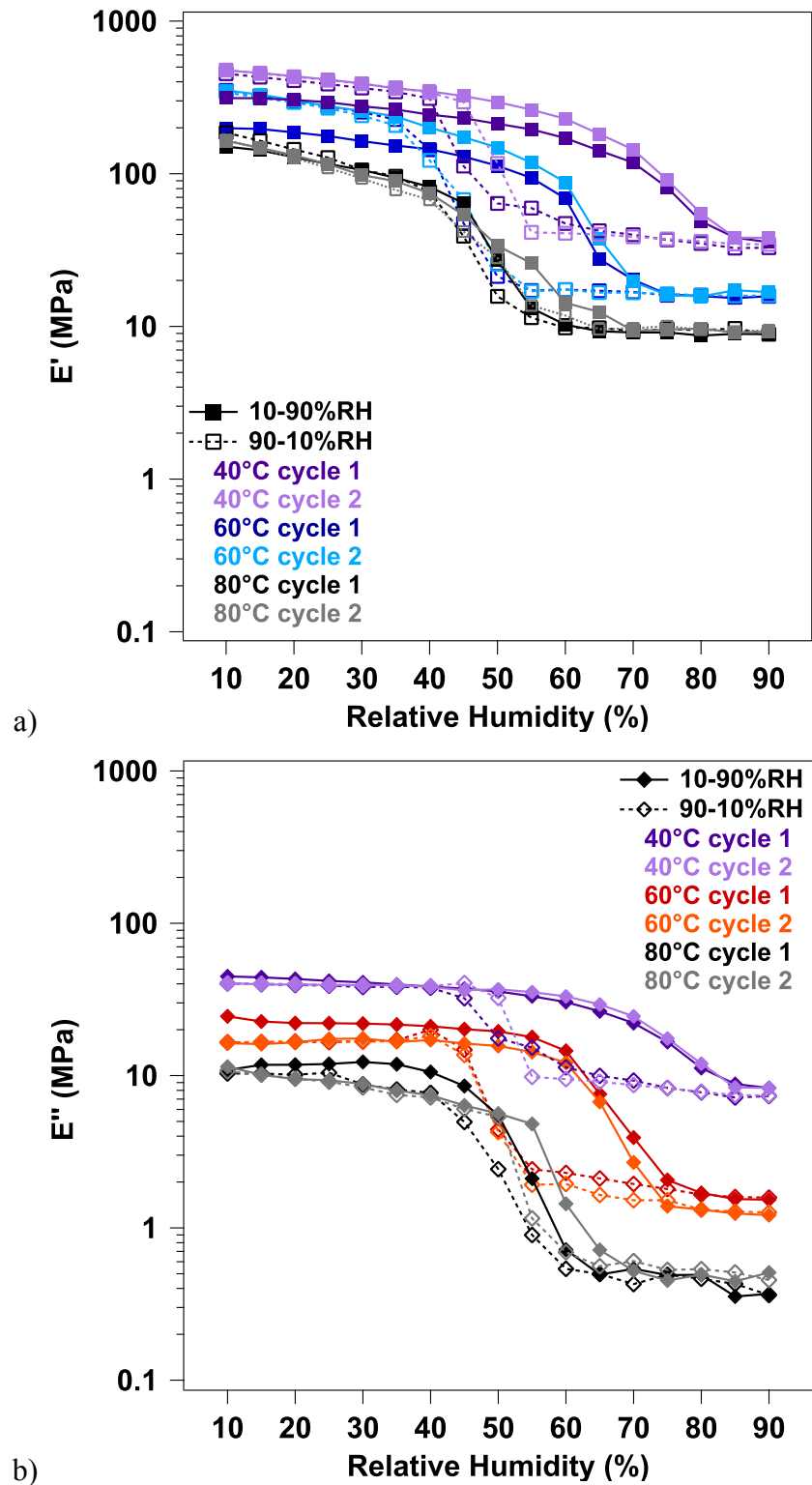
Figure 7.11: a) Storage modulus and b) loss modulus vs. relative humidity at 40°C (purple), 60°C (blue/red), and 80°C (black).

Dynamic mechanical analysis was performed while ramping humidity. The storage and loss moduli displayed a sharp decrease during humidification, this transition was reversible between the dry and hydrated states, but the humidity at which the transition occurs displayed hysteresis from humidification to dehumidification. The dynamic moduli were normalized to water content, i.e. lambda, to eliminate the effects of sorption/desorption kinetics, but hysteresis between humidification and dehumidification remained. Ionic conductivity was measured as a function of humidity, and the onset for increased conductivity corresponded to mechanical softening of the membrane. The correlation between conductivity and mechanical softening suggest that bulk mechanical properties could be used to determine the operational humidity levels required to facilitate ion transport. Additional DMA testing confirmed that hygromechanical hysteresis was a function of temperature, with hysteresis being inversely proportional to temperature. Interestingly, while the onset of mechanical stiffening during humidification was dependent on temperature, all samples completed this transition at the same humidity, 40%RH, regardless of temperature. The relationship between ion conduction and mechanical softening is important to understanding AEM performance, and will lead to the development of robust, well-performing anion exchange membranes.

7.6 Acknowledgements

CHAPTER 8 : CONCLUSIONS AND RECOMMENDATIONS

8.1 Summary and Conclusions

Anion exchange membranes are promising for use as solid polymer electrolytes in alkali fuel cells and other electrochemical energy conversion devices. AEMs must have a high ionic conductivity and be chemically and mechanically stable over the lifetime of the device. The fuel cell is a dynamic environment requiring that AEMs operate at a range of hydration levels. Water is critical to ion transport, but also leads to dimensional swelling and mechanical instability of the membrane. Sorption and desorption of water produces hygrothermal stresses in the membrane, over multiple humidity cycles these stresses lead to pinholes, cracks, and mechanical failure. The inversely proportional relationship between conductivity and mechanical performance makes designing a robust, well-performing AEM a challenge, and makes simultaneous study ionic conductivity and mechanical properties necessary. The goals of this thesis were to establish mechanical properties metrics for AEMs to evaluate the mechanical performance of novel AEM chemistries. Establishing mechanical metrics and testing AEMs at a range of hydrations will help guide development of durable, well-performing AEMs.

As a relatively new area of study, characterizing the basic mechanical properties of well-studied AEMs is necessary to establish benchmark data for future AEM research and development. An extensional rheometer fixture was utilized to measure tensile properties of three well-established AEMs at a range of temperature and humidity conditions. Water absorbed by the polymer membrane acts as a plasticizer, increasing elasticity and elongation, and reducing film strength. Reinforcement of an AEM in a non-conductive matrix reduces water sorption and swelling, resulting in stable mechanical properties over a range of humidities, but also limiting conductivity as a result of reduced ion concentration. Freestanding, non-reinforced, membranes

128

had a higher degree of in-plane swelling, about 25%, and mechanical properties changed dramatically with hydration. Water sorption causes softening, 50 - 75% reduction in Young's modulus, and weakening, 20 - 70% reduction in strength, of the freestanding membranes. Achieving an AEM with adequate elasticity and elongation at dry conditions and sufficient strength at hydrated conditions is a challenge, but a narrow range of mechanical properties as a function of hydration would improve mechanical performance and extend lifetime.

Metrics were developed to define the acceptable range of mechanical properties (Young's modulus, strength, and elongation) for AEMs based on the mechanical performance of the benchmarking AEMs and Nafion[®], the industry standard for PEMs. Some of the AEMs studied were overly stiff at dry conditions but severely softened when hydrated. Membranes that are too stiff, with Young's moduli above 450 MPa, have a tendency to become brittle and do not have adequate elasticity to accommodate swelling associated with water sorption. At hydrated
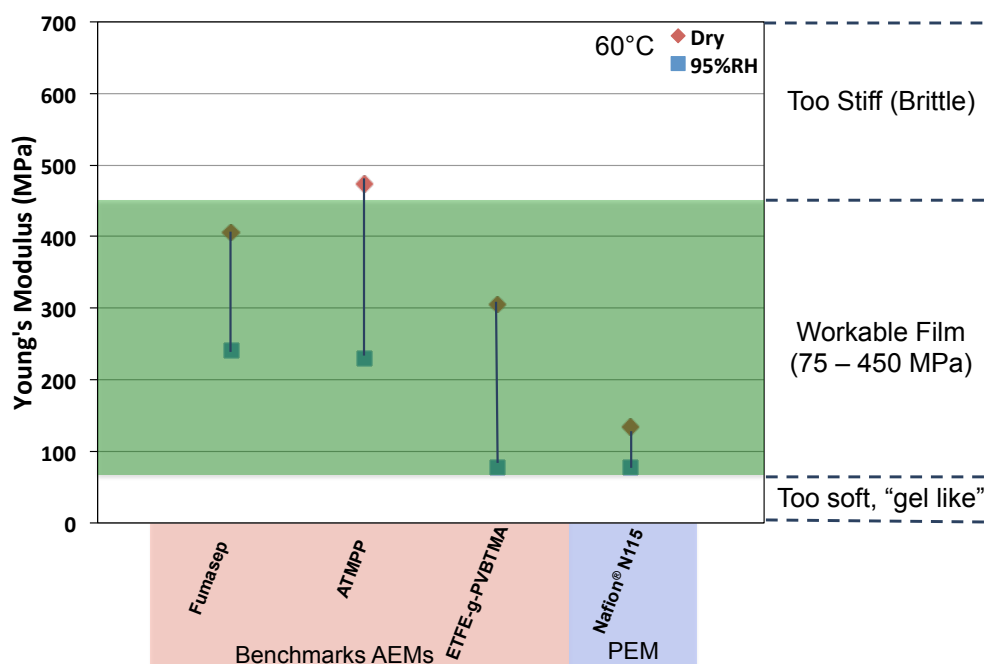
Figure 8.1: AEM metric for Young's modulus defined between 75 - 450 MPa, indicated by green box, and measured values for benchmarking AEMs and Nafion[®] at 60°C under dry and saturated humidity conditions.

conditions, water acts as a plasticizer, softening the membrane, but an excess reduction in modulus can be detrimental to membrane integrity. Ideally an AEM would have a moderate modulus with only minor changes between dry and hydrated conditions, so the metric range for the Young's modulus was defined between 75 and 450 MPa (Figure 8.1).

AEMs need to have adequate strength to remain a semi-permeable barrier, and have sufficient elongation to accommodate dimensional swelling. Membranes tend to weaken due to plasticization by water, so the minimum strength requirement, 25 MPa, was based on the stress at break of the non-reinforced benchmarking AEMs (Figure 8.2). As discussed, AEMs must have sufficient elongation to accommodate dimensional swelling; ideally all swelling will occur within the elastic region to prevent irreversible deformation that would reduce membrane performance and lifetime. In an attempt to contain swelling effects to the elastic deformation region, the minimum elongation metric, above 100%, was chosen to be similar to the elongation
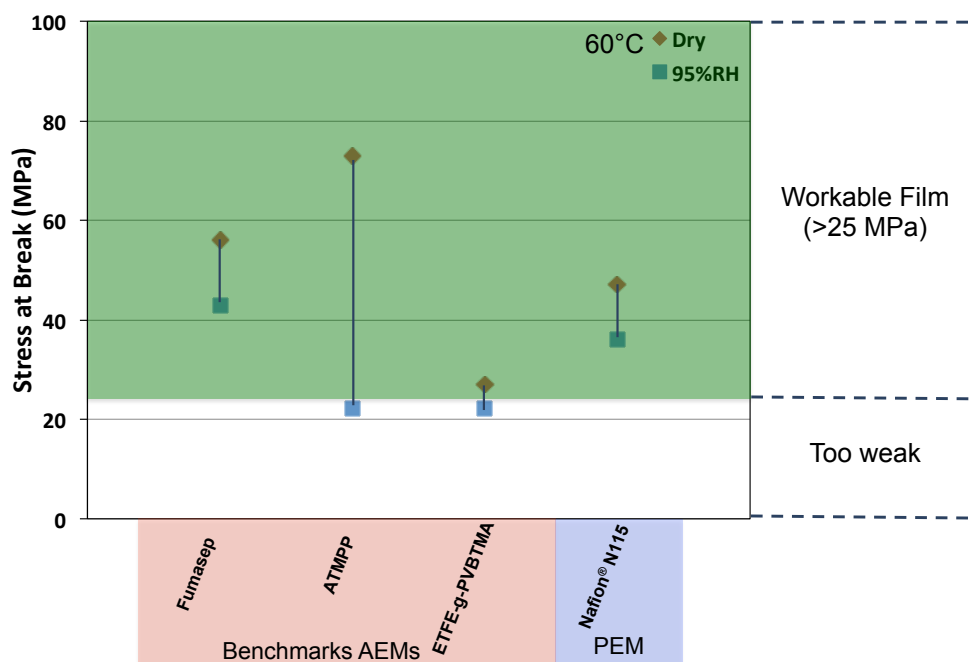
Figure 8.2: AEM metric for stress at break (strength) defined above 25 MPa, indicated by green box, and measured values for benchmarking AEMs and Nafion® at 60°C under dry and saturated humidity conditions.

for Nafion® at dry conditions which exceeds the lower elongations seen in benchmarking AEMs (Figure 8.3). The mechanical metrics established here will be used to evaluate novel AEM membranes and identify favorable polymer chemistries for robust AEMs.
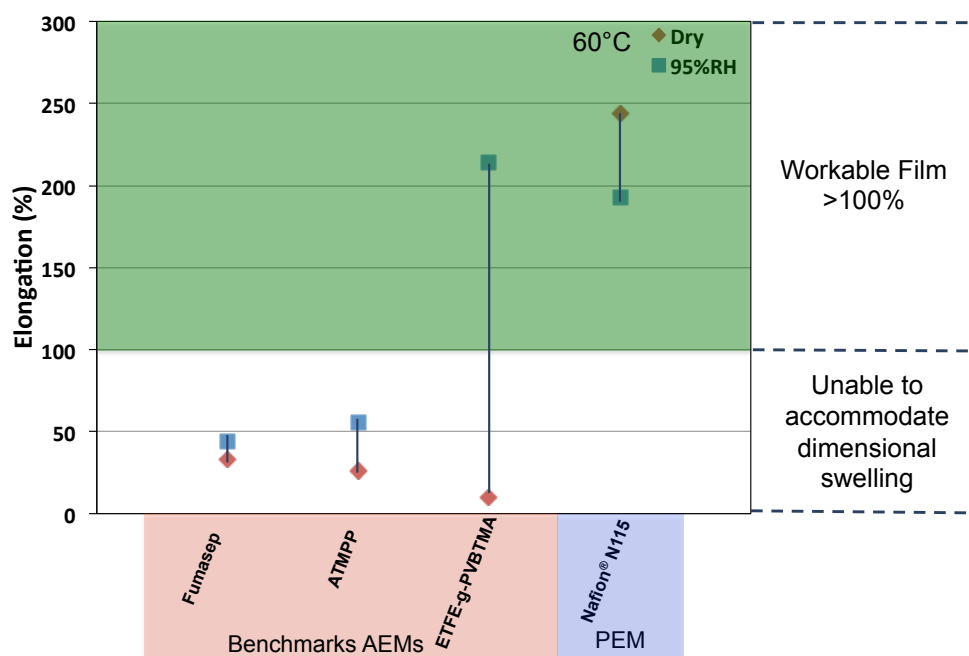
Figure 8.3: AEM metric for elongation defined above 100%, indicated by green box, and measured values for benchmarking AEMs and Nafion® at 60°C under dry and saturated humidity conditions.

Block copolymers are intriguing due to their ability to self-assemble into organized morphologies on the nanoscale scale. Ordered, phase separated materials benefit from well-defined ionic pathways while still maintaining mechanical integrity and resisting excess swelling. A polystyrene-b-poly(vinylbenzyl trimethylammonium) diblock was investigated as a potential AEM. The polystyrene diblock displayed nanometer scale phase separation, with increased ordering upon hydration, and good conductivity (30 mS cm^{-1} at 50°C/95%RH, [Cl$^-$] form). The mechanical properties of the PS-b-PVBTMA were investigated and compared to the neutral precursor polymer. The addition of cationic functionalities reduced elasticity and elongation, making the films stiff and brittle. Under hydrated conditions, membrane elasticity and elongation

improved, but strength was still low, and overall the mechanical performance of the PS-b-PVBTMA was not adequate for electrochemical devices.

The cationic nature of AEMs inherently increases membrane stiffness; in an attempt to prevent extreme stiffening, rubbery polyisoprene-based, random copolymers were studied. These copolymers can be solution processed and subsequently chemically crosslinked to produce a solid polymer film. The addition of polystyrene to the polymer matrix produced a higher IEC polymer that could still be rendered insoluble by crosslinking. Crosslinking was performed by thermal treatment at two durations and photocrosslinking using a dithiol linkage. The higher IEC terpolymer displayed higher conductivity than the copolymer, but both systems lost solid membrane integrity, and flowed, when hydrated at higher temperatures. The crosslinked films had relatively high water uptake and significant dimensional swelling that could be detrimental to device stability. Crosslinking caused films to be stiff under dry conditions, with reduced elasticity as the degree of crosslinking was increased, but all films were severely softened and weakened when hydrated. The vast discrepancy between mechanical properties at dry conditions compared to hydrated conditions is problematic, as AEM performance must be stable over all device operating conditions.

Since the polystyrene diblock displayed favorable phase separation and high conductivity, but had inadequate elasticity, a new block copolymer with a rubbery, polyethylene, neutral block was synthesized to improve film elasticity. The polyethylene-b-poly(vinylbenzyl bromide) polymer could be solution cast into large, thin (12 μm) polymer films and further functionalized with vinylbenzyl trimethylammonium cations. The polyethylene diblock had good ionic conductivity and low dimensional swelling. The membrane displayed a good elastic modulus and adequate strength and elongation at dry conditions. At hydrated conditions, the membrane had

only minor changes in strength and elongation, but a significant (95%) reduction in elastic modulus. Dynamic mechanical analysis identified a sharp transition in the storage and loss moduli at 65%RH during humidification at 60°C. This transition was reversible, but displayed hysteresis, with the transition shifting down to 45%RH during dehumidification. Measuring conductivity as a function of humidity showed a possible correlation between mechanical softening and the onset of increased conductivity. The relationship between ion conduction and mechanical softening is important to understanding AEM performance, and could help identify operating conditions for maintaining membrane and device performance.

Production of robust, well-performing AEMs is a continued challenge. Water sorption is critical to hydrate ionic sites and facilitate ion transport, but water also acts as a plasticizer that can soften and weaken the membrane. Maintaining high ionic conductivity and sufficient mechanical performance is a difficult balance in AEMs. Basic mechanical properties remain highly dependent on polymer chemistry, ion concentration, and water sorption. Block copolymers are of great interest, but use of glassy polystyrene as the hydrophobic block produced membranes that were stiff and brittle, particularly after functionalization to their cationic form. Replacing the glassy polystyrene block with a rubbery polyethylene block greatly improved film elasticity allowing production of large films that were flexible and relatively strong. While the polyethylene based AEMs exhibited decent mechanical performance, the elastic modulus was reduced by an order of magnitude when hydrated. A comparison of conductivity as a function of humidity to the storage modulus suggests that mechanical softening, indicating an increase in chain mobility, may help facilitate ion conduction at higher hydrations. Additional studies of other AEMs are needed to confirm a correlation between mechanical softening and ion conduction, because ion conduction is already highly dependent on hydration

133

level. If the correlation between mechanical softening and ionic transport is consistent for AEMs, it will make accurate characterization of mechanical performance over the range operating conditions critical to understand AEM performance. The mechanical performance of the novel AEMs tested all fell outside the "workable film" range defined based on the benchmark AEMs and PEM performance (Figure 8.4), indicating that additional chemistries are needed that have adequate elasticity, strength, and elongation at all hydration levels.
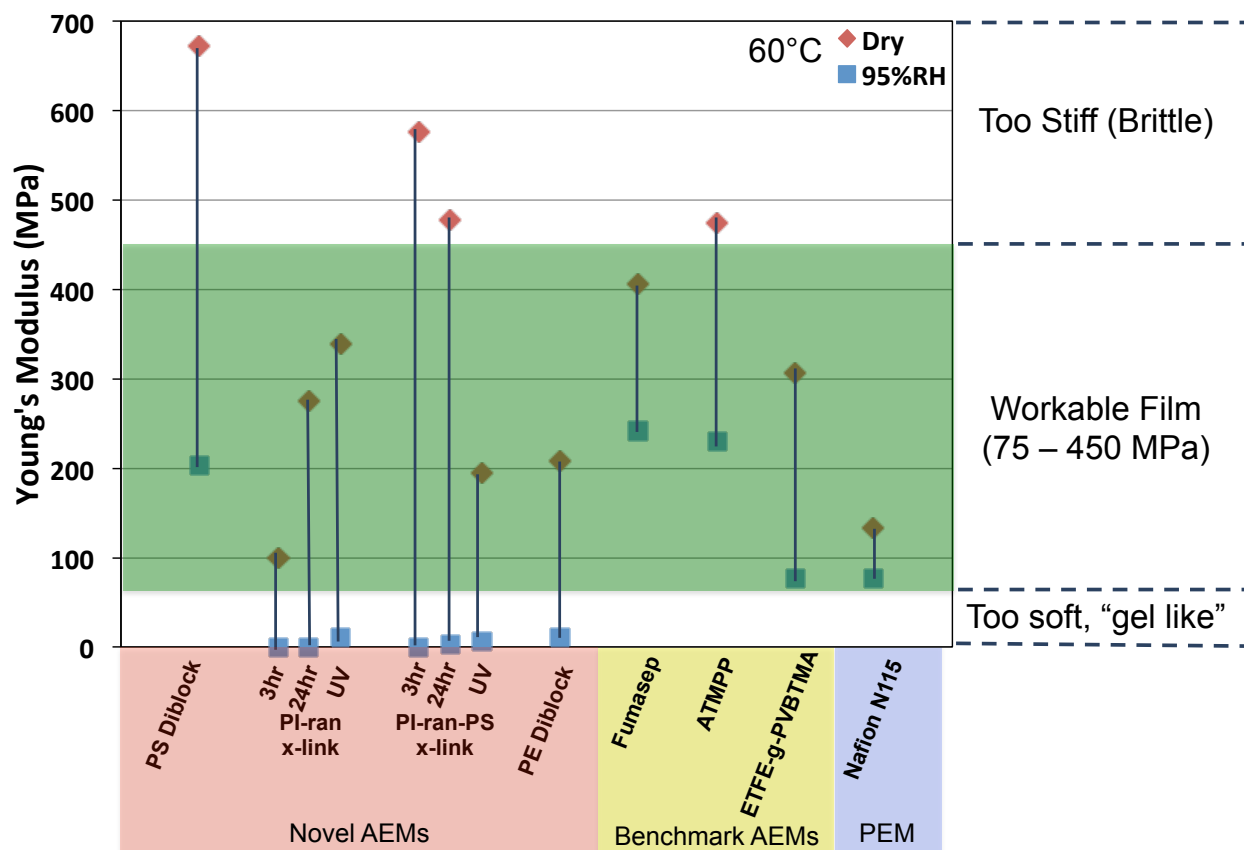
Figure 8.4: Mechanical performance, in terms of Young's Modulus, for the novel AEMs, benchmarking AEMs, and Nafion®. All novel AEMs fall outside the "workable film" range at one or more hydration conditions.

8.2 Recommendations for future work

The high chemical stability and mechanical durability of perfluorinated polymers, along with the vast literature on perfluorinated PEMs, make the development of perfluorinated AEMs a continued interest. The sulfonamide linkage described in the previous study was unstable and

suffered degradation in alkali environments. Replacing the cation linkage with a more stable chemistry is necessary to produce a base stable AEM. Attaching an alkyl to the sulfonyl group can be achieved using novel chemistry, such as a Grignard reagent, and will increase base stability of the cation attachment. Tailoring reaction chemistry will allow functionalization of various cation species that have been identified to have high alkali stability. A base stable, mechanically durable perfluorinated AEM will be able to operate in an alkali fuel cell at higher operating conditions, 80°C, which will help mitigate the effect of carbonate formation that reduces ionic conductivity and creates a pH gradient across the membrane.

Polyisoprene based, crosslinkable copolymers warrant further study due to environmentally favorable processing and good conductivity performance; however, mechanical durability at hydrated conditions must be improved. Photocrosslinking using a dithiol crosslinker and adding glassy polystyrene to the polymer matrix proved to increase film durability and reduced dimensional swelling, so continued study should focus on optimizing polymer chemistry in terms of IEC and crosslinking chemistry. An ongoing study is investigating different dithiol chemistries with different hydrophobicities. Changing crosslinker hydrophobicity will have a significant impact on water uptake and dimensional stability. A hydrophilic crosslinking agent could increase water sorption and hydrate the ionic groups to facilitate greater ion conduction at lower ion concentrations, as high ion concentration tends to make films stiff and brittle. After crosslinking chemistry is optimized, IEC can be tailored to maximize conductivity without succumbing to excess swelling or dissolution at higher humidity conditions.

Beyond new polymer chemistries, investigations into the effects of molecular weight and chain entanglements on the mechanical properties of AEMs would be very beneficial. Increasing molecular weight has been shown to increase tensile strength [131]. Increasing molecular weight

will increase chain density and entanglement that will provide increased resistance to deformation [132, 133]. While increasing molecular weight is expected to increase mechanical performance, it will also effect morphology and ion conduction, particularly in block copolymer AEMs. The morphology of block copolymer is dependent on block length and block ratio [89]. Increasing molecular weight, keeping block ratio constant, will produce longer lengths of both blocks. It is expected that increasing block length would increase the domain spacing, but could also lessen phase separation and ordering, as longer chains will have less mobility to phase separated into organized domains. Ideally, a single block copolymer chemistry would be synthesized at a range of molecular weights (50 - 500 kg/mol), maintaining the same block ratio for a constant IEC, and characterized in terms of ion conduction, morphology, and mechanical properties. This investigation would confirm the increased performance of AEM by increasing molecular weight, but also provide insight into potential changes in ion conduction and morphology.

In addition to studying entanglements by altering molecular weight, investigation into entanglements of polymer chains in solution would be beneficial to determine the effect of casting viscosity on film morphology and strength. Empirical evidence throughout this thesis work has shown that increasing solution viscosity, by increasing polymer concentration, during casting improves film integrity and mechanical performance. Increasing polymer concentration increases chain interaction and entanglement that is imparted to the final film. At higher viscosities the casting solution must be drawn to produce a film of the desired thickness, so the solution must be transferable and be able to be drawn to a consistent film. On-going studies are investigating the viscosity of a pentablock polymer from Kraton Performance Polymer Inc. in tetrahydrofuran at concentrations from 1 to 20 wt%. The viscosity has three regimes

corresponding dilute (1 - 9 wt%), semi-dilute (10 - 15 wt%), and entangled (16 - 20 wt%). Casting from the entangled regime will produce films of higher strength due to a higher degree of chain entanglement. The semi-dilute regime would produce weaker films and the dilute regimes will not produce freestanding solid films. The pentablock polymer can be partially brominated to produce reactive sites for conversion to cations to produce an AEM polymer. Understanding the effect of casting viscosity on membrane strength will help optimize film casting conditions to improve membrane strength and durability.

Polymer membranes are heterogeneous in terms of their surface properties compared to the bulk, and consideration of these differences are necessary to understand AEM performance. Membrane interfaces interact with different elements (i.e. casting substrate, air, gas, and water) than the bulk polymer, and this can result in significantly different surface properties in terms of resistance and transport compared to the bulk. The surface resistance of the membrane to ion transport can be significantly different than the bulk, which influences the shape of the impedance spectra when measuring conductivity [134]. Nafion has been shown to change surface composition based on whether it is in contact with air, hydrophobic regions on surface, or water, sulfonate groups on surface [135, 136]. Ionic groups on the surface take up water causing swelling at the surface, which can bend the film due to the difference in swelling between the surface in contact with water and the rest of the membrane [135]. This local swelling produces stresses in the membrane, the wet side being in compression while the dry side is in tension [135]. Differences in hydration between the two interfaces of the membrane can result in stress gradients across the membrane. These stresses, like the hygrothermal stresses due to temperature and humidity changes, can lead to mechanical degradation of the membrane.

Surface energy effects should be investigated by measuring contact angle with water and observing any physical deformation of a freestanding membrane in contact with water.

The suite of mechanical tests available for characterization of AEMs was developed throughout the course of this dissertation: an extensional rheometer fixture was modified to accommodate thin, solid polymer films; upgrades to the ARES G2 rheometer allowed dynamic, oscillatory measurements on solid films in a tension geometry; and a custom sample chamber allowed independent control of temperature and humidity to measure mechanical properties and identify mechanical transitions as a function of hydration. Combined, these tools will provide in-depth characterization of AEM mechanical performance as a function of hydration. Extensional testing has been verified to accurately measure tensile properties and can be performed between 30 - 90°C and 10 - 90%RH. Current tests have limited conditions to 30°C or 60°C, and dry or saturated conditions, to match literature data and other test methods available (i.e. vapor sorption, conductivity, etc.). If optimized AEM fuel cell operating conditions are identified, future extensional testing can focus on characterizing mechanical performance at these conditions. Additionally, extensional testing at intermediate humidity conditions would be advantageous to understanding AEM performance when operating conditions change.

Axial testing in a tension geometry has shown significant promise in characterizing the dynamic mechanical properties of AEM films. DMA analysis identified mechanical transitions as a function of humidity, or water content. The onset for increased conductivity occurred at humidities similar to mechanical softening of the membrane, suggesting chain mobility may help facilitate ionic transport in AEMs. Further testing of other AEM systems is needed to confirm that mechanical softening enhances ion transport. If this hypothesis is confirmed, future AEM development will need to identify the level of chain flexibility necessary to conduct ions and the

corresponding hydration conditions necessary for fuel cell operation. Plasticization has been shown to improve conductivity in polymer electrolyte batteries, by lowering the glass transition and increasing ion dissociation [137, 138]. Ion dissociation tends to be lower in AEMs, compared to PEMs, due to weakly basic cation species such as quaternary ammoniums [9, 18, 102]. Low ion dissociation, along with the stiff nature of AEMs at dry conditions, may make plasticization by water necessary to facilitate ion conduction. While softening may be necessary for ion conduction, excess softening will reduce film durability, and ultimately shorten device lifetime. Identifying the minimum level of softening, minimum Young's modulus, required for efficient ion conduction will guide development of high performance, durable AEMs for sustained use in electrochemical devices. Benchmarking the dynamic mechanical properties and conductivity of common AEMs as a function of humidity, similar to the extensional benchmarking study in Chapter 4, would be beneficial to understand how mechanical softening impacts conductivity in AEMs.

Hygrothermal stresses develop in AEMs during dehydration because the membrane is constrained between electrodes preventing dimensional changes. The axial tension geometry can be used to measure the stress induced in the membrane due to dehydration. Current experiments have loaded humidified samples in the film/fiber geometry and applied a small axial force, about 0.01 N, to the film. The sample is held at a constant gap height while the environment is dehumidified by dry gas flow. The stress on the film is measured as the sample is dehydrated, and the change in stress between saturated and dry states is termed the "water stress". Identifying the stress associated with water sorption/desorption is beneficial to understand stress cycles in the membrane and developing protocols for accelerated stress testing of AEMs. Accelerate stress testing by cycling humidity, while measuring gas crossover, can accurately predict relative

lifetime of a fuel cell membrane [27, 139]. But this testing requires a specialized apparatus to measure gas permeability while controlling humidity. DMA testing utilizing the measured "water stress" as the oscillatory stress could be developed as an accelerated stress testing for gauging membrane durability. Developing accelerated test methods that could be applied with standard analytical equipment, such as a DMA, would be beneficial to characterize and screen AEMs in terms of mechanical performance.

REFERENCES

[1]   Vielstich, W., Lamm, A., Gasteiger, H.A. (Eds.), Handbook of Fuel Cells: Fundamentals, Technology, Applications, John Wiley & Sons, 2003.

[2]   Hickner, M.A., Ghassemi, H., Kim, Y.S., Einsla, B.R., et al., Alternative Polymer Systems for Proton Exchange Membranes (PEMs). *Chem. Rev.* 2004, *104*, 4587–4612.

[3]   Smitha, B., Sridhar, S., Khan, A.A., Solid polymer electrolyte membranes for fuel cell applications—a review. *J Membrane Sci* 2005, *259*, 10–26.

[4]   Di Noto, V., Zawodzinski, T.A., Herring, A.M., Giffin, G.A., et al., Polymer electrolytes for a hydrogen economy. *International Journal of Hydrogen Energy* 2012, *37*, 6120–6131.

[5]   Neburchilov, V., Martin, J., Wang, H., Zhang, J., A review of polymer electrolyte membranes for direct methanol fuel cells. *Journal of Power Sources* 2007, *169*, 221–238.

[6]   Borup, R., Meyers, J., Pivovar, B., Kim, Y.S., et al., Scientific Aspects of Polymer Electrolyte Fuel Cell Durability and Degradation. *Chem. Rev.* 2007, *107*, 3904–3951.

[7]   Rodgers, M.P., Bonville, L.J., Kunz, H.R., Slattery, D.K., et al., Fuel Cell Perfluorinated Sulfonic Acid Membrane Degradation Correlating Accelerated Stress Testing and Lifetime. *Chem. Rev.* 2012, *112*, 6075–6103.

[8]   Couture, G., Alaaeddine, A., Boschet, F., Ameduri, B., Polymeric materials as anion-exchange membranes for alkaline fuel cells. *Progress in Polymer Science* 2011, *36*, 1521–1557.

[9]   Varcoe, J.R., Slade, R.C.T., Prospects for Alkaline Anion-Exchange Membranes in Low Temperature Fuel Cells. *Fuel Cells* 2005, *5*, 187–200.

[10]   Merle, G.R., Wessling, M., Nijmeijer, K., Anion Exchange Membranes for Alkaline Fuel Cells: A Review. *J Membrane Sci* 2011, 1–90.

[11]   McLean, G.F., Niet, T., Prince-Richard, S., Djilali, N., An assessment of alkaline fuel cell technology. *International Journal of Hydrogen Energy* 2002, *27*, 507–526.

[12]   Varcoe, J.R., Atanassov, P., Dekel, D.R., Herring, A.M., et al., Anion-exchange membranes in electrochemical energy systems. *Energy Environ. Sci.* 2014, *7*, 3135–3191.

[13]   Wang, Y., Li, L., Hu, L., Zhuang, L., et al., A feasibility analysis for alkaline membrane direct methanol fuel cell: thermodynamic disadvantages versus kinetic advantages. *Electrochemistry Communications* 2003, *5*, 662–666.

[14]   Couture, G., Alaaeddine, A., Boschet, F., Ameduri, B., Polymeric Materials as Anion-Exchange Membranes for Alkaline Fuel Cells. *Progress in Polymer Science* 2011.

[15]   Hayes, W.M., CRC Handbook of Chemistry and Physics, 92nd ed., CRC Press, Inc., 2011.

[16]   Marx, D., Chandra, A., Tuckerman, M.E., Aqueous Basic Solutions: Hydroxide Solvation, Structural Diffusion, and Comparison to the Hydrated Proton. *Chem. Rev.* 2010, *110*, 2174–2216.

[17]   Chempath, S., Boncella, J.M., Pratt, L.R., Henson, N., et al., Density Functional Theory Study of Degradation of Tetraalkylammonium Hydroxides. *J. Phys. Chem. C* 2010, *114*, 11977–11983.

[18]   Merle, G.R., Wessling, M., Nijmeijer, K., Anion exchange membranes for alkaline fuel cells: A review. *J Membrane Sci* 2011, *377*, 1–35.

[19]   Subianto, S., Pica, M., Casciola, M., Cojocaru, P., et al., Physical and chemical modification routes leading to improved mechanical properties of perfluorosulfonic acid membranes for PEM fuel cells. *Journal of Power Sources* 2013, *233*, 216–230.

[20]   Herring, A.M., Yandrasits, M.A., Aieta, N.V., Stanis, R.J., et al., Dynamics of PFSA Polymer Hydration Measured in Situ by SAXS. *ECS Transactions* 2006, *3*, 915–921.

[21]   Kreuer, K.-D., Schuster, M., Obliers, B., Diat, O., et al., Short-side-chain proton conducting perfluorosulfonic acid ionomers: Why they perform better in PEM fuel cells. *Journal of Power Sources* 2008, *178*, 499–509.

[22]   Robertson, N.J., Kostalik, H.A., IV, Clark, T.J., Mutolo, P.F., et al., Tunable high performance cross-linked alkaline anion exchange membranes for fuel cell applications. *J. Am. Chem. Soc.* 2010, *132*, 3400–3404.

[23]   Giffin, G.A., Lavina, S., Pace, G., Di Noto, V., Interplay between the Structure and Relaxations in Selemion AMV Hydroxide Conducting Membranes for AEMFC Applications. *J. Phys. Chem. C* 2012, *116*, 23965–23973.

[24]   Tang, H., Peikang, S., Jiang, S.P., Wang, F., et al., A degradation study of Nafion proton exchange membrane of PEM fuel cells. *Journal of Power Sources* 2007, *170*, 85–92.

[25]   Tang, Y., Karlsson, A.M., Santare, M.H., Gilbert, M., et al., An experimental investigation of humidity and temperature effects on the mechanical properties of perfluorosulfonic acid membrane. *Materials Science and Engineering: A* 2006, *425*, 297–304.

[26]   Patil, Y.P., Jarrett, W.L., Mauritz, K.A., Deterioration of mechanical properties: a cause for fuel cell membrane failure. *J Membrane Sci* 2010, *356*, 7–13.

[27]   Pestrak, M., Li, Y., Case, S.W., Dillard, D.A., et al., The effect of mechanical fatigue on the lifetimes of membrane electrode assemblies. *J. Fuel Cell Sci. Technol.* 2010, *7*, 041009.

[28]   Lai, Y.-H., Mittelsteadt, C.K., Gittleman, C.S., Dillard, D.A., Viscoelastic Stress Analysis of Constrained Proton Exchange Membranes Under Humidity Cycling. *J. Fuel Cell Sci. Technol.* 2009, *6*, 021002.

[29]   Dillard, D.A., Li, Y., Grohs, J.R., Case, S.W., et al., On the use of pressure-loaded blister tests to characterize the strength and durability of proton exchange membranes. *J. Fuel Cell Sci. Technol.* 2009, *6*, 031014.

[30]   Hibbs, M.R., Hickner, M.A., Alam, T.M., McIntyre, S.K., et al., Transport properties of hydroxide and proton conducting membranes. *Chem Mater* 2008, *20*, 2566–2573.

[31]   Hibbs, M.R., Fujimoto, C.H., Cornelius, C.J., Synthesis and Characterization of Poly(phenylene)-Based Anion Exchange Membranes for Alkaline Fuel Cells. *Macromolecules* 2009, *42*, 8316–8321.

[32]   Jung, H., Fujii, K., Tamaki, T., Ohashi, H., et al., Low fuel crossover anion exchange pore-filling membrane for solid-state alkaline fuel cells. *J Membrane Sci* 2011, *373*, 107–111.

[33]   Glatter, O., Kratky, O. (Eds.), Small Angle X-ray Scattering, Academic Press, London 1982.

[34]   Krebs, F.C., Fabrication and processing of polymer solar cells: A review of printing and coating techniques. *Solar Energy Materials and Solar Cells* 2009, *93*, 394–412.

[35]   Li, J., Park, J.K., Moore, R.B., Madsen, L.A., Linear coupling of alignment with transport in a polymer electrolyte membrane. *Nat Mater* 2011, *10*, 507–511.

[36]   Villar, M.A., Rueda, D.R., Fernando, A., Thomas, E.L., Studey of oriented block copolymer films obtained by roll-casting. *Polymer* 2002, *43*, 5139–5145.

[37]   Saccà, A., Carbone, A., Pedicini, R., Portale, G., et al., Structural and electrochemical investigation on re-cast Nafion membranes for polymer electrolyte fuel cells (PEFCs) application. *J Membrane Sci* 2006, *278*, 105–113.

[38]   Sentmanat, M.L., Miniature universal testing platform: from extensional melt rheology to solid-state deformation behavior. *Rheol Acta* 2004, *43*, 657–669.

[39]   Menard, K.P., Dynamic Mechanical Analysis, A Practical Introduction, 2nd ed., CRC Press, Inc., Boca Raton 2008.

[40]   Instruments, T.A. (Ed.), Determining the Optimum Sample Size for Testing a Film in the DMA 2980, 1999.

[41]   DeLuca, N.W., Elabd, Y.A., Polymer electrolyte membranes for the direct methanol fuel cell: A review. *J Polym Sci Pol Phys* 2006, *44*, 2201–2225.

[42]   Varcoe, J.R., Slade, R.C., Lam How Yee, E., Poynton, S.D., et al., Poly (ethylene-co-tetrafluoroethylene)-derived radiation-grafted anion-exchange membrane with properties specifically tailored for application in metal-cation-free alkaline polymer electrolyte fuel cells. *Chem Mater* 2007, *19*, 2686–2693.

[43]   Yan, J., Hickner, M.A., Anion Exchange Membranes by Bromination of Benzylmethyl-Containing Poly(sulfone)s. *Macromolecules* 2010, *43*, 2349–2356.

[44]   Mauritz, K.A., Moore, R.B., State of Understanding of Nafion. *Chem. Rev.* 2004, *104*, 4535–4586.

[45]   Kong, X., Wadhwa, K., Verkade, J.G., Schmidt-Rohr, K., Determination of the Structure of a Novel Anion Exchange Fuel Cell Membrane by Solid-State Nuclear Magnetic Resonance Spectroscopy. *Macromolecules* 2009, *42*, 1659–1664.

[46]   Jung, M.-S.J., Arges, C.G., Ramani, V., A perfluorinated anion exchange membrane with a 1,4-dimethylpiperazinium cation. *J. Mater. Chem.* 2011, *21*, 6158–6160.

[47]   Salerno, H.L.S., Beyer, F.L., Elabd, Y.A., Anion exchange membranes derived from nafion precursor for the alkaline fuel cell. *J Polym Sci Pol Phys* 2012, *50*, 552–562.

[48]   Arges, C., Jung, M., Johnson, G., Parrondo, J., et al., Anion Exchange Membranes (AEMs) with Perfluorinated and Polysulfone Backbones with Different Cation Chemistries. *ECS Transactions* 2011, *41*, 1795–1816.

[49]   Edson, J.B., Macomber, C.S., Pivovar, B.S., Boncella, J.M., Hydroxide based decomposition pathways of alkyltrimethylammonium cations. *J Membrane Sci* 2012, *399-400*, 49–59.

[50]   Matsui, K., Kikuchi, Y., Hiyama, T., Kondo, K., et al., Fluorocarbon Anion Exchangers and Processes for their Preparation, 4,659,774, 1987.

[51]   Stejskal, E.O., Tanner, J.E., Spin diffusion measurements: Spin echoes in the presence of a time-dependent field gradient. *J. Chem. Phys.* 1965, *42*, 288.

[52]   Stallmach, F., Galvosas, P., Spin echo NMR diffusion studies. *Annual Reports on NMR Spectroscopy* 2007, *61*, 51–131.

[53]   Perusich, S.A., FTIR equivalent weight determination of perfluorosulfonate polymers. *J Appl Polym Sci* 2010, *120*, 165–183.

[54]   Swaminathan, P., Disley, P.F., Assender, H.E., Surface modification of ion exchange membrane using amines. *J Membrane Sci* 2004, *234*, 131–137.

[55]   Danilczuk, M., Lin, L., Schlick, S., Hamrock, S.J., et al., Understanding the fingerprint region in the infra-red spectra of perfluorinated ionomer membranes and corresponding model compounds: Experiments and theoretical calculations. *Journal of Power Sources* 2011, *196*, 8216–8224.

[56]   Kim, Y.S., Kim, D.-S., Labouriau, A., Fujimoto, C., et al., FY 2010 Annual Progress Report, DOE Hydrogen Program, Arlington, VA 2010.

[57]   Halseid, R., Vie, P.J.S., Tunold, R., Influence of ammonium on conductivity and water content of Nafion 117 membranes. *J. Electrochem. Soc.* 2004, *151*, A381.

[58]   Slade, R.C.T., Varcoe, J.R., Investigations of conductivity in FEP-based radiation-grafted alkaline anion-exchange membranes. *Solid State Ionics* 2005, *176*, 585–597.

[59]   Fujimura, M., Hashimoto, T., Kawai, H., Small-Angle X-ray Scattering of Perfluorinated Ionomer Membranes. 1. Origin of Two Scattering Maxima. *Macromolecules* 1981, *14*, 1309–1315.

[60]   Gebel, G., Lambard, J., Small-Angle Scattering Study of Water-Swollen Perfluorinated Ionomer Membranes. *Macromolecules* 1997, *30*, 7914–7920.

[61]   Simpson, J., Carr, H., Diffusion and nuclear spin relaxation in water. *Physical Review* 1958, *111*, 1201–1202.

[62]   Klaus, Z., Diffusion, 3rd ed., Bruker, Rheinstetten, Germany 2009.

[63]   Zhao, Q., Majsztrik, P., Benziger, J., Diffusion and Interfacial Transport of Water in Nafion. *J. Phys. Chem. B* 2011, *115*, 2717–2727.

[64]   Kidena, K., Ohkubo, T., Takimoto, N., Ohira, A., PFG-NMR approach to determining the water transport mechanism in polymer electrolyte membranes conditioned at different temperatures. *European Polymer Journal* 2010, *46*, 450–455.

[65]   Park, J.K., Li, J., Divoux, G.M., Madsen, L.A., et al., Oriented Morphology and Anisotropic Transport in Uniaxially Stretched Perfluorosulfonate Ionomer Membranes. *Macromolecules* 2011, *44*, 5701–5710.

[66]   Tsushima, S., Teranishi, K., Hirai, S., Water diffusion measurement in fuel-cell SPE membrane by NMR. *Energy* 2005, *30*, 235–245.

[67]   Gebel, G., Aldebert, P., Pineri, M., Structure and Related Properties Perfluorosulfonated Ionomer Films. *Macromolecules* 1987, *20*, 1425–1430.

[68]   Aieta, N.V., Stanis, R.J., Horan, J.L., Yandrasits, M.A., et al., Clipped Random Wave Morphologies and the Analysis of the SAXS of an Ionomer Formed by Copolymerization of Tetrafluoroethylene and CF 2═CFO(CF 2) 4SO 3H. *Macromolecules* 2009, *42*, 5774–5780.

[69]   Steele, B.C., Heinzel, A., Materials for fuel-cell technologies. *Nature* 2001, *414*, 345–352.

[70]   Hickner, M.A., Herring, A.M., Coughlin, E.B., Anion exchange membranes: Current status and moving forward. *J Polym Sci Pol Phys* 2013, *51*, 1727–1735.

[71]   Aindow, T.T., O'Neill, J., Use of mechanical tests to predict durability of polymer fuel cell membranes under humidity cycling. *Journal of Power Sources* 2011, *196*, 3851–3854.

[72]   Schmittinger, W., Vahidi, A., A review of the main parameters influencing long-term performance and durability of PEM fuel cells. *Journal of Power Sources* 2008, *180*, 1–14.

[73]   Satterfield, M.B., Benziger, J.B., Viscoelastic properties of Nafion at elevated temperature and humidity. *J Polym Sci Pol Phys* 2009, *47*, 11–24.

[74]   Fumatech, Technical Datasheet - fumasep FAA-PK, Fumatech, 2012.

[75]   Fujimoto, C., Kim, D.-S., Hibbs, M., Wrobleski, D., et al., Backbone stability of quaternized polyaromatics for alkaline membrane fuel cells. *J Membrane Sci* 2012, *423-424*, 438–449.

[76]   Janarthanan, R., Horan, J.L., Caire, B.R., Ziegler, Z.C., et al., Understanding anion transport in an aminated trimethyl polyphenylene with high anionic conductivity. *J Polym Sci Pol Phys* 2013, *51*, 1743–1750.

[77]   Deavin, O.I., Murphy, S., Ong, A.L., Poynton, S.D., et al., Anion-exchange membranes for alkaline polymer electrolyte fuel cells: comparison of pendent benzyltrimethylammonium-and benzylmethylimidazolium-head-groups. *Energy Environ. Sci.* 2012, *5*, 8584–8597.

[78]   Mazin, P.V., Kapustina, N.A., Tarasevich, M.R., Direct ethanol oxidation fuel cell with anionite membrane and alkaline electrolyte. *Russian Journal of Electrochemistry* 2011, *47*, 275–281.

[79]   Chikvaidze, G., Gabrusenoks, J., Kleperis, J., Vaivars, G., Application of micro Raman spectroscopy to industrial FC membranes. *J. Phys.: Conf. Ser.* 2007, *93*, 012026.

[80]   Majsztrik, P.W., Bocarsly, A.B., Benziger, J.B., Viscoelastic Response of Nafion. Effects of Temperature and Hydration on Tensile Creep. *Macromolecules* 2008, *41*, 9849–9862.

[81]   Berer, M., Major, Z., Pinter, G., Constantinescu, D.M., et al., Investigation of the dynamic mechanical behavior of polyetheretherketone (PEEK) in the high stress tensile regime. *Mech Time-Depend Mater* 2013.

[82]   Li, X., Wang, Z., Lu, H., Zhao, C., et al., Electrochemical properties of sulfonated PEEK used for ion exchange membranes. *J Membrane Sci* 2005, *254*, 147–155.

[83]   Rusanov, A.L., Likhachev, D.Y., Kozlova, O.V., Harris, F.W., Highly arylated bis-cyclopentadienones in the synthesis of aromatic condensation monomers and polymers. *Progress in Polymer Science* 2006, *31*, 749–810.

[84]   De Focatiis, D.S.A., Gubler, L., Uniaxial deformation and orientation of ethylene-tetrafluoroethylene films. *Polymer Testing* 2013, *32*, 1423–1435.

[85]   DuPont, DuPont Nafion PFSA Membranes, data sheet, 2009.

[86]   Cheng, S.Z., Cao, M.Y., Wunderlich, B., Glass transition and melting behavior of poly (oxy-1, 4-phenyleneoxy-1, 4-phenylenecarbonyl-1, 4-phenylene)(PEEK). *Macromolecules* 1986, *19*, 1868–1876.

[87]   Vandiver, M.A., Horan, J.L., Yang, Y., Tansey, E.T., et al., Synthesis and characterization of perfluoro quaternary ammonium anion exchange membranes. *J Polym Sci Pol Phys* 2013, *51*, 1761–1769.

[88]   Janarthanan, R., Kishore Pilli, S., Horan, J.L., Gamarra, D.A., et al., A Direct Methanol Alkaline Fuel Cell Based on Poly(phenylene) Anion Exchange Membranes. *J. Electrochem. Soc.* 2014, *161*, F944–F950.

[89]   Bates, F.S., Fredrickson, G.H., Block Copolymers—Designer Soft Materials. *Phys. Today* 1999, *52*, 32.

[90]   Gadjourova, Z., Andreev, Y.G., Tunstall, D.P., Bruce, P.G., Ionic conductivity in crystalline polymer electrolytes. *Nature* 2001, *412*, 520–523.

[91]   Bates, F.S., Polymer-polymer phase behavior. *Science* 1991, *251*, 898–905.

[92]   Tsai, T.-H., Maes, A.M., Vandiver, M.A., Versek, C., et al., Synthesis and structure-conductivity relationship of polystyrene- block-poly(vinyl benzyl trimethylammonium) for alkaline anion exchange membrane fuel cells. *J Polym Sci Pol Phys* 2012, *51*, 1751–1760.

[93]   Sudre, G., Inceoglu, S., Cotanda, P., Balsara, N.P., Influence of Bound Ion on the Morphology and Conductivity of Anion-Conducting Block Copolymers. *Macromolecules* 2013, *46*, 1519–1527.

[94]   Li, Y., Block Copolymer for Alkaline Fuel Cell Membrane Materials, Colorado School of Mines, 2014.

[95]   Schlichting, G.J., Horan, J.L., Jessop, J.D., Nelson, S.E., et al., A Hybrid Organic/Inorganic Ionomer from the Copolymerization of Vinylphosphonic Acid and Zirconium Vinylphosphonate. *Macromolecules* 2012, *45*, 3874–3882.

[96]   Liu, Y., Horan, J.L., Schlichting, G.J., Caire, B.R., et al., A Small-Angle X-ray Scattering Study of the Development of Morphology in Films Formed from the 3M Perfluorinated Sulfonic Acid Ionomer. *Macromolecules* 2012, 120911063431009.

[97]   Vandiver, M.A., Caire, B.R., Carver, J.R., Waldrop, K., et al., Mechanical Characterization of Anion Exchange Membranes by Extensional Rheology under Controlled Hydration. *J. Electrochem. Soc.* 2014, *161*, H677–H683.

[98]   Zawodinski, T.A.J., Springer, T.E., Davey, J., Jestel, R., et al., A Comparative Study of Water Uptake by and Transport Through Ionomeric Fuel Cell Membranes. *J. Electrochem. Soc.* 1993, *140*, 1981–1985.

[99]   Burnett, D.J., Garcia, A.R., Thielmann, F., Measuring moisture sorption and diffusion kinetics on proton exchange membranes using a gravimetric vapor sorption apparatus. *Journal of Power Sources* 2006, *160*, 426–430.

[100]   Park, M.J., Downing, K.H., Jackson, A., Gomez, E.D., et al., Increased Water Retention in Polymer Electrolyte Membranes at Elevated Temperatures Assisted by Capillary Condensation. *Nano Lett.* 2007, *7*, 3547–3552.

[101]   Li, Y.S., Zhao, T.S., Yang, W.W., Measurements of water uptake and transport properties in anion-exchange membranes. *International Journal of Hydrogen Energy* 2010, *35*, 5656–5665.

[102]   Lin, X., Wu, L., Liu, Y., Ong, A.L., et al., Alkali resistant and conductive guanidinium-based anion-exchange membranes for alkaline polymer electrolyte fuel cells. *Journal of Power Sources* 2012, *217*, 373–380.

[103]   Wang, J., Li, S., Zhang, S., Novel Hydroxide-Conducting Polyelectrolyte Composed of an Poly(arylene ether sulfone) Containing Pendant Quaternary Guanidinium Groups for Alkaline Fuel Cell Applications. *Macromolecules* 2010, *43*, 3890–3896.

[104]   Silberstein, M.N., Boyce, M.C., Constitutive modeling of the rate, temperature, and hydration dependent deformation response of Nafion to monotonic and cyclic loading. *Journal of Power Sources* 2010, *195*, 5692–5706.

[105]   Sgreccia, E., Chailan, J.F., Khadhraoui, M., Di Vona, M.L., et al., Mechanical properties of proton-conducting sulfonated aromatic polymer membranes: Stress-strain tests and dynamical analysis. *Journal of Power Sources* 2010, *195*, 7770–7775.

[106]   Yuan, X.Z., Li, H., Zhang, S., Martin, J., et al., A review of polymer electrolyte membrane fuel cell durability test protocols. *Journal of Power Sources* 2011, *196*, 9107–9116.

[107]   Vandiver, M.A., Caire, B.R., Waldrop, K., Herring, A.M., et al., Mechanical Characterization of Anion Exchange Membranes. *ECS Transactions* 2013, *58*, 1543–1550.

[108]   Zhang, S., Yuan, X., Wang, H., MErida, W., et al., A review of accelerated stress tests of MEA durability in PEM fuel cells. *International Journal of Hydrogen Energy* 2009, *34*, 388–404.

[109]   Flory, P.J., Rehner, J., Statistical Mechanics of Cross-Linked Polymer Networks I. Rubberlike Elasticity. *J. Chem. Phys.* 1943, *11*, 512.

[110]   Nielsen, L.E., Cross-linking–effect on physical properties of polymers. *Journal of Macromolecular Science, Part C: Polymer Reviews* 1969, *3*, 69–103.

[111]   Clark, T.J., Robertson, N.J., Kostalik, H.A., IV, Lobkovsky, E.B., et al., A Ring-Opening Metathesis Polymerization Route to Alkaline Anion Exchange Membranes: Development of Hydroxide-Conducting Thin Films from an Ammonium-Functionalized Monomer. *J. Am. Chem. Soc.* 2009, *131*, 12888–12889.

[112]   Zha, Y., Disabb-Miller, M.L., Johnson, Z.D., Hickner, M.A., et al., Metal-Cation-Based Anion Exchange Membranes. *J. Am. Chem. Soc.* 2012, *134*, 4493–4496.

[113]   Pandey, A.K., Goswami, A., Sen, D., Mazumder, S., et al., Formation and characterization of highly crosslinked anion-exchange membranes. *J Membrane Sci* 2003, *217*, 117–130.

[114]   Varcoe, J.R., Slade, R.C.T., Lam How Yee, E., An alkaline polymer electrochemical interface: a breakthrough in application of alkaline anion-exchange membranes in fuel cells. *Chem. Commun.* 2006, 1428.

[115]   Pan, J., Li, Y., Zhuang, L., Lu, J., Self-crosslinked alkaline polymer electrolyte exceptionally stable at 90 °C. *Chem. Commun.* 2010, *46*, 8597.

[116]   Zhao, Y., Yu, H., Yang, D., Li, J., et al., High-performance alkaline fuel cells using crosslinked composite anion exchange membrane. *Journal of Power Sources* 2013, *221*, 247–251.

[117]   Gu, S., Cai, R., Yan, Y., Self-crosslinking for dimensionally stable and solvent-resistant quaternary phosphonium based hydroxide exchange membranes. *Chem. Commun.* 2011, *47*, 2856–2858.

[118]   Tsai, T.-H., Ionic Copolymers for Alkaline Anion Exchange Membrane Fuel Cells, University of Massachusetts Amherst, 2014.

[119]   Roddecha, S., Dong, Z., Wu, Y., Anthamatten, M., Mechanical properties and ionic conductivity of electrospun quaternary ammonium ionomers. *J Membrane Sci* 2012, *389*, 478–485.

[120]   Xu, S., Zhang, G., Zhang, Y., Zhao, C., et al., Synthesis and properties of a novel side-chain-type hydroxide exchange membrane for direct methanol fuel cells (DMFCs). *Journal of Power Sources* 2012, *209*, 228–235.

[121]   Wang, J., Wang, J., Li, S., Zhang, S., Poly(arylene ether sulfone)s ionomers with pendant quaternary ammonium groups for alkaline anion exchange membranes: Preparation and stability issues. *J Membrane Sci* 2011, *368*, 246–253.

[122]   Zhang, B., Gu, S., Wang, J., Liu, Y., et al., Tertiary sulfonium as a cationic functional group for hydroxide exchange membranes. *RSC Advances* 2012, *2*, 12683–12685.

[123]   Liu, Y., Wang, J., Yang, Y., Brenner, T.M., et al., Anion Transport in a Chemically Stable, Sterically Bulky α-C Modified Imidazolium Functionalized Anion Exchange Membrane. *J. Phys. Chem. C* 2014, *118*, 15136–15145.

[124]   Li, Y., Jackson, A.C., Beyer, F.L., Knauss, D.M., Poly(2,6-dimethyl-1,4-phenylene oxide) Blended with Poly(vinylbenzyl chloride)- b-polystyrene for the Formation of Anion Exchange Membranes. *Macromolecules* 2014, 140923073242003.

[125]   Kostalik, H.A., IV, Clark, T.J., Robertson, N.J., Mutolo, P.F., et al., Solvent Processable Tetraalkylammonium-Functionalized Polyethylene for Use as an Alkaline Anion Exchange Membrane. *Macromolecules* 2010, *43*, 7147–7150.

[126]   Zhang, M., Kim, H.K., Chalkova, E., Mark, F., et al., New Polyethylene Based Anion Exchange Membranes (PE–AEMs) with High Ionic Conductivity. *Macromolecules* 2011, *44*, 5937–5946.

[127]   Faraj, M., Boccia, M., Miller, H., Martini, F., et al., New LDPE based anion-exchange membranes for alkaline solid polymeric electrolyte water electrolysis. *International Journal of Hydrogen Energy* 2012, *37*, 14992–15002.

[128]   Sherazi, T.A., Sohn, J.Y., Lee, Y.M., Guiver, M.D., Polyethylene-based radiation grafted anion-exchange membranes for alkaline fuel cells. *J Membrane Sci* 2013, *441*, 148–157.

[129]   Vandiver, M.A., Caire, B.R., Poskin, Z., Li, Y., Durability and performance of polystyrene-b-poly (vinylbenzyl trimethylammonium) diblock copolymer and equivalent blend anion exchange membranes. *Journal of Applied …* 2015, *132*, 41596.

[130]   Park, A.M., Pintauro, P.N., Alkaline Fuel Cell Membranes from Electrospun Fiber Mats. *Electrochem Solid St* 2012, *15*, B27.

[131]   Flory, P.J., Tensile strength in relation to molecular weight of high polymers. *J. Am. Chem. Soc.* 1945, *67*, 2048–2050.

[132]   Grijpma, D.W., Penning, J.P., Pennings, A.J., Chain entanglement, mechanical properties and drawability of poly (lactide). *Colloid and Polymer Science* 1994, *272*, 1068–1081.

[133]   Fetters, L.J., Lohse, D.J., Milner, S.T., Graessley, W.W., Packing Length Influence in Linear Polymer Melts on the Entanglement, Critical, and Reptation Molecular Weights. *Macromolecules* 1999, *32*, 6847–6851.

[134] Buck, R.P., Kinetics of bulk and interfacial ionic motion: microscopic bases and limits for the nernst—planck equation applied to membrane systems. *J Membrane Sci* 1984, *17*, 1–62.

[135] Goswami, S., Klaus, S., Benziger, J., Wetting and Absorption of Water Drops on Nafion Films. *Langmuir* 2008, *24*, 8627–8633.

[136] Kim, Y.-H., Oblas, D., Angelopoulos, A.P., Fossey, S.A., et al., Adsorption of a Cationic Polyacrylamide onto the Surface of a Nafion Ionomer Membrane. *Macromolecules* 2001, *34*, 7489–7495.

[137] Kim, J.Y., Kim, S.H., Ionic conduction behavior of network polymer electrolytes based on phosphate and polyether copolymers. *Solid State Ionics* 1999, *124*, 91–99.

[138] Pradhan, D.K., Choudhary, R., Samantaray, B.K., Studies of dielectric relaxation and AC conductivity behavior of plasticized polymer nanocomposite electrolytes. *Int J Electrochem Sci* 2008, *3*, 597–608.

[139] Mathias, M.F., Makharia, R., Gasteiger, H.A., Conley, J.J., et al., Two fuel cell cars in every garage? *Interface-Electrochemical Society* 2005, *14*, 24–36.

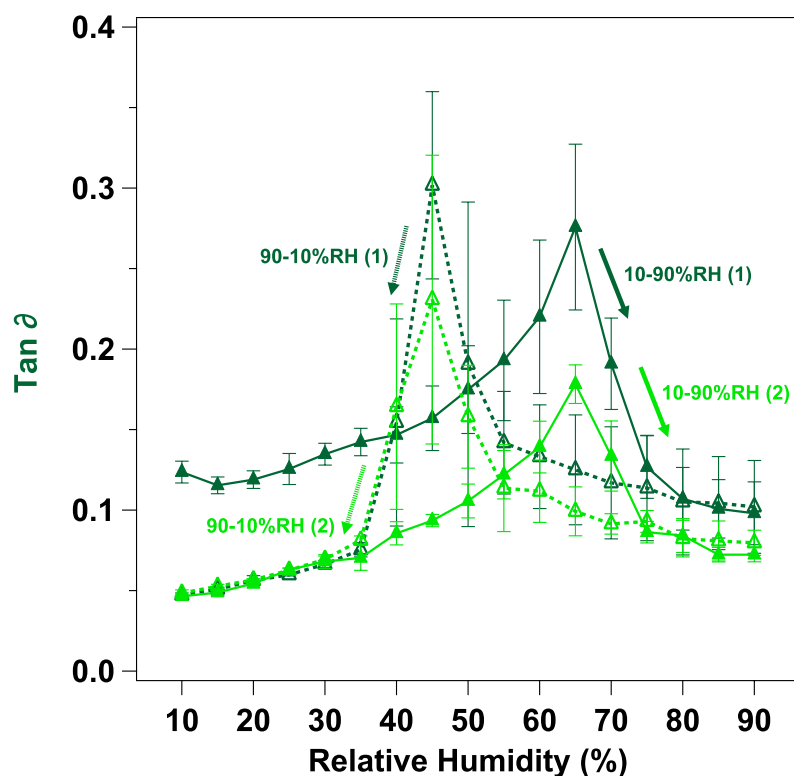This Appendix contains the supplemental figures referenced in Chapter 7 showing error bars for data.

Figure A.1: Tan δ vs. relative humidity, the solid markers are during humidification and open are markers are during dehumidification. Dark green corresponds to cycle 1 and light green to cycle 2.
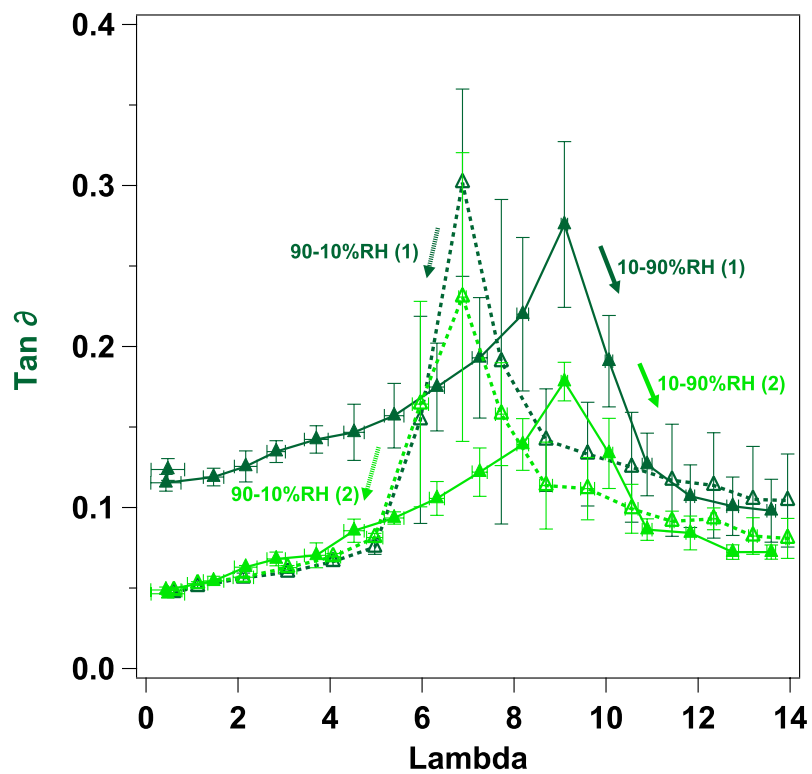
Figure A.2: Tan δ vs. lambda, the solid markers are during humidification and open are markers are during dehumidification. Dark green corresponds to cycle 1 and light green to cycle 2.
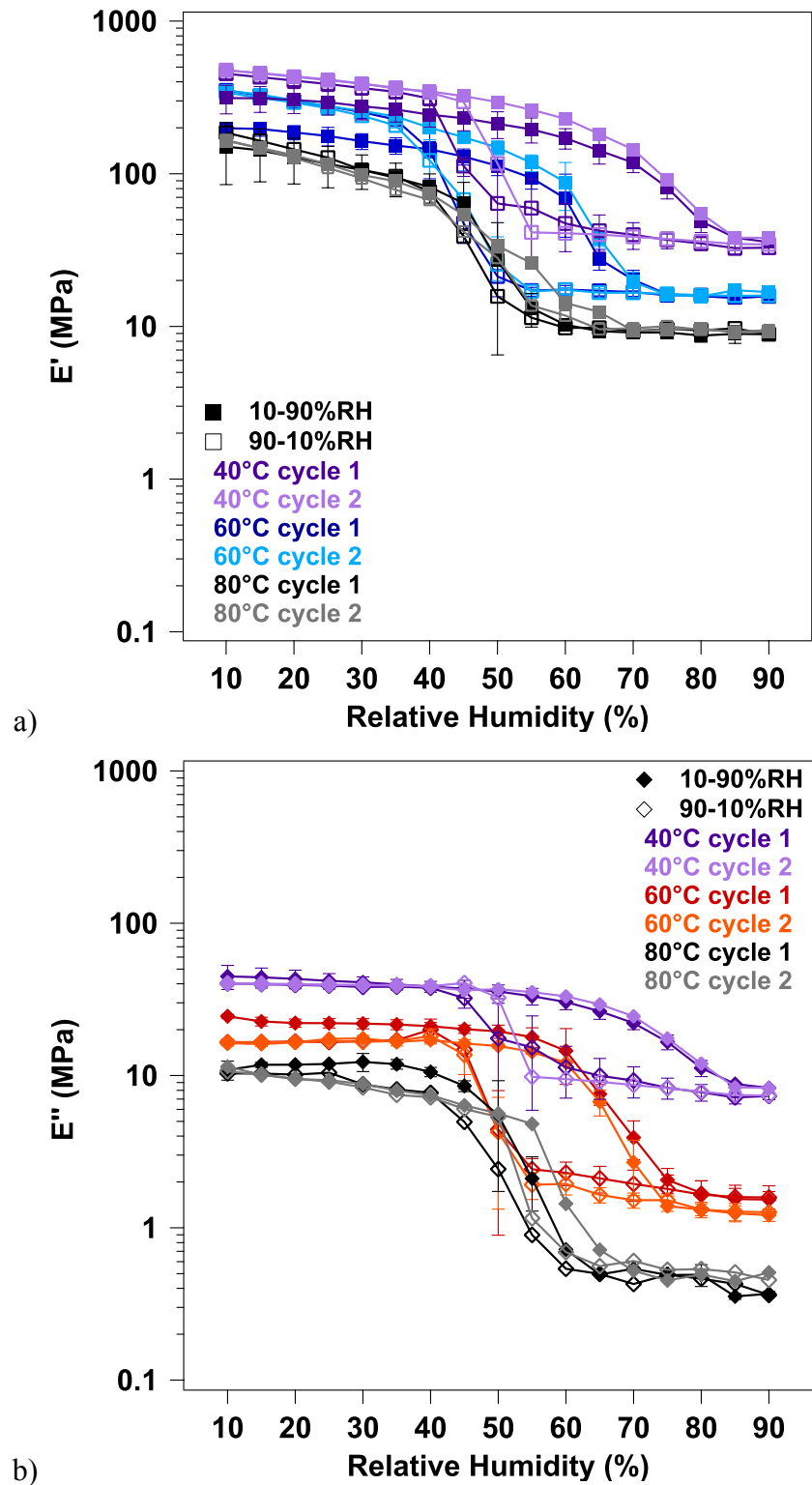
Figure A.3: a) Storage modulus and b) loss modulus vs. relative humidity at 40°C (purple), 60°C (blue/red), and 80°C (black).
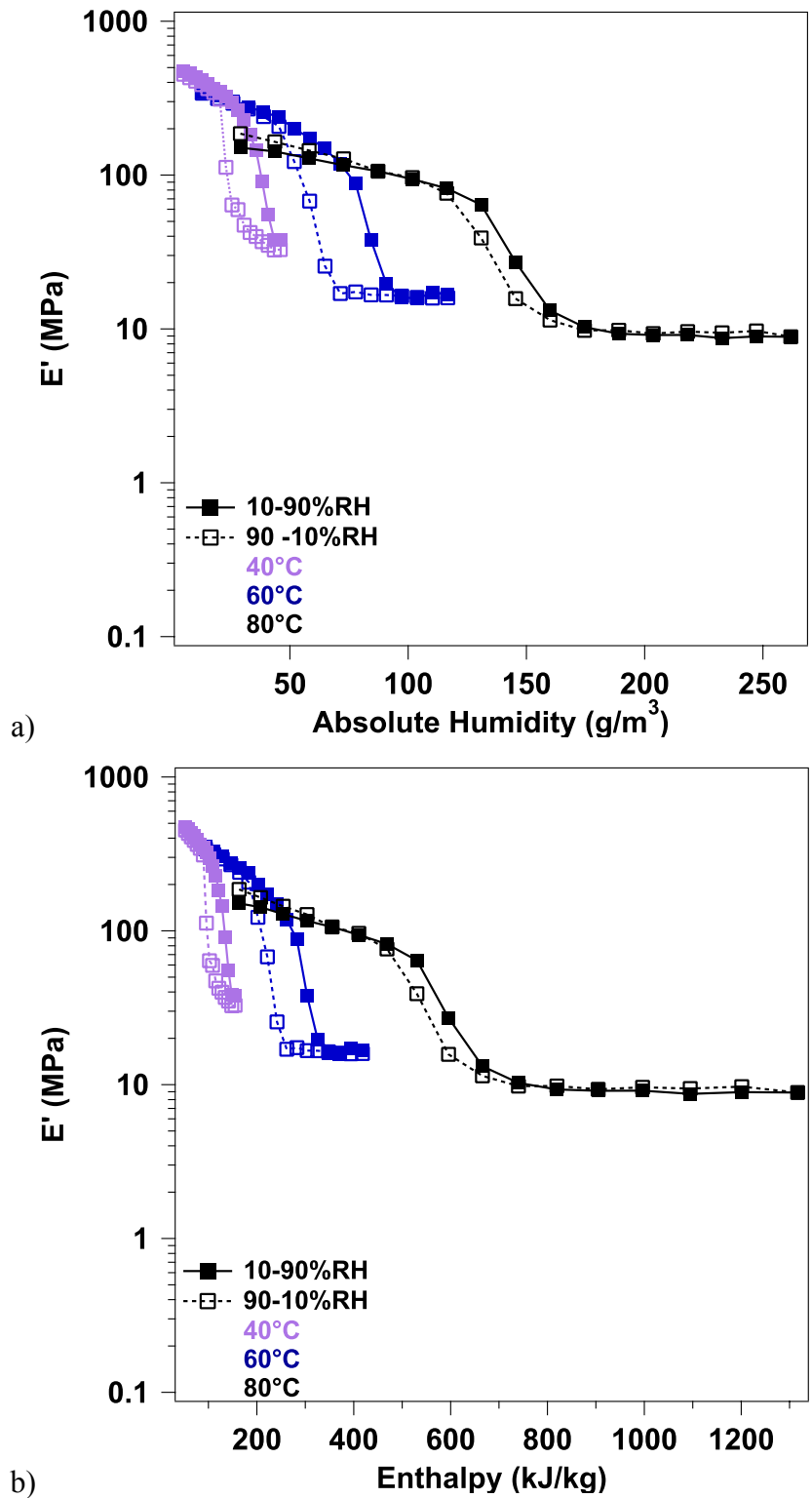
a)

b)

Figure A.4: Storage modulus vs. a) absolute humidity and b) enthalpy at 40°C (purple), 60°C (blue), and 80°C (black).

This Appendix includes expressed, written permission from the copyright holders granting permission for republication of the material contained in Chapters 3 (John Wiley and Sons) and 5 (John Wiley and Sons) of this thesis. The material in Chapter 4 was published as open-access and the copyright is held by the authors, the Creative Commons Attribution 4.0 License is included for reference. Written consent for republication from all Co-authors is also included.

<div style="text-align:center">

JOHN WILEY AND SONS LICENSE
TERMS AND CONDITIONS

Nov 12, 2014

</div>

This is a License Agreement between Melissa Vandiver ("You") and John Wiley and Sons ("John Wiley and Sons") provided by Copyright Clearance Center ("CCC"). The license consists of your order details, the terms and conditions provided by John Wiley and Sons, and the payment terms and conditions.

All payments must be made in full to CCC. For payment instructions, please see information listed at the bottom of this form.

License Number	3506640086514
License date	Nov 12, 2014
Licensed content publisher	John Wiley and Sons
Licensed content publication	Journal of Polymer Science Part B: Polymer Physics
Licensed content title	Synthesis and characterization of perfluoro quaternary ammonium anion exchange membranes
Licensed copyright line	Copyright © 2012 Wiley Periodicals, Inc.
Licensed content author	Melissa A. Vandiver,James L. Horan,Yuan Yang,Emily T. Tansey,Söenke Seifert,Matthew W. Liberatore,Andrew M. Herring
Licensed content date	Sep 26, 2012
Start page	1761
End page	1769
Type of use	Dissertation/Thesis
Requestor type	Author of this Wiley article
Format	Print and electronic
Portion	Full article
Will you be translating?	No
Title of your thesis / dissertation	CONTROLLED FILM PROCESSING TO IMPROVE MECHANICAL DURABILITY OF ANION EXCHANGE MEMBRANES
Expected completion date	Jan 2015
Expected size (number of pages)	130
Total	0.00 USD
Terms and Conditions	

<div style="text-align:center">

TERMS AND CONDITIONS

</div>

This copyrighted material is owned by or exclusively licensed to John Wiley & Sons, Inc. or one of its group companies (each a"Wiley Company") or handled on behalf of a society with

which a Wiley Company has exclusive publishing rights in relation to a particular work (collectively "WILEY"). By clicking �accept� in connection with completing this licensing transaction, you agree that the following terms and conditions apply to this transaction (along with the billing and payment terms and conditions established by the Copyright Clearance Center Inc., ("CCC's Billing and Payment terms and conditions"), at the time that you opened your Rightslink account (these are available at any time at http://myaccount.copyright.com).

Terms and Conditions

- The materials you have requested permission to reproduce or reuse (the "Wiley Materials") are protected by copyright.

- You are hereby granted a personal, non-exclusive, non-sub licensable (on a stand-alone basis), non-transferable, worldwide, limited license to reproduce the Wiley Materials for the purpose specified in the licensing process. This license is for a one-time use only and limited to any maximum distribution number specified in the license. The first instance of republication or reuse granted by this licence must be completed within two years of the date of the grant of this licence (although copies prepared before the end date may be distributed thereafter). The Wiley Materials shall not be used in any other manner or for any other purpose, beyond what is granted in the license. Permission is granted subject to an appropriate acknowledgement given to the author, title of the material/book/journal and the publisher. You shall also duplicate the copyright notice that appears in the Wiley publication in your use of the Wiley Material. Permission is also granted on the understanding that nowhere in the text is a previously published source acknowledged for all or part of this Wiley Material. Any third party content is expressly excluded from this permission.

- With respect to the Wiley Materials, all rights are reserved. Except as expressly granted by the terms of the license, no part of the Wiley Materials may be copied, modified, adapted (except for minor reformatting required by the new Publication), translated, reproduced, transferred or distributed, in any form or by any means, and no derivative works may be made based on the Wiley Materials without the prior permission of the respective copyright owner. You may not alter, remove or suppress in any manner any copyright, trademark or other notices displayed by the Wiley Materials. You may not license, rent, sell, loan, lease, pledge, offer as security, transfer or assign the Wiley Materials on a stand-alone basis, or any of the rights granted to you hereunder to any other person.

- The Wiley Materials and all of the intellectual property rights therein shall at all times remain the exclusive property of John Wiley & Sons Inc, the Wiley Companies, or their respective licensors, and your interest therein is only that of having possession of and the right to reproduce the Wiley Materials pursuant to Section 2 herein during the continuance of this Agreement. You agree that you own no right, title or interest in or to the Wiley Materials or any of the intellectual property rights therein. You shall have no rights hereunder other than the license as provided for above in Section 2. No right, license or interest to any trademark, trade name, service mark or other branding

("Marks") of WILEY or its licensors is granted hereunder, and you agree that you shall not assert any such right, license or interest with respect thereto.

- NEITHER WILEY NOR ITS LICENSORS MAKES ANY WARRANTY OR REPRESENTATION OF ANY KIND TO YOU OR ANY THIRD PARTY, EXPRESS, IMPLIED OR STATUTORY, WITH RESPECT TO THE MATERIALS OR THE ACCURACY OF ANY INFORMATION CONTAINED IN THE MATERIALS, INCLUDING, WITHOUT LIMITATION, ANY IMPLIED WARRANTY OF MERCHANTABILITY, ACCURACY, SATISFACTORY QUALITY, FITNESS FOR A PARTICULAR PURPOSE, USABILITY, INTEGRATION OR NON-INFRINGEMENT AND ALL SUCH WARRANTIES ARE HEREBY EXCLUDED BY WILEY AND ITS LICENSORS AND WAIVED BY YOU

- WILEY shall have the right to terminate this Agreement immediately upon breach of this Agreement by you.

- You shall indemnify, defend and hold harmless WILEY, its Licensors and their respective directors, officers, agents and employees, from and against any actual or threatened claims, demands, causes of action or proceedings arising from any breach of this Agreement by you.

- IN NO EVENT SHALL WILEY OR ITS LICENSORS BE LIABLE TO YOU OR ANY OTHER PARTY OR ANY OTHER PERSON OR ENTITY FOR ANY SPECIAL, CONSEQUENTIAL, INCIDENTAL, INDIRECT, EXEMPLARY OR PUNITIVE DAMAGES, HOWEVER CAUSED, ARISING OUT OF OR IN CONNECTION WITH THE DOWNLOADING, PROVISIONING, VIEWING OR USE OF THE MATERIALS REGARDLESS OF THE FORM OF ACTION, WHETHER FOR BREACH OF CONTRACT, BREACH OF WARRANTY, TORT, NEGLIGENCE, INFRINGEMENT OR OTHERWISE (INCLUDING, WITHOUT LIMITATION, DAMAGES BASED ON LOSS OF PROFITS, DATA, FILES, USE, BUSINESS OPPORTUNITY OR CLAIMS OF THIRD PARTIES), AND WHETHER OR NOT THE PARTY HAS BEEN ADVISED OF THE POSSIBILITY OF SUCH DAMAGES. THIS LIMITATION SHALL APPLY NOTWITHSTANDING ANY FAILURE OF ESSENTIAL PURPOSE OF ANY LIMITED REMEDY PROVIDED HEREIN.

- Should any provision of this Agreement be held by a court of competent jurisdiction to be illegal, invalid, or unenforceable, that provision shall be deemed amended to achieve as nearly as possible the same economic effect as the original provision, and the legality, validity and enforceability of the remaining provisions of this Agreement shall not be affected or impaired thereby.

- The failure of either party to enforce any term or condition of this Agreement shall not constitute a waiver of either party's right to enforce each and every term and condition of this Agreement. No breach under this agreement shall be deemed waived or excused by either party unless such waiver or consent is in writing signed by the party granting such waiver or consent. The waiver by or consent of a party to a breach of

any provision of this Agreement shall not operate or be construed as a waiver of or consent to any other or subsequent breach by such other party.

- This Agreement may not be assigned (including by operation of law or otherwise) by you without WILEY's prior written consent.

- Any fee required for this permission shall be non-refundable after thirty (30) days from receipt by the CCC.

- These terms and conditions together with CCC�s Billing and Payment terms and conditions (which are incorporated herein) form the entire agreement between you and WILEY concerning this licensing transaction and (in the absence of fraud) supersedes all prior agreements and representations of the parties, oral or written. This Agreement may not be amended except in writing signed by both parties. This Agreement shall be binding upon and inure to the benefit of the parties' successors, legal representatives, and authorized assigns.

- In the event of any conflict between your obligations established by these terms and conditions and those established by CCC�s Billing and Payment terms and conditions, these terms and conditions shall prevail.

- WILEY expressly reserves all rights not specifically granted in the combination of (i) the license details provided by you and accepted in the course of this licensing transaction, (ii) these terms and conditions and (iii) CCC�s Billing and Payment terms and conditions.

- This Agreement will be void if the Type of Use, Format, Circulation, or Requestor Type was misrepresented during the licensing process.

- This Agreement shall be governed by and construed in accordance with the laws of the State of New York, USA, without regards to such state�s conflict of law rules. Any legal action, suit or proceeding arising out of or relating to these Terms and Conditions or the breach thereof shall be instituted in a court of competent jurisdiction in New York County in the State of New York in the United States of America and each party hereby consents and submits to the personal jurisdiction of such court, waives any objection to venue in such court and consents to service of process by registered or certified mail, return receipt requested, at the last known address of such party.

WILEY OPEN ACCESS TERMS AND CONDITIONS

Wiley Publishes Open Access Articles in fully Open Access Journals and in Subscription journals offering Online Open. Although most of the fully Open Access journals publish open access articles under the terms of the Creative Commons Attribution (CC BY) License only, the subscription journals and a few of the Open Access Journals offer a choice of Creative Commons Licenses:: Creative Commons Attribution (CC-BY) license Creative Commons Attribution Non-Commercial (CC-BY-NC) license and Creative Commons

161

Use by non-commercial users

For non-commercial and non-promotional purposes, individual users may access, download, copy, display and redistribute to colleagues Wiley Open Access articles, as well as adapt, translate, text- and data-mine the content subject to the following conditions:

- The authors' moral rights are not compromised. These rights include the right of "paternity" (also known as "attribution" - the right for the author to be identified as such) and "integrity" (the right for the author not to have the work altered in such a way that the author's reputation or integrity may be impugned).

- Where content in the article is identified as belonging to a third party, it is the obligation of the user to ensure that any reuse complies with the copyright policies of the owner of that content.

- If article content is copied, downloaded or otherwise reused for non-commercial research and education purposes, a link to the appropriate bibliographic citation (authors, journal, article title, volume, issue, page numbers, DOI and the link to the definitive published version on **Wiley Online Library**) should be maintained. Copyright notices and disclaimers must not be deleted.

- Any translations, for which a prior translation agreement with Wiley has not been agreed, must prominently display the statement: "This is an unofficial translation of an article that appeared in a Wiley publication. The publisher has not endorsed this translation."

Use by commercial "for-profit" organisations

Use of Wiley Open Access articles for commercial, promotional, or marketing purposes requires further explicit permission from Wiley and will be subject to a fee. Commercial purposes include:

- Copying or downloading of articles, or linking to such articles for further redistribution, sale or licensing;

- Copying, downloading or posting by a site or service that incorporates advertising with such content;

- The inclusion or incorporation of article content in other works or services (other than normal quotations with an appropriate citation) that is then available for sale or licensing, for a fee (for example, a compilation produced for marketing purposes, inclusion in a sales pack)

- Use of article content (other than normal quotations with appropriate citation) by for-profit organisations for promotional purposes

- Linking to article content in e-mails redistributed for promotional, marketing or educational purposes;

- Use for the purposes of monetary reward by means of sale, resale, licence, loan, transfer or other form of commercial exploitation such as marketing products

- Print reprints of Wiley Open Access articles can be purchased from: corporatesales@wiley.com

Further details can be found on Wiley Online Library http://olabout.wiley.com/WileyCDA /Section/id-410895.html

Other Terms and Conditions:

v1.9

Questions? customercare@copyright.com or +1-855-239-3415 (toll free in the US) or +1-978-646-2777.

Gratis licenses (referencing $0 in the Total field) are free. Please retain this printable license for your reference. No payment is required.

JOHN WILEY AND SONS LICENSE
TERMS AND CONDITIONS

Nov 12, 2014

This is a License Agreement between Melissa Vandiver ("You") and John Wiley and Sons ("John Wiley and Sons") provided by Copyright Clearance Center ("CCC"). The license consists of your order details, the terms and conditions provided by John Wiley and Sons, and the payment terms and conditions.

All payments must be made in full to CCC. For payment instructions, please see information listed at the bottom of this form.

License Number	3506631279387
License date	Nov 12, 2014
Licensed content publisher	John Wiley and Sons
Licensed content publication	Journal of Applied Polymer Science
Licensed content title	Durability and performance of polystyrene-b-poly(vinylbenzyl trimethylammonium) diblock copolymer and equivalent blend anion exchange membranes
Licensed copyright line	Copyright © 2014 Wiley Periodicals, Inc.
Licensed content author	Melissa A. Vandiver,Benjamin R. Caire,Zach Poskin,Yifan Li,Sönke Seifert,Daniel M. Knauss,Andrew M. Herring,Matthew W. Liberatore
Licensed content date	Nov 1, 2014
Start page	n/a
End page	n/a
Type of use	Dissertation/Thesis
Requestor type	Author of this Wiley article
Format	Print and electronic
Portion	Full article
Will you be translating?	No
Title of your thesis / dissertation	CONTROLLED FILM PROCESSING TO IMPROVE MECHANICAL DURABILITY OF ANION EXCHANGE MEMBRANES
Expected completion date	Jan 2015
Expected size (number of pages)	130
Total	0.00 USD
Terms and Conditions	

TERMS AND CONDITIONS

This copyrighted material is owned by or exclusively licensed to John Wiley & Sons, Inc. or

one of its group companies (each a"Wiley Company") or handled on behalf of a society with which a Wiley Company has exclusive publishing rights in relation to a particular work (collectively "WILEY"). By clicking �accept� in connection with completing this licensing transaction, you agree that the following terms and conditions apply to this transaction (along with the billing and payment terms and conditions established by the Copyright Clearance Center Inc., ("CCC's Billing and Payment terms and conditions"), at the time that you opened your Rightslink account (these are available at any time at http://myaccount.copyright.com).

Terms and Conditions

- The materials you have requested permission to reproduce or reuse (the "Wiley Materials") are protected by copyright.

- You are hereby granted a personal, non-exclusive, non-sub licensable (on a stand-alone basis), non-transferable, worldwide, limited license to reproduce the Wiley Materials for the purpose specified in the licensing process. This license is for a one-time use only and limited to any maximum distribution number specified in the license. The first instance of republication or reuse granted by this licence must be completed within two years of the date of the grant of this licence (although copies prepared before the end date may be distributed thereafter). The Wiley Materials shall not be used in any other manner or for any other purpose, beyond what is granted in the license. Permission is granted subject to an appropriate acknowledgement given to the author, title of the material/book/journal and the publisher. You shall also duplicate the copyright notice that appears in the Wiley publication in your use of the Wiley Material. Permission is also granted on the understanding that nowhere in the text is a previously published source acknowledged for all or part of this Wiley Material. Any third party content is expressly excluded from this permission.

- With respect to the Wiley Materials, all rights are reserved. Except as expressly granted by the terms of the license, no part of the Wiley Materials may be copied, modified, adapted (except for minor reformatting required by the new Publication), translated, reproduced, transferred or distributed, in any form or by any means, and no derivative works may be made based on the Wiley Materials without the prior permission of the respective copyright owner. You may not alter, remove or suppress in any manner any copyright, trademark or other notices displayed by the Wiley Materials. You may not license, rent, sell, loan, lease, pledge, offer as security, transfer or assign the Wiley Materials on a stand-alone basis, or any of the rights granted to you hereunder to any other person.

- The Wiley Materials and all of the intellectual property rights therein shall at all times remain the exclusive property of John Wiley & Sons Inc, the Wiley Companies, or their respective licensors, and your interest therein is only that of having possession of and the right to reproduce the Wiley Materials pursuant to Section 2 herein during the continuance of this Agreement. You agree that you own no right, title or interest in or to the Wiley Materials or any of the intellectual property rights therein. You shall have no rights hereunder other than the license as provided for above in Section 2. No right,

165

license or interest to any trademark, trade name, service mark or other branding ("Marks") of WILEY or its licensors is granted hereunder, and you agree that you shall not assert any such right, license or interest with respect thereto.

- NEITHER WILEY NOR ITS LICENSORS MAKES ANY WARRANTY OR REPRESENTATION OF ANY KIND TO YOU OR ANY THIRD PARTY, EXPRESS, IMPLIED OR STATUTORY, WITH RESPECT TO THE MATERIALS OR THE ACCURACY OF ANY INFORMATION CONTAINED IN THE MATERIALS, INCLUDING, WITHOUT LIMITATION, ANY IMPLIED WARRANTY OF MERCHANTABILITY, ACCURACY, SATISFACTORY QUALITY, FITNESS FOR A PARTICULAR PURPOSE, USABILITY, INTEGRATION OR NON-INFRINGEMENT AND ALL SUCH WARRANTIES ARE HEREBY EXCLUDED BY WILEY AND ITS LICENSORS AND WAIVED BY YOU

- WILEY shall have the right to terminate this Agreement immediately upon breach of this Agreement by you.

- You shall indemnify, defend and hold harmless WILEY, its Licensors and their respective directors, officers, agents and employees, from and against any actual or threatened claims, demands, causes of action or proceedings arising from any breach of this Agreement by you.

- IN NO EVENT SHALL WILEY OR ITS LICENSORS BE LIABLE TO YOU OR ANY OTHER PARTY OR ANY OTHER PERSON OR ENTITY FOR ANY SPECIAL, CONSEQUENTIAL, INCIDENTAL, INDIRECT, EXEMPLARY OR PUNITIVE DAMAGES, HOWEVER CAUSED, ARISING OUT OF OR IN CONNECTION WITH THE DOWNLOADING, PROVISIONING, VIEWING OR USE OF THE MATERIALS REGARDLESS OF THE FORM OF ACTION, WHETHER FOR BREACH OF CONTRACT, BREACH OF WARRANTY, TORT, NEGLIGENCE, INFRINGEMENT OR OTHERWISE (INCLUDING, WITHOUT LIMITATION, DAMAGES BASED ON LOSS OF PROFITS, DATA, FILES, USE, BUSINESS OPPORTUNITY OR CLAIMS OF THIRD PARTIES), AND WHETHER OR NOT THE PARTY HAS BEEN ADVISED OF THE POSSIBILITY OF SUCH DAMAGES. THIS LIMITATION SHALL APPLY NOTWITHSTANDING ANY FAILURE OF ESSENTIAL PURPOSE OF ANY LIMITED REMEDY PROVIDED HEREIN.

- Should any provision of this Agreement be held by a court of competent jurisdiction to be illegal, invalid, or unenforceable, that provision shall be deemed amended to achieve as nearly as possible the same economic effect as the original provision, and the legality, validity and enforceability of the remaining provisions of this Agreement shall not be affected or impaired thereby.

- The failure of either party to enforce any term or condition of this Agreement shall not constitute a waiver of either party's right to enforce each and every term and condition of this Agreement. No breach under this agreement shall be deemed waived or excused by either party unless such waiver or consent is in writing signed by the party

granting such waiver or consent. The waiver by or consent of a party to a breach of any provision of this Agreement shall not operate or be construed as a waiver of or consent to any other or subsequent breach by such other party.

- This Agreement may not be assigned (including by operation of law or otherwise) by you without WILEY's prior written consent.

- Any fee required for this permission shall be non-refundable after thirty (30) days from receipt by the CCC.

- These terms and conditions together with CCC�s Billing and Payment terms and conditions (which are incorporated herein) form the entire agreement between you and WILEY concerning this licensing transaction and (in the absence of fraud) supersedes all prior agreements and representations of the parties, oral or written. This Agreement may not be amended except in writing signed by both parties. This Agreement shall be binding upon and inure to the benefit of the parties' successors, legal representatives, and authorized assigns.

- In the event of any conflict between your obligations established by these terms and conditions and those established by CCC�s Billing and Payment terms and conditions, these terms and conditions shall prevail.

- WILEY expressly reserves all rights not specifically granted in the combination of (i) the license details provided by you and accepted in the course of this licensing transaction, (ii) these terms and conditions and (iii) CCC�s Billing and Payment terms and conditions.

- This Agreement will be void if the Type of Use, Format, Circulation, or Requestor Type was misrepresented during the licensing process.

- This Agreement shall be governed by and construed in accordance with the laws of the State of New York, USA, without regards to such state�s conflict of law rules. Any legal action, suit or proceeding arising out of or relating to these Terms and Conditions or the breach thereof shall be instituted in a court of competent jurisdiction in New York County in the State of New York in the United States of America and each party hereby consents and submits to the personal jurisdiction of such court, waives any objection to venue in such court and consents to service of process by registered or certified mail, return receipt requested, at the last known address of such party.

WILEY OPEN ACCESS TERMS AND CONDITIONS

Wiley Publishes Open Access Articles in fully Open Access Journals and in Subscription journals offering Online Open. Although most of the fully Open Access journals publish open access articles under the terms of the Creative Commons Attribution (CC BY) License only, the subscription journals and a few of the Open Access Journals offer a choice of Creative Commons Licenses:: Creative Commons Attribution (CC-BY) license Creative

Commons Attribution Non-Commercial (CC-BY-NC) license and Creative Commons Attribution Non-Commercial-NoDerivs (CC-BY-NC-ND) License. The license type is clearly identified on the article.

Copyright in any research article in a journal published as Open Access under a Creative Commons License is retained by the author(s). Authors grant Wiley a license to publish the article and identify itself as the original publisher. Authors also grant any third party the right to use the article freely as long as its integrity is maintained and its original authors, citation details and publisher are identified as follows: [Title of Article/Author/Journal Title and Volume/Issue. Copyright (c) [year] [copyright owner as specified in the Journal]. Links to the final article on Wiley�s website are encouraged where applicable.

The Creative Commons Attribution License

The Creative Commons Attribution License (CC-BY) allows users to copy, distribute and transmit an article, adapt the article and make commercial use of the article. The CC-BY license permits commercial and non-commercial re-use of an open access article, as long as the author is properly attributed.

The Creative Commons Attribution License does not affect the moral rights of authors, including without limitation the right not to have their work subjected to derogatory treatment. It also does not affect any other rights held by authors or third parties in the article, including without limitation the rights of privacy and publicity. Use of the article must not assert or imply, whether implicitly or explicitly, any connection with, endorsement or sponsorship of such use by the author, publisher or any other party associated with the article.

For any reuse or distribution, users must include the copyright notice and make clear to others that the article is made available under a Creative Commons Attribution license, linking to the relevant Creative Commons web page.

To the fullest extent permitted by applicable law, the article is made available as is and without representation or warranties of any kind whether express, implied, statutory or otherwise and including, without limitation, warranties of title, merchantability, fitness for a particular purpose, non-infringement, absence of defects, accuracy, or the presence or absence of errors.

Creative Commons Attribution Non-Commercial License

The Creative Commons Attribution Non-Commercial (CC-BY-NC) License permits use, distribution and reproduction in any medium, provided the original work is properly cited and is not used for commercial purposes.(see below)

Creative Commons Attribution-Non-Commercial-NoDerivs License

The Creative Commons Attribution Non-Commercial-NoDerivs License (CC-BY-NC-ND) permits use, distribution and reproduction in any medium, provided the original work is properly cited, is not used for commercial purposes and no modifications or adaptations are made. (see below)

Use by non-commercial users

For non-commercial and non-promotional purposes, individual users may access, download, copy, display and redistribute to colleagues Wiley Open Access articles, as well as adapt, translate, text- and data-mine the content subject to the following conditions:

- The authors' moral rights are not compromised. These rights include the right of "paternity" (also known as "attribution" - the right for the author to be identified as such) and "integrity" (the right for the author not to have the work altered in such a way that the author's reputation or integrity may be impugned).

- Where content in the article is identified as belonging to a third party, it is the obligation of the user to ensure that any reuse complies with the copyright policies of the owner of that content.

- If article content is copied, downloaded or otherwise reused for non-commercial research and education purposes, a link to the appropriate bibliographic citation (authors, journal, article title, volume, issue, page numbers, DOI and the link to the definitive published version on **Wiley Online Library**) should be maintained. Copyright notices and disclaimers must not be deleted.

- Any translations, for which a prior translation agreement with Wiley has not been agreed, must prominently display the statement: "This is an unofficial translation of an article that appeared in a Wiley publication. The publisher has not endorsed this translation."

Use by commercial "for-profit" organisations

Use of Wiley Open Access articles for commercial, promotional, or marketing purposes requires further explicit permission from Wiley and will be subject to a fee. Commercial purposes include:

- Copying or downloading of articles, or linking to such articles for further redistribution, sale or licensing;

- Copying, downloading or posting by a site or service that incorporates advertising with such content;

- The inclusion or incorporation of article content in other works or services (other than normal quotations with an appropriate citation) that is then available for sale or licensing, for a fee (for example, a compilation produced for marketing purposes, inclusion in a sales pack)

- Use of article content (other than normal quotations with appropriate citation) by for-profit organisations for promotional purposes

- Linking to article content in e-mails redistributed for promotional, marketing or educational purposes;

- Use for the purposes of monetary reward by means of sale, resale, licence, loan, transfer or other form of commercial exploitation such as marketing products

- Print reprints of Wiley Open Access articles can be purchased from: corporatesales@wiley.com

Further details can be found on Wiley Online Library http://olabout.wiley.com/WileyCDA /Section/id-410895.html

Other Terms and Conditions:

v1.9

Questions? customercare@copyright.com or +1-855-239-3415 (toll free in the US) or +1-978-646-2777.

Gratis licenses (referencing $0 in the Total field) are free. Please retain this printable license for your reference. No payment is required.

171

[More info](#).

You may also use a license listed as compatible at https://creativecommons.org/compatiblelicenses

[More info](#).

A commercial use is one primarily intended for commercial advantage or monetary compensation.

[More info](#).

Merely changing the format never creates a derivative.

[More info](#).

Melissa Vandiver <mvandive@mymail.mines.edu>

Thesis - permission to reproduce

Jim Horan <jhoran@mines.edu>   Mon, Nov 17, 2014 at 9:21 PM
To: Melissa Vandiver <mvandive@mymail.mines.edu>

Melissa,

I hope the statement below will be satisfactory to allow you to include the published manuscript in your thesis. Let me know if you need anything else.

I hereby permit Melissa Vandiver to reproduce the work entitled " Synthesis and characterization of perfluoro quaternary ammonium anion exchange membranes" published in the *Journal of Polymer Science, Part B: Polymer Physics* (2013), **51**, 1761-1769, DOI: 10.1002/polb.23171 as part of her thesis.

James L. Horan

Melissa Vandiver <mvandive@mymail.mines.edu>

Thesis - permission to reproduce

Yuan Yang <yuanyang@mines.edu>   Mon, Nov 17, 2014 at 3:26 PM
To: Melissa Vandiver <mvandive@mymail.mines.edu>

I hereby permit Melissa Vandiver to reproduce the work entitled " Synthesis and characterization of perfluoro quaternary ammonium anion exchange membranes" published in the *Journal of Polymer Science, Part B: Polymer Physics* (2013), **51**, 1761-1769, DOI: 10.1002/polb.23171 as part of her thesis.

-Yuan Yang

Yuan Yang
Research Assistant Professor
NMR Facility Manager
Department of Chemistry and Geochemistry
121 Coolbaugh Hall
Colorado School of Mines
Golden, CO 80401
303-384-2109

Melissa Vandiver <mvandive@mymail.mines.edu>

Thesis - permission to reproduce

emily Tansey <emily.t.tansey@gmail.com>
To: Melissa Vandiver <mvandive@mymail.mines.edu>

Tue, Nov 18, 2014 at 3:05 AM

Dear Melissa,

That's great news, I'm excited to hear you'll be defending your thesis soon. Below is the statemtent of permission.

I hereby permit Melissa Vandiver to reproduce the work entitled "Synthesis and characterization of perfluoro quaternary ammonium anion exchange membranes" published in the *Journal of Polymer Science, Part B: Polymer Physics* (2013), **51**, 1761-1769, DOI: 10.1002/polb.23171 as part of her thesis.

-Emily Tansey

Good luck finishing everything up! Wishing you all the best, greetings to everyone in the work group from me in Germany! I'm currently studying and filling some prerequisites to start my masters at the Universität Bremen. I miss Colorado, though...

All the best,
Emily

Sent from Samsung tablet
[Quoted text hidden]

Melissa Vandiver <mvandive@mymail.mines.edu>

Thesis - permission to reproduce

seifert <seifert@anl.gov>   Tue, Nov 18, 2014 at 12:39 AM
To: Melissa Vandiver <mvandive@mymail.mines.edu>

I hereby permit Melissa Vandiver to reproduce the following works as part of her thesis:

"Synthesis and characterization of perfluoro quaternary ammonium anion exchange membranes" published in the *Journal of Polymer Science, Part B: Polymer Physics* (2013), **51**, 1761-1769, DOI: 10.1002/polb.23171

"Durability and performance of polystyrene-b-poly(vinylbenzyl trimethylammonium) diblock copolymer and equivalent blend anion exchange membranes" published" published in the *Journal of Applied Polymer Science*, (2015), **132**, 41596, DOI: 10.1002/app.41596

Sincerely,

Soenke Seifert, Ph.D.

APS/ANL 433E008
Argonne National Laboratory
9700 South Cass Avenue
Argonne, Illinois 60439
office: 630 252 0391

Melissa Vandiver <mvandive@mymail.mines.edu>

Thesis - permission to reproduce

Benjamin Caire <bcaire@mymail.mines.edu>
To: Melissa Vandiver <mvandive@mymail.mines.edu>

Mon, Nov 17, 2014 at 2:47 PM

I hereby permit Melissa Vandiver to reproduce the following works as part of her thesis:

"Mechanical Characterization of Anion Exchange Membranes by Extensional Rheology under Controlled Hydration" published in the *Journal of The Electrochemical Society*, (2014), **161**, H677-H683, DOI: 10.1149/2.0971410jes

"Durability and performance of polystyrene-b-poly(vinylbenzyl trimethylammonium) diblock copolymer and equivalent blend anion exchange membranes" published" published in the *Journal of Applied Polymer Science*, (2015), **132**, 41596, DOI: 10.1002/app.41596

-Benjamin R. Caire

Benjamin Caire
bcaire@mymail.mines.edu
bcaire@gmail.com
(504) 214-7552 Mobile
[Quoted text hidden]

Melissa Vandiver <mvandive@mymail.mines.edu>

Thesis - permission to reproduce

Jordan Carver <j.r.carver23@gmail.com>   Mon, Nov 17, 2014 at 4:44 PM
To: Melissa Vandiver <mvandive@mymail.mines.edu>

I hereby permit Melissa Vandiver to reproduce the work entitled: "Mechanical Characterization of Anion Exchange Membranes by Extensional Rheology under Controlled Hydration" published in the *Journal of The Electrochemical Society*, (2014), **161**, H677-H683, DOI: 10.1149/2.0971410jes as part of her thesis.

- Jordan R. Carver

Congratulations!!!!!!!!!! What's next for you?
[Quoted text hidden]

Melissa Vandiver <mvandive@mymail.mines.edu>

Thesis - permission to reproduce

Krysta Waldrop <krysta.waldrop@gmail.com>   Mon, Nov 17, 2014 at 7:09 PM
To: Melissa Vandiver <mvandive@mymail.mines.edu>

I hereby permit Melissa Vandiver to reproduce the work entitled: "Mechanical Characterization of Anion Exchange Membranes by Extensional Rheology under Controlled Hydration" published in the *Journal of The Electrochemical Society*, (2014), **161**, H677-H683, DOI: 10.1149/2.0971410jes as part of her thesis.

Krysta Lee Waldrop

[Quoted text hidden]

Melissa Vandiver <mvandive@mymail.mines.edu>

Thesis - permission to reproduce

Hibbs, Michael <mhibbs@sandia.gov>   Mon, Nov 17, 2014 at 4:59 PM
To: Melissa Vandiver <mvandive@mymail.mines.edu>

Hi Melissa,

I hereby permit Melissa Vandiver to reproduce the work entitled: "Mechanical Characterization of Anion Exchange Membranes by Extensional Rheology under Controlled Hydration" published in the *Journal of The Electrochemical Society*, (2014), **161**, H677-H683, DOI: 10.1149/2.0971410jes as part of her thesis.

Good luck with getting everything ready to submit!

Michael Hibbs

From: Melissa Vandiver [mailto:mvandive@mymail.mines.edu]
Sent: Monday, November 17, 2014 2:56 PM
To: Hibbs, Michael
Subject: [EXTERNAL] Thesis - permission to reproduce

[Quoted text hidden]

Melissa Vandiver <mvandive@mymail.mines.edu>

Thesis - permission to reproduce

j.varcoe@surrey.ac.uk <j.varcoe@surrey.ac.uk>   Mon, Nov 17, 2014 at 3:33 PM
To: mvandive@mymail.mines.edu

Hi Melissa,

"I hereby permit you (Melissa Vandiver) to reproduce the work entitled: "Mechanical Characterization of Anion Exchange Membranes by Extensional Rheology under Controlled Hydration" published in the *Journal of The Electrochemical Society*, (2014), **161**, H677-H683, DOI: 10.1149/2.0971410jes as part of your thesis.

Regards

Prof John Varcoe

Sent from my ipad
[Quoted text hidden]

Melissa Vandiver <mvandive@mymail.mines.edu>

Thesis - permission to reproduce

Zach Poskin <zposkin@gmail.com>   Mon, Nov 17, 2014 at 2:44 PM
To: Melissa Vandiver <mvandive@mymail.mines.edu>

Hey Melissa,

Good luck with your submission and defense! Hope all goes well. Here is the permission statement:

I hereby permit Melissa Vandiver to reproduce the work entitled "Durability and performance of polystyrene-b-poly(vinylbenzyl trimethylammonium) diblock copolymer and equivalent blend anion exchange membranes" published in the *Journal of Applied Polymer Science*, (2015), **132**, 41596, DOI: 10.1002/app.41596 as part of her thesis.

-Zach Poskin
[Quoted text hidden]
--
Zach Poskin
Graduate Research Assistant
Biomedical Engineering
University of Wisconsin
zposkin@wisc.edu
(913) 488-1166

Melissa Vandiver <mvandive@mymail.mines.edu>

Thesis - permission to reproduce

Yifan Li <malfurionless@gmail.com>   Mon, Nov 17, 2014 at 7:19 PM
To: Melissa Vandiver <mvandive@mymail.mines.edu>

I hereby permit Melissa Vandiver to reproduce the work entitled "Durability and performance of polystyrene-b-poly(vinylbenzyl trimethylammonium) diblock copolymer and equivalent blend anion exchange membranes" published in the *Journal of Applied Polymer Science*, (2015), **132**, 41596, DOI: 10.1002/app.41596 as part of her thesis.

Yifan Li

On Mon, Nov 17, 2014 at 3:42 PM, Melissa Vandiver <mvandive@mymail.mines.edu> wrote:
> Hello Yifan,
>
> I hope all is well with you and you're enjoying the new job.
>
> I will be submitting/defending my thesis this December, and the thesis formatting rules require permission from all co-authors to include published manuscripts. I would like your permission to reproduce the article listed below that you are a co-author. If you could please copy the quoted texted below and respond to this email, or send a new message, and include your full name as signature, I would greatly appreciate it.
>
> "I hereby permit Melissa Vandiver to reproduce the work entitled "Durability and performance of polystyrene-b-poly(vinylbenzyl trimethylammonium) diblock copolymer and equivalent blend anion exchange membranes" published in the *Journal of Applied Polymer Science*, (2015), **132**, 41596, DOI: 10.1002/app.41596 as part of her thesis.
>
> -Your full Name"
>
> Thank you for your help,
>
> --
> Melissa Vandiver
> PhD Candidate
> Colorado School of Mines
> (970)-946-5413
> mvandive@mymail.mines.edu